Protein Engineering of Bacterioferritin: Applications to Bionanotechnology

by

Anton Michiel van der Ven

A thesis

presented to the University of Waterloo

in fulfilment of the

thesis requirement for the degree of

Master of Science

in

Chemistry

Waterloo, Ontario, Canada, 2014

I hereby declare that I am the sole author of this thesis. This is a true copy of the thesis, including any required final revisions, as accepted by my examiners.

I understand that my thesis may be made electronically available to the public.

Abstract

Biological protein assemblies are the products of evolutionary necessity that have arisen to protect the cell, improve reaction rates, and/or compartmentalize biological systems. Belonging to this category of sel-assembling bionano-structures are cage proteins. Cage proteins are composed of multiple protomers (subunits) that self-assemble into many unique structures, all having interior, exterior, and interface surfaces available for controllable modification. Bacterioferritins (Bfr) are a set of cage proteins belonging to the ferritin superfamily of iron storage proteins, are roughly spherical with a 12 nm exterior diameter and an 8 nm interior diameter, are composed of 24 identical protomers, and contain 12 heme cofactors. An important feature of Bfr that was utilized for advancement in platform development was the locality of the N- and C- termini. These termini point towards the exterior and interior of the protein cage, which made them ideal for genetic engineering these two surfaces. Polyhistidine amino acid sequences (His6-tags) were added to the C-termini of the Bfr protein subunits in order to provide new selective affinity interactions on the interior protein surface of this multiprotein cavity. This His6-tag affinity interaction allowed for Ni^{2+}-dependent complexation between the host Bfr and two guest molecules modified with a nitrilotriacetic (NTA) acid. The two proof of concept guests studied in our laboratory were streptavidin binding a biotin-XNTA functionality, and a gold nanoparticle (GNP) containing NTA functionalities. This approach was designed to make both streptavidin and GNPs addressable to the interior surface of Bfr through the NTA/His6-tag affinity interaction. The purpose of these experiments was to explore various methodologies to form controllable interactions between guest molecules and internal protein cavity surfaces. Additionally, the endogenous heme molecules were exchanged for fluorescently-modified hemes as a further approach to engineer this cage protein

for host-guest interactions. The information gained from the above experiments will help develop the bionanotechnology applications of Bfr.

Acknowledgements

I would like to thank and acknowledge all the guidance and hard work that Dr. John Honek has put towards my personal development as a student and scientist. Much less would have been accomplished if not for his commitment to his students

I would also like to thank the members of the Honek group that worked tirelessly, who I owe much too, and who have been integral in the success of the work in this thesis, in no particular order: Dr. Elisabeth Daub, Anthony Petrie, Robert Taylor, Denise Lieuson, Amanda Poole, Danny Liu, Jessy Mathos, and all those before me who worked hard to get the Bfr project off the ground, notably Dr. Uthaiwan Suttisansanee and Liz Gargatsougias.

Acknowledgement must be made to the funding agencies of NSERC and OGS for recognizing the potential in the research performed. Without this funding much of the research would be impossible to do.

Lastly, I want to thank family, friends, and my girlfriend, Joanna, for their understanding when hours were late, and gatherings missed.

Table of Contents

List of Figures

List of Tables

Appendix

Reaction Schemes

Abbreviations

AAF: 5-(Aminoacetamido)Fluorescein

aaRS: aminoacyl-tRNA synthetase

AFM: Atomic force microscopy

Ala: Alanine

Arg: Arginine

Asn: Asparagine

Asp: Aspartate

Bfr: Bacterioferritin

Biotin-XNTA: Biotin nitrilotriacetic acid

CCMV: Cowpea chlorotic mottle virus

Cox: Cytochrome c oxidase

CPMV: Cowpea mosaic virus

Cys: Cysteine

DCCH: 7-Diethylaminocoumarin-3-Carboxylic Acid, Hydrazide

DLS: Dynamic light scattering

DMF: Dimethylformamide

DMSO: Dimethyl Sulfoxide

Dps: DNA-binding proteins from starved cells

EDC: N-(3-dimethylaminopropyl-N’-ethyl)-carbodiimide

EPL: Expressed protein ligation

EPR: Enhanced permeability and retention

FRET: Förster resonance energy transfer

FSTC: Fluorescein-5-Thiosemicarbazide

GFP: Green Fluorescent Protein

Gln: Glutamine

Glu: Glutamate

Gly: Glycine

GndHCl: Guanidine HCl

His: Histidine

His6-tag: Hexahistidine affinity tag

HRP: Horseradish peroxidase

Hsp: Heat-shock protein

Ile: Isoluecine

kDa: Kilodalton

keV: Kiloelectron volt

Leu: Leucine

LY: Lucifer Yellow

Lys: Lysine

Lys-NTA: Nα,Nα-Bis(carboxymethyl)-L-lysine

Met: Methionine

MW: Molecular Weight

NBA: N-butylamine

Native PAGE: Native polyacrylamide gel electrophoresis

NCL: Native chemical ligation

NHS: N-hydroxysuccinimide

NP: Nanoparticle

NTA: Nitrilotriacetic acid

P450: Cytochrome P450

PalB: *Pseudozyma antarctica* lipase B

PEG: Polyethylene glycol

Phe: Phenylalanine

Pro: Proline

QD: Quantum dots

SDS-PAGE: Sodium dodecyl sulfate polyacrylamide gel electrophoresis

SEC: Size exclusion chromatography

Ser: Serine

TEM: Transmission electron microscopy

Thr: Threonine

Trp: Tryptophan

Tyr: Tyrosine

Val: Valine

VLP: Virus-like proteins

1. Chapter 1: Introduction

1.1. Summary of Research

Although proteins are complex molecules, they can be engineered and repurposed through a combination of recombinant genetic and chemical approaches. Multiprotein complexes, such as cellular housekeeping cage proteins and viral coat proteins fall within the category of bio-nanoparticles, and are being investigated with intense interest as potential platforms for drug delivery, unique materials generation, biosensors, and other novel applications.[1-5] These protein shells vary in size from the largest virus with a 750 nm diameter shell to the smaller protein complexes with diameters of 10 nm [6,7] (Figure 1.1). This diversity in size, and function, provides a reservoir of cage proteins all governed by similar assembly principles, which could be used in many unique applications. Of importance to these applications is understanding how host-guest interactions are central for encapsulating novel guest molecules, which modifications to the protein cage outer surface can be made to direct it to particular surfaces, and how native features can be exploited to the user's advantage.

The purpose of the proposed experimental research described herein was to better characterize the properties and limits of one such biomolecular system, bacterioferritin (Bfr), as a platform for host-guest interactions and surface targeting. This entailed three major areas of investigation: engineering of host-guest encapsulation interactions, surface targeting by protein cage modifications, and chemical modification of propionate groups on the native heme cofactor. In this chapter, the application of bio-nanomolecular systems will be outlined, and the relevant background information on cage proteins, encapsulation strategies, and labeling cofactors will be discussed.

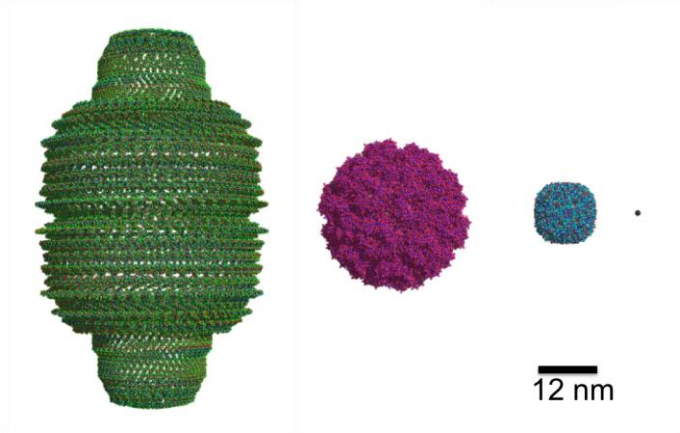

Figure 1.1: Size comparison of three commonly cited cage proteins investigated compared to a C60 fullerene. From left to right are the vault protein, CCMV, Bfr, and a C60 fullerene. Images were generated in Pymol using PDB IDs: 2QZV, 1CWP, and 1BFR.

1.2. Biological Molecules in Nanotechnology: The Emergence of Bionanotechnology-Driven Applications

1.2.1. Encapsulation of Functional Guests in Cage Proteins

Host-guest interactions, or the methods to encapsulate guest molecules within protein cages are essential in the design of drug delivery vehicles, nano-reactors, and unique biomolecular platforms. Understanding the methods used to encapsulate guest molecules will be important for future development of successful host-guest interactions. Presented below will be a discussion of three methods of encapsulation along with the various unique features of hosts that are exploited to encapsulate targeted guests.

Encapsulating novel guest molecules within a cage protein remains a challenging pursuit. Developing methodologies to probe the capabilities of host cage proteins remains an important, but poorly understood area. This point was emphasized by J. Cornelissen in his *Nature Chemistry* publication on viral encapsulation wherein he highlighted that outer surface modifications to cage proteins are generally much easier than the series of careful choices that must be made for successful encapsulation, and proper host interaction with the guest[8]. Methodologies to encapsulate guest molecules, generally, require disassembly of the protein cage, which allows

guest molecules to interact with the interior surface of the host. Once the guest interacts with the interior of the host surface, reformation of the cage permits the trapping and encapsulation of the target guest molecule(s). The contacts that maintain the host and guest interaction can be subdivided into three categories: concentration dependent encapsulation, covalent or genetically engineered linkages, and non-covalent affinity interactions (Figure 2). Presentation of examples will be given here to exemplify each category.

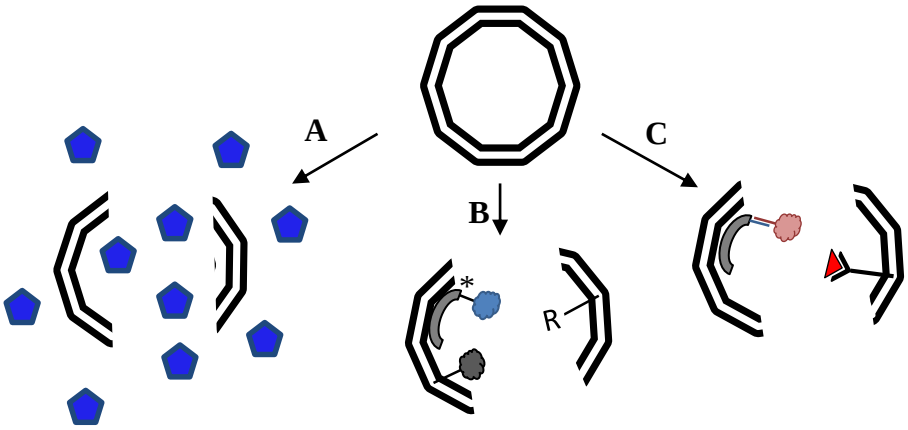

Figure 1.2: Demonstration of the three categories of encapsulation methods. The first method (A) is non-specific and only passively accumulates guest molecules. The second method (B) uses a covalent linker to associate guest molecules to the interior through genetically engineering, a covalent modification (R) to amino acids, or either genetic or chemical linkage to scaffolding proteins (*). The third type (C) is a specific, and non-covalent method of encapsulation.

1.2.1.1. Concentration Dependant Encapsulation

This first category is less well represented in the literature because it is an unspecific method. The methodology involves the disassembly of the host cage protein in the presence of high concentrations of the desired guest molecule (Figure 2A). Upon reassembly of the host cage protein some population of guest is encapsulated through mere chance. This method is less desirable because there is no driving attractive force between host and guest, and so minor repulsive forces preventing the guest from interacting with the host can be unfavourable for encapsulation. Cowpea chloritic

mosaic virus (CCMV) was able to encapsulate horseradish peroxidase using this non-specific technique.[9] Triggering of CCMV to disassemble was accomplished by a switch in the pH, incubation with the guest enzyme, and then adjustment of the pH to reform the CCMV capsid. Encapsulation of a small molecule drug cisplatin in ferritin was performed by adding cisplatin in high concentrations, followed by dissociating ferritin with an alkaline pH, and was then re-assembled by decreasing the pH.[10] Some other papers described similar methods that use excess guest molecule. This is an acceptable procedure when the guest can be used in excess amounts, or when there is some innate positive interaction already present, such as electrostatics or native metal ligation. In these instances, the researcher is taking advantage of the intrinsic properties without having to engineer in new functionality. Despite the success of this method, more investigations have focused on directed encapsulation of guest molecules.

1.2.1.2. Covalent and Genetically Engineered Encapsulation

Covalent methods for encapsulation can be used to directly link guest molecules to the interior of cage proteins. The interaction is irreversible, which can be either disadvantageous or advantageous depending on the nature of the application. When the guest molecule is a protein or peptide, it is possible to genetically engineer the guest molecule onto an associating protein, or to some part of the capsid sequence. The Douglas laboratory has used genetic engineering to localize guest proteins to the inner surface by modifying a scaffolding protein, which associates to the interior of an assembling bacteriophage P22 virus (Figure 2B).[11-16] Scaffolding proteins, as in P22, are highly modular towards incorporation of proteins of appropriate sizes. The group has performed studies for the purposes of co-expressing and encapsulating aggregation prone guest proteins to improve purification techniques. They have encapsulated a wide variety of enzymes, such as: CelB glycosidase, alcohol dehydrogenase, and have simultaneously encapsulated three enzymes involved in a cascade reaction. This methodology excellently utilizes the native scaffolding

protein for the purposes of encapsulating guest molecules through covalent linkage to the interior surface.

Direct labelling through covalent modification of an amino acid is a familiar method to biochemists, and has been employed in encapsulation of novel guest molecules. A photodynamic therapeutic was covalently attached to the interior surface of bacteriophage MS2 by incorporation of a Cys residue by site-specific mutagenesis of the virus capsid interior, followed by reaction with a maleimide functionalized photodynamic therapeutic agent[17]. The host protein with photodynamic payload was directed to cancerous cell surfaces by modification of the exterior surface with an aptamer specific for the cell surface. Covalent addition was also used to attach a fluorescent dye to the interior of a heat shock protein in combination with a peptide that targeted macrophages[18]. The dye was covalently attached to an interior Cys residue through a maleimide containing dye, which was able to detect signs of atherosclerosis. Cys labelling was also used in bacteriophage P22 to place a catalytic initiator on the interior that allowed for the polymerization of poly(2-aminoethyl methacrylate) within the confined environment of the cage protein[19]. The controlled nature of polymerization within a cage limited the size, and size distribution of the resulting polymers, which can be of great interest in the synthesis of narrow molecular weight distributed polymers. The specific applications of covalent encapsulation are those that do not require a guest molecule to be released. Cell imaging, encapsulation of catalysts or enzymes, and some therapeutics work well with covalent approaches for encapsulation. Other applications require or benefit from a more dynamic interaction for encapsulation.

1.2.1.3. Non-covalent Directed Encapsulation

This mode of encapsulation can be further divided into two groups: those that use an accessory coat protein, and those that do not. As is somewhat familiar in virus capsids, multiple proteins can be involved in formation of a complete viral coat (Figure 2C). Scaffolding and accessory

proteins exist that associate to the interior and act as excellent handles for genetic modification. The Cornelissen group has used this successfully with CCMV in the past, using a genetically engineered addition of a leucine zipper cognate pair to associate a guest molecule to the interior of CCMV[20]. Similarly, vault associating protein has been used to encapsulate drug molecules and gold nanoparticles to the interior using genetic modifications to the associating protein to non-covalently link the guest molecule to the interior. In the first case the associating protein had an amphipathic helix addition to associate lipid nanodisks saturated with drug molecules to the interior space of the vault protein[21]. In the second example a His-tag on the vault associating protein interacted with gold nanoparticles displaying a nitrilotriacetic acid (NTA) moiety on the surface[22]. In another example of metal coordination, a 5-iodoacetamido-1,10-phenanthroline was labelled to the interior of the P22 bacteriophage protein coat, which was shown to coordinate the metal templated growth of 1,3-di-1,10-phenanthrolin-5-ylthiourea[23]. Genetic mutations were made to interior residues of the P22 coat protein to generate a K118C and S39C mutant. These Cys mutants were covalently labelled with 5-iodoacetamido-1,10-phenanthroline, which could co-coordinate a Ni^{2+} ion with a 1,3-di-1,10-phenanthrolin-5-ylthiourea (bis form of-iodoacetamido-1,10-phenanthroline). This was of interest because it demonstrated another mode for metal based affinity interactions. Another study utilized Rh-norbornadiene and labelled an interior Cys residue on ferritin to initiate the polymerization of phenylacetylene[24].

Genetically integrating a binding motif can be a very versatile approach to introduce new affinity interactions. A p19 RNA binding protein was engineered as a fusion to the HBV virus, which created a chimeric virus that could bind siRNA therapeutics[25]. This was a very versatile development because the p19 RNA binding protein could bind multiple types of siRNA without having to make modifications to the therapeutic siRNA structure. In addition, the surface was functionalized with an RGD cyclic peptide motif to address the virus complex to cancerous cells. Similarly, bacteriophage

MS2 through the use of the MS2 bacteriophage's intrinsic RNA binding affinity was able to encapsulate multiple therapeutics and deliver them to hepatocellular carcinoma cells[1]. The interaction was able to encapsulate cargo containing an RNA motif known to be bound by the interior of MS2 cargo, which included: quantum dots, therapeutic drugs, siRNA, and ricin toxins. Daunomycin and doxorubicin have both been encapsulated within ferritin through the incorporation of a poly-aspartic acid sequence, and the co-coordination of a Cu between the native metal binding site of ferritin and the drug, respectively [2,26]. Both technologies showed potential for drug delivery, but only the latter was modified with a cyclic RGD peptide and evaluated for its ability to target *in vitro* and *in vivo* cancerous cells. Non-covalent interactions between host and guest creates a more dynamic interaction, which can be beneficial for release of cargo, but can also be of interest for more stable arrangements.

1.2.2. Drug Delivery

Bio-nanoparticles encompass a large natural catalog of particles, ranging from DNA to lipids to protein, as well as various combinations of these. The two areas of research where bio-nanoparticles are most actively pursued are the medical and material science fields. Within the medical area there are two main projects: drug delivery and imaging, or image enhancement[27]. The bio-nanoparticles used typically have a hollow centre, and a surface amenable to modification. This facilitates the protection of a drug, contrast agent, fluorescent molecule, or photodynamic therapeutic, which is combined with the ability to target cells displaying specific antigens, or receptors. The development of these vehicles is a complex process necessitating many requirements. An ideal bio-nanoparticle should be: stable enough to retain all of its cargo, large enough to be excluded from renal clearance but small enough to avoid opsonisation (enhanced permeability and retention effect [EPR])[28-30], able to carry molecules that can be released from the interior upon encountering a target[31], have a ligand or marker on the surface that is highly specific to the desired target[32], is non-

recognizable by the immune system[33,34], contains non-toxic components or metabolic products, and likely other factors that have not been accounted for.

Liposomal delivery particles continue to be the largest contributors in this area[35]. Proteins, however, are persistently being explored as potential targets due to several advantageous features, some specific only to proteins[26,36-44]. Many proteins are non-toxic, easily metabolized, can present polyvalent markers, have sizes that comply with the EPR effect, are stable, are amenable to exquisite chemical and genetic modification, have a structurally uniform population, are frequently easy to produce, and have structural data available with atomic resolution. The protein systems that have been reported have included virus-like-particles (VLP) and protein cages, which include ferritins, vault protein, GroEL, heat shock proteins (Hsp), and other protein cages. Protein cages are not derived from a single peptide chain, but many identical, self-assembling units. Repetition of the same unit in the structure provides labelling advantages. Modifications designed for any one structural unit will be repeated throughout the overall structure; in this there is a built-in propensity for avidity. Cage proteins, therefore, have a great potential for directed therapeutic delivery.

Specific drug delivery to diseased cells has the potential to revolutionize the way drugs are taken and diminish the side effects seen in patients. Advances in drug delivery have not yet replaced the current treatment schemes, and much primary research still remains to be performed. Currently, cage proteins are being investigated as a small but growing subset of delivery vehicles for their ability to encapsulate therapeutics, and to target specific cells. For therapeutic delivery the ideal scenario is to trap the drug molecule within the vehicle, and upon delivery to the target cell release the drug in an unaltered, active form. Some methods of encapsulation include disulphide and acid labile linkages[45,46]. Two nonspecific cellular mechanisms exist that will liberate a guest molecule

from the host cage protein. One is the reductive nature of the cellular environment, which can reduce disulphide bridges. Therefore, any drug covalently bound through a disulphide linkage should be released upon entering the reducing environment of the cell. The second mechanism relies on acid sensitivity, where endocytosed molecules are targeted to the lysosome. The lysosome has an acidic environment, and can cause the release of acid labile hydrazine linkers. Other linkers include the attachment to RNA, which can be released by degradation with RNases. In this case a drug is linked to an RNA molecule, which is then readily degraded by RNases found in the body[47]. Peptides can also be degraded by the metalloproteinases overexpressed in regions containing solid tumors, which can release encapsulated drug molecules[48,49].

Designing triggers to release therapeutics is as important as being able to encapsulate drugs that are otherwise not soluble in aqueous solutions. Cyclodextrin has been used to associate hydrophobic drug molecules within protein cages, which then slowly leach out into the cell [45]. Poly-aspartic acid has also been used to specifically locate daunomycin to the interior of ferritin[50]. Use of an RNA label to specifically encapsulate multiple types of therapeutics, including small molecule drugs, natural toxins, and imaging QDs was used as a versatile targeted encapsulation method[1]. All of these methods have a common theme, and that is the use of some linker that can be controllably released upon interaction with the desired cell type. Some of the studies mentioned here have investigated the efficacy of these approaches in mammalian cells and mouse models. These studies have reported the accumulation of the active ingredient in the target cell type, and an improvement in the therapeutic effect of the drug.

The second aspect to drug delivery is the need for targeting a unique cell type. This has been effectively accomplished by identifying unique or over-expressed receptors on the surface of target cells. Protein cages are particularly adept for targeting to cells due to their ability to be multiply

labelled with ligands or receptors. This ability should greatly increase the interaction with a target cell through an effect known as avidity. For solid tumors there is an additional effect called the EPR, which results from the prolonged circulation and passive accumulation at the sites of "leaky" tumors due to epithelial fenestrations and accelerated angiogenesis at solid tumors[29]..

Viruses have been used in the past, and although many mammalian viruses possess the native ability to penetrate cell interiors to deliver their genetic payloads, many of the drug delivery vehicles being designed are from plant based viruses, or non-viral cage proteins. Therefore, ligands must be engineered onto the surface of these cage proteins to direct them towards specific cells. Small molecules can be used to target receptors, such as folic acid, which binds the folic acid receptor[47]. A common ligand to target tumor surfaces is the arginylglycylaspartic acid (RGD) peptide, which targets overexpressed integrin $\alpha_v\beta_3$ receptors[2,25]. RDG is a peptide based ligand, and hence this sequence can be genetically engineered onto the protein cage surface. Peptide based markers are generally easier to place precisely within the protein architecture using established molecular genetic techniques. Peptide markers include: epidermal growth factor, LyP-1 peptide, SP94 peptide, and peptides derived from phage display[1,47,51,52]. Like phage display, which can generate affinity peptides for both organic and inorganic targets, aptamer technology has arisen as a means to generate highly specific receptors for desired targets. Aptamers have been used to label host surfaces to direct them to target cells for photodynamic treatment, but this approach could be extended to therapeutic delivery as well[17]. Selecting the appropriate cell identifier and the complimentary ligand or receptor will be essential in design of drug delivery vehicles to ensure that drugs are appropriately addressed.

1.2.3. Directed Placement of Novel Metal Centres

Ferritins and other protein complexes have been utilized for diverse generation of metal centres that fall within the categories of quantum dots (QDs) and nanoparticles. Generation of QDs or metal clusters remains an interesting area of research in materials science since QDs can exhibit superparamagnetic, semiconductor, and fluorescent properties[53].

Marriage of biological molecules with materials through bioconjugation serves interesting applications in the creation of biosensors and controlled delivery of inorganic nanocrystaline material. Localization of ferritin onto silica surfaces has been accomplished by electrostatic attraction, for example: ferritin was found to associate with 100 nm spaced positive spots using 3-aminopropyltriethoxysilane on silica[54]. The ability to specifically position a single ferritin is an important display of controlled placement useful in the area of bioelectronics. These types of delivery methods have been applied to floating nanodot gate memory field effect transistors by placing mono-layers of semiconductor NP on a transistor, which was accomplished through the use of a poly(ethyleneimine)-modified transistor that could electrostatically attract ferritin-containing metal cores of CoO[55,56]. A similar approach was used to develop a low-temperature polycrystalline silicon thin film transistor flash memory device, again using ferritin to ferry metal cores generated in its interior into location to form the required mono-layer [57]. Ferrying metal cores can be used for more than bioelectronics purposes. The generation of a Förster resonance energy transfer (FRET) based biosensor was possible by use of specifically placed ZnSe NPs on Si substrate, where ferritin acted as the ferry [58]. Use of encapsulated QDs in viruses can also be utilized for cellular imaging. Simian virus 40 protein capsids was employed to encapsulate QDs functionalized with DNA ligands, and subsequently used to target cells *in vitro*[59]. This approach suggests possible use of such biomolecular frameworks in cellular imaging, which would utilize the improved properties of QD compared to organic fluorophores.

1.2.4. Catalytic Confinement

Encapsulation of catalysts and enzymes into cage proteins for development of nano-reactors has revealed some interesting enzymatic properties, some of which remain to be fully explained. The ability to study single enzyme reaction rates, and to alter the local environment of the encapsulated guest molecules may lead to a better understanding of enzymes and improvements of enzymatic turnover. There have been a series of experiments that have reported that encapsulated enzymes and catalysts results in an increase in the catalytic turnover, no change at all, or alteration of other kinetic parameters, such as Km. One of the first investigations of enzyme encapsulation was that of encapsulating horseradish peroxidase (HRP) within CCMV.[9] The HRP enzyme was non-specifically encapsulated within CCMV and it was determined that each capsid contained only one enzyme molecule. The authors did not perform enzymatic studies, but were able to demonstrate that enzymes could be encapsulated within a protein capsid without totally disrupting enzymatic function. The next level of analysis was to encapsulate an enzyme and evaluate the kinetic parameters. The school of thought concerning the effects of encapsulation on enzyme activity was that substrate turnover should increase because of the apparent increase in concentration of substrate or enzyme within the confined capsid space. When a substrate leaves the bulk solution and enters a VLP, or protein cage, the volume drastically decreases, and hence the concentration of the enzyme, the substrate, or both is significantly magnified within the viral capsid. Similarly, if multiple enzymes involved in a cascade reactions are placed within the confines of a cage protein the rates should increase since the substrates and products are "shuttled" from one reaction centre to the next. Recent evidence has shed light on the question of how enzyme kinetics are effected within the confined molecular space of viral capsids. Encapsulation of *Pseudozyma antarctica* lipase B (PalB) within CCMV was shown to have increased turnover compared to the non-encapsulated enzyme.[60] The researchers encapsulated PalB by a non-covalent coiled coil

affinity interaction between the enzyme and the capsid protein. It was observed that the activity of PalB was highest when there were fewer enzymes encapsulated (one or two). This was suspected to be a result of the limitation of substrate transition into the capsid interior and to active sites. The Km did not appear to change and so the explanation for increased rates at lower enzyme encapsulation numbers was that the reaction rate was increased. The results seemed to fit previous work done with enzymes within vesicles, where smaller vesicles increased the turnover number of the encapsulated enzymes[61]. Conversely, encapsulation of CelB glycosidase and alcohol dehydrogenase within bacteriophage P22 showed no increases in turnover between encapsulated and free enzyme.[11,13] Encapsulation of alcohol dehydrogenase showed a decrease in both turnover and Km, which could be a result of over-crowding, as was observed in the case of PalB when excess enzyme was present. The optimal amount of PalB was 3.5 fold lower than the alcohol dehydrogenase concentrations found in P22, and so there may exist an upper limit when considering enzymatic loading. Although great improvements to rates of enzyme reactions were not observed, the measured enzyme rates do not appear to decrease upon encapsulation. Encapsulation within bacteriophage P22 of three enzymes involved in the metabolism of lactose was investigated to evaluate the principle of proximity effects with co-encapsulated enzymes.[15] Interestingly, no increase in turnover was observed in the co-encapsulated enzymes from the free enzymes and singly encapsulated enzymes. This null result prompted further exploration, which resulted in a mathematical model that suggested a fine-tuning of the kinetic balance between enzymes. By modulating the first enzyme activity with an inhibitor (Tris buffer) the combination of enzymes was observed to outperform the individual enzymes under the same conditions. This sheds light on the complexities of encapsulated enzymes, and some of the misunderstanding in the field. Further investigations on both the encapsulation of single enzymes as well

as multiple enzymes will enhance the scope and capabilities of studying and manipulating these catalysts.

Even if enzymes do not show improvements in rate after encapsulation, capsids could still be useful for enzymatic studies since free enzymes have been shown to decrease activity upon attachment to surfaces.[62,63] Using a cage protein as a scaffold to house the encapsulated enzymes and protect them from surface labelling, degradation could circumvent the decrease in enzymatic activity due to covalent attachment to a surface.

Parallel to the enzyme encapsulation studies are experiments that have been reported on inorganic catalyst encapsulation. One study reported the encapsulation of a Pt nanoparticle within a heat shock protein. This host-guest complex was able to generate H_2 gas at the efficiency level of some naturally occurring hydrogenases.[64] By preventing Pt from aggregating in solution by protecting it within a host cage protein, the nanoparticle was able to generate H_2 gas by light driven photo-activation of a Ru complex. The Ru complex would transfer an electron to methyl viologen, which in turn donated the electron to the Pt nanoparticle to reduce protons to H_2 gas. Methyl viologen degraded quickly in the solution due to exposure to Pt, however, and further improvements must be made. More importantly, this study demonstrated a step towards integration of inorganic nanoparticles with biological scaffolds for the purpose of catalytically generating a highly useful fuel substance.

1.2.5. Novel Metal Centres

Even before the exact mechanism of the ferroxidase centre was elucidated there had been experimentation to utilize the machinery of ferritins to introduce new metals into ferritin to form cores of defined and uniform size. The development of novel nanoparticles of defined size has revolved largely around the use of commercial horse spleen ferritin and some viral protein shells (capsids).[65] There have been many different

approaches to the generation of nanoparticles, including utilizing the inherent ferroxidase centre[66], by addition of hexacyanoferrate(III)[67], or encapsulation of a metal of interest followed by the addition of an appropriate nucleating agent, wherein the protein cage acts as a physical enclosure to limit core growth.[68-70] The types of metals and metal composites utilized are diverse in form, crystallinity, composition (Mn, Co, Cu, Ni, Cr, Pd, CdS, ZnSe, Fe_2O_3) and properties (magnetic, semiconductor, and fluorescence).[65,68,69,71] The nanoparticles harvested from these protein cage systems are good examples of how ferritins, and indeed other cage systems, can aid in materials development.

1.2.6. Cofactor Modification

Protein cofactors provide an expanded range of functionalities that the 20 canonical amino acids cannot otherwise provide. Such cofactors include: NAD(P)H, flavins, metal atoms or clusters, pyridoxal phosphate (PLP), pterins, biotin, quinones, protoporphyrins, chlorins, and many others. A critical role of some cofactors is to handle the processing of electrons, either single electrons or pairs of electrons. Most notably are the flavin, metal centres or clusters, and protoporphyrin cofactors in their unique ability to handle single electron transfers. Most redox proteins, and electron shuttling proteins involve the use of one or multiples of these cofactors to transmit electrons. These classes of enzymes and proteins are of particular interest because of the ubiquity of the cofactors, the diversity of enzymes and protein functions, and their integration into devices. Each cofactor having its limitations and advantages that lend it to applications in the aforementioned areas.

1.2.6.1. Applications of Chlorin and Heme Modifications

Separate from the class of flavins and NAD(P)H cofactors are the protoporphyrins, which are certainly one of the most diverse cofactors found in nature. An excellent publication on the aspects of heme and protoporphyrins in biology can be accessed for more in depth review.[72] Diversity of functions include: catalysis, substrate transport (oxygen in hemoglobin), and electron relay. Such a seemingly large range of purposes from a single class of cofactor are possible through several points of variation. For instance, modulation of the redox properties of protoporphyrins can be accomplished by changes to the coordinating residues on the transition metal (Figure 1.3). Amino acid residues coordinating the metal in protoporphyrins can provide ligation of the metal in one or two positions. Some such known residues are His, His-His, His-Met, Cys, Met-Met, and Tyr-His.[72]

As might be expected from the diversity of functions, the architecture of heme binding proteins is not conserved, and many structures exist. Hemoglobin, a text book example of molecule transport, uses a heme-b protoporphyrin and is coordinated by proximal His(F8). Pre-oxygen binding, the iron is pentacoordinated, which becomes hexacoordinated upon oxygen binding[73]. A distal His(E7) co-coordinates with the dioxygen molecule while it binds to the ferrous iron of heme-b (Figure 5). The iron atom must be ferrous to bind and transport oxygen, and the proximal His is essential in the mechanism and fine tuning of heme for this purpose.[74]

His-His interactions can be seen with cytochrome c oxidase (Cox), which is a Cu-heme membrane protein involved in the reduction of molecular oxygen to water in the electron transport chain.[75] Cox coordinates two heme-a cofactors, one with a bis-His coordination. This bis-His coordinated heme transports a total of four electrons and shuttles them to the second heme reaction centre to eventually reduce molecular oxygen[76]. Redox potentials associated with the heme-a cofactors have been reported to range between 260 mV and 340 mV, compared to the heme-b situated in hemoglobins which can have a redox

potential of -52 mV.[77] This demonstrates how even though the same residues coordinate the heme group, modifications to the macrocycle and changes in the protein architecture can greatly modulate the heme redox potential. An example of Cys (thio/thiolate) coordination of heme cofactors can be seen in the enzymes termed cytochrome P450 (P450).[78] This class of enzymes has great importance in the metabolism of fatty acids, steroids, and xenobiotics. The role of heme in P450 is to activate molecular oxygen at the heme iron to an iron-oxo intermediate, which is then primed to react with substrates.[79] The thiol-ligated heme-b in P450s has a redox potential in the substrate free form of approximately -220 mV, which changes as substrates bind and the spin state of iron changes.[80] Lastly, a bis-Met coordinated heme-b cofactor example can be seen in the Bfr class of proteins. As mentioned previously Bfr is a storage protein, used to maintain a repository of iron within cells. Although the function of heme had been debated, recent evidence has emerged supporting its role in triggering iron release from the cage interior, as outlined below. Bfr heme-b has been shown to interact with a Bfr-associating protein that derives electrons from ferredoxin, and was proposed to transfer electrons to the ferroxide centres inside the Bfr cage.[81] The observed redox potentials in Bfr have been between -475 to -225 mV depending on whether the iron core is present or not[82].

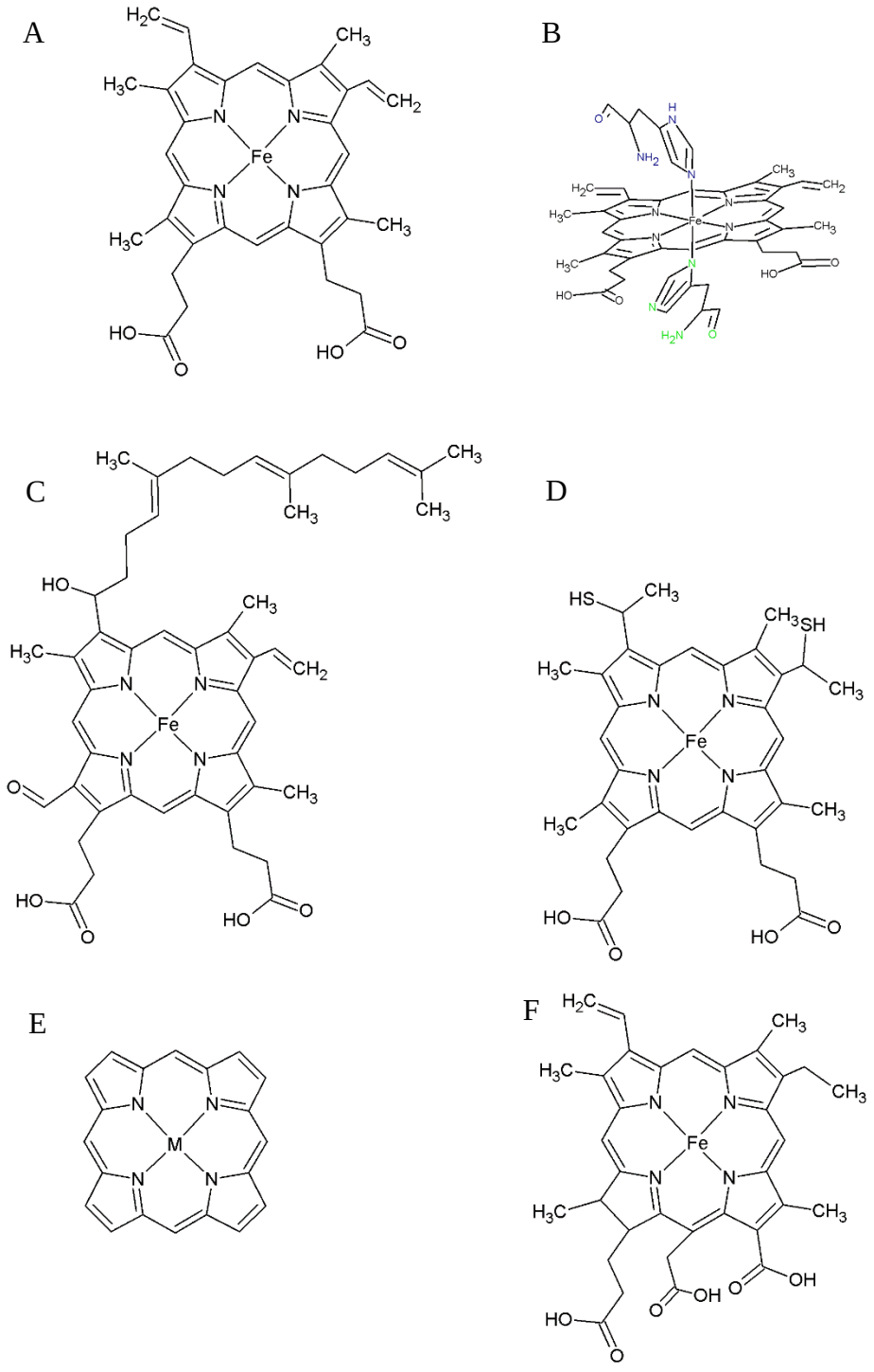

Figure 1.3: Some of the most common forms of heme in nature, and a chlorin. Heme-b (A) is one of the common types of heme found in nature. The iron metal can be coordinated by two histidine residues (B), by single histidine residues, or by other amino acids like methionine, and cysteine. Variations of heme are seen in nature, such as heme-a (C), and heme-c (D). Variations of chlorin (E) can also be used to substitute heme in some proteins, for instance chlorin E6 (F) has been used to incorporate within bacterioferritin.

The propionate groups found on heme have a somewhat unexpected role, and are important in the handling of single electrons. P450s and peroxidases may delocalize single electrons to the carboxylate groups on the propionates, and may be somewhat involved in the transfer of electrons, as evidenced by crystallographic data showing interaction between peroxidase substrates and the propionate groups of its heme cofactor.[83] If indeed the propionate groups are more critical for the function of heme containing proteins than previously thought, then surely the pKa of the carboxylate groups would be important. This very property has been observed in heme-containing proteins where changes to the propionate local environment, and thus the pKa, appeared to modulate the redox potential of the heme.[84] For these reasons, and reasons discussed in previous paragraphs, hemes have been touted as one of the most versatile cofactors in biology, with a reported range of 800 mV in redox potential.[85,86]

In addition to native heme diversity, investigation into the modification of heme and heme proteins has also become of interest for the biotechnological and bionanotechnological community. There is great interest in enzymes, specifically redox enzymes, in biotechnology for the production of chiral compounds, biofuels, and in the disposal of harmful waste compounds.[87-90] Protoporphyrin containing enzymes have been explored for these purposes to improve some industrial applications in synthesis and degradation. The major contender in this area is P450, with the notable addition of cellobiose dehydrogenases. P450s are primarily used for the production of new compounds, pharmaceuticals, optically pure molecules, and for bioremediation.[91] Biofuel cells are more commonly mentioned with cellobiose dehydrogenases and glucose oxidase.[89,90] By linking either direct or mediated electron transfer to an electrode from the cellobiose dehydrogenase, researchers have been able to generate electrical current.[89] These literature examples show that distinct heme coordinating proteins can be used for the development of industrially relevant technologies. This means that understanding the modes of

electron transfer and how to modulate them will be essential for further development and understanding in this field.

Research has also been reported on modification of the propionate groups as well as the macrocycle itself, as outlined below. Modification to the Macrocycle can alter the electrochemical properties of the heme, as seen with the differences between chlorins and protoporphyrins.[92] Chlorins, generally, are easier to oxidize than protoporphyrins, and chlorins have been demonstrated to be exchanged with heme in heme proteins.[93] Although the macrocycle is a powerful place to modulate these characteristics, macrocycle modification as it relates to replacement in heme proteins has been less explored in research.

More interest has been paid to the exploration of the propionate groups on protoporphyrins and heme. Labelling of heme propionate groups usually follows a similar synthetic route, activating the carboxylic acid with a carbodiimide followed by the addition of a desired amine containing label. The Niemeyer group has labelled heme propionate with DNA for the purposes of directing horseradish peroxidase and myoglobin to surfaces containing the partner DNA strand (Figure 1.4).[94-97] Heme was doubly labelled, and singly labelled with DNA oligonucleotides followed by evaluation of the enzymatic activity upon surface binding. Interestingly, the group also demonstrated selective labelling of individual propionate groups on a single heme through use of a glass support.[98] They were capable of labelling a single heme with both a single stranded DNA oligomer and a photosensitive ruthenium complex. The ruthenium complex was photo-activatable and able to reduce the heme iron. The single stranded DNA was used to associate the heme to a surface presenting the complementary DNA strand. Similar to this type of reduction, another group has reported the attachment of the myoglobin heme to a CdTe quantum dot that could photo-reduce the heme through the photo-activation of the CdTe quantum dot.[99] Using a thiol containing label, they were able to directly attach multiple myoglobin proteins to the CdTe quantum dot through the heme moiety. These examples show how heme proteins can be attached to surfaces and reduced

when coupled to photo-activatable groups.

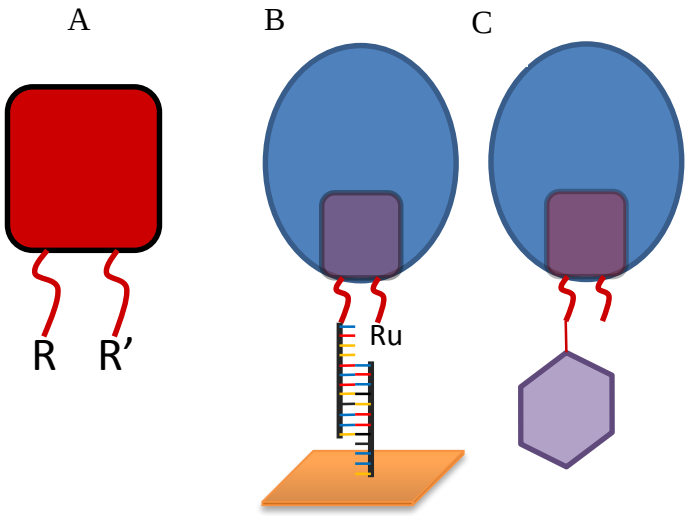

Figure 1.4: Examples of the modifications that have been made to the propionate groups of heme-b. Modifications to heme demonstrate how additional functionalities can be introduced to heme containing proteins (A). Through addition of a DNA oligomer researchers were able to attach myoglobin to a surface and label the second propionate group with a photo-activatable ruthenium complex (B).[98] Heme has also been labelled directly to a CdTe QD, which was able to reduce the iron centre upon photo-activation (C).[99]

Myoglobin and horseradish peroxidase have shown enhanced rates of reaction with the addition of N,N-Di(carboxylate)-1,3,5-Benzenetricaboxamide) derivatives to the heme propionate groups. Functionalization of the propionate groups with N,N-Di(carboxylate)-1,3,5-Benzenetricaboxamide was shown to enhance the rate of peroxidase activity of myoglobin towards 2-methoxyphenol[100]. This increased activity could possibly be due to the aromatic benzene ring interacting with the phenol ring of the substrate. Similar work was performed that discovered increased thermo and solvent stability of myoglobin after heme modifications were made.[101]

Biosensor development through direct electron transfer from heme proteins to electrodes is another possibility for heme proteins.[102] Electron tunneling through proteins is very distance dependent, and proper positioning of the heme moiety is essential for efficient electron transfer in heme proteins. Orientation of heme in the heme protein at an electrode surface is important for

biosensors, and can be applied to most electrode modifications with heme containing electron transfer proteins. For example, heme has been attached to a titanium nano-rod through its propionate groups, which coordinated horseradish peroxidase for the purpose of developing a peroxide biosensor.[103] The many examples of chlorin/protoporphyrin cofactor modification provide foundational evidence for the breadth of interest and application of a ubiquitous class of cofactors.

1.2.7. Bioconjugates

Bioconjugation is an essential component to many of the studies outlined in this chapter. Conjugation is required to specifically anchor guest molecules to the host cage proteins, and/or to provide affinity linkers between multiprotein complexes and various guests.

1.2.7.1. Bioorthogonal Reactions

Ideal reagents for covalent modification of proteins would have the following properties: solubility in water, selectivity to a particular functional group, reactivity producing high yields, and an ability to undergo reaction at physiological temperatures and pH. These requirements have spawned development of bioorthogonal and "click" chemistry reactions. The first bioorthogonal reaction was derived from the Staudinger reduction reaction (Table 1). A phosphine reacts with azides, a functional group not found in proteins, and is thus very selective and has minimal side reactions. Subsequent modification of this reaction, termed the Staudinger ligation, allowed for chemical attachment of functionalities to the azide group (Table 1).[104] Both reactions require two components: an organophosphine and an organoazide.[105] These functional groups are compatible with biological systems such as proteins and cells. The reagents can be made water soluble, and the ligation reaction can proceed under physiological pH and temperature. The difference between the reduction and the ligation reactions is that the ligation reaction uses a diphenylphosphine-containing arene with an ester *ortho* to the phosphine moiety. This arrangement allows for the formation of an intermediate aza-ylide

that rearranges to form a stable amide. The phosphorus atom remains in the product.[105] This reaction is possible *in vivo*, but problems arise with the labile phosphine reagent and the length of time it takes to react. However, this is not as much of an issue for *in vitro* protein labelling. A related ligation strategy has arisen from a reaction based on a copper catalyzed azide-acetylene cycloaddition developed by Huisgen (Table 1).[106] Although the $Cu^{(I)}$ catalyzed reaction is still applicable for *in vitro* synthesis the $Cu^{(I)}$ catalyst is somewhat toxic to cells. Formation of the disubstituted 1,2,3-triazole is found in both the Cu-catalyzed azide-alkyne cycloaddition and the cyclooctyne azide addition, a reaction developed to eliminate the need for copper catalysis for the cyscloaddition reaction (Table 1).

Diels-Alder-based cycloaddition reactions have recently been developed to be water soluble and capable of use in bioconjugation reactions. Attachment of a diene to a protein followed by cycloaddition of a derivatized maleimide can allow for attachment of small molecules such as fluorophores or peptides (Table 1).[107] All of these reactions have been developed for use under aqueous conditions, but most require functionality not found in proteins (azides, alkynes, and aldehydes for example). There are several methods available to introduce these unique functionalities into proteins, or to take advantage of the functional groups already present in the protein.

Table 1: **A summary of the bioorthogonal reactions discussed with the associated chemical mechanisms**

Reaction	Mechanism
Staudinger reduction[108]	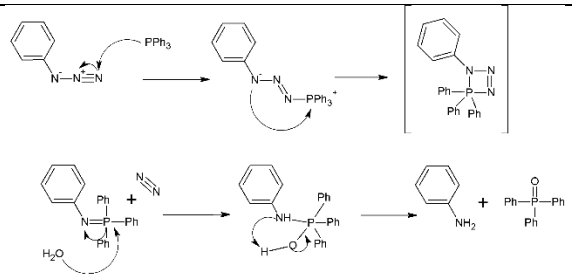
Staudinger ligation[109]	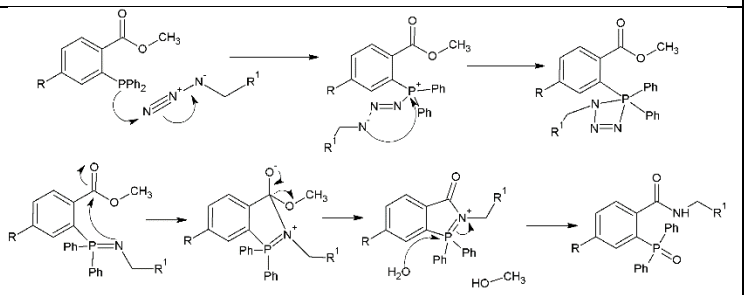
Cyclooctyne azide addition[109]	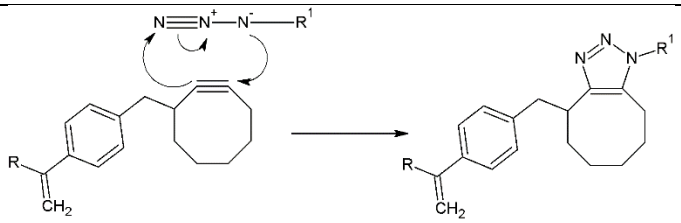
Diels-Alder cycloaddition[107]	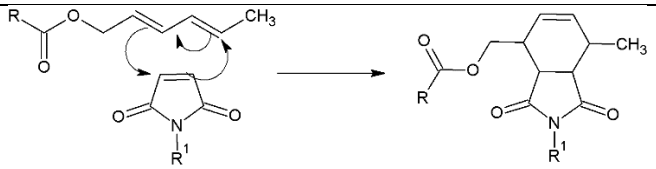

1.2.7.2. Natural Amino Acid Modifications

In order to accomplish the above bioorthogonal ligation reactions with proteins it is necessary to introduce the appropriate chemical functionality into the protein scaffold. There are solutions to incorporate these functionalities, as well as other functionalities, into proteins: site directed mutations introducing natural but reactive amino acids, unnatural amino acid incorporation, recombinant genetic fusion peptides, and enzymatic modifications. Naturally reactive amino acids, either native to the sequence or generated through recombinant point mutations, have the ability to decorate a protein with unique

functionalities. The most common amino acids used for these types of reactions are cysteine (Cys), lysine (Lys), tyrosine (Tyr), glutamate (Glu), and aspartate (Asp). Cys is the most frequently utilized for these purposes.

Cys is unique because of its reactive thiol, and its generally low sequence abundance. There have been many studies that have introduced a Cys residue into a protein sequence for downstream chemical modification.[110] Such modifications can be between the very reactive cysteine thiol with maleimide analogs derivatized with a functionality of interest (Figure 1.5).[31] The maleimide reacts with the thiol of Cys to produce a stable carbon thioether bond.[111] Lys residues in proteins can also be modified under basic conditions.[112] The ε amino group on Lys can react with an activated ester to form an amide bond, or can react with isothiocyanate.[113]

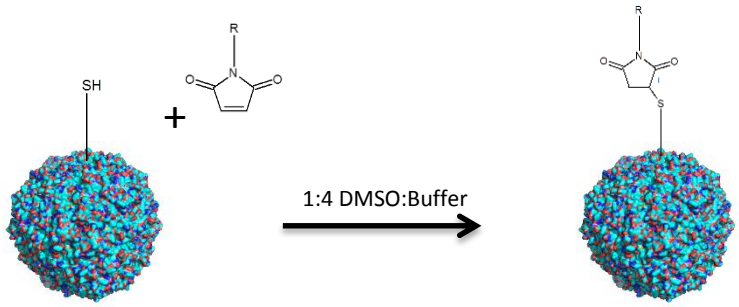

Figure 1.5: An example of possible cysteine labelling with maleimide on the surface of Bfr. The R group on maleimide could be fluorescein, nanogold, or biotin for example[114]. Images generated using Pymol (PDB ID: 1BFR), and ChemSketch

Tyr can be conjugated to diazonium salts, which attack *ortho* to the phenolic group on Tyr to form a disubstituted hydrazine.[115] Tyr can also be modified by the π-allyl species activated with Pd-based catalysts to form an ether linkage with the *para* hydroxyl.[116] Glu and Asp can both be modified with N-(3-dimethylaminopropyl)-N'-ethylcarbodiimide (EDC) to activate the carboxylic acid to react with an amine to form an amide bond; an interesting application used EDC to attach alkylamines to ferritin to make ferritin completely soluble in dichloromethane.[117]

At times, modification of natural amino acids does not suit the application of the particular system due to cross reactivity or multiple activated residues, and so other methods of conjugation have been developed.

1.2.7.3. Unnatural Amino Acid Substitution

A number of synthetic unnatural amino acid analogs that utilize the native aminoacyl tRNA synthetase (aaRS)/tRNA pair can be incorporated in a residue-specific manner into proteins. There are a select number of unnatural amino acids (Met analogs have been popular[118]) that can be added to the growth media of auxotrophic bacterial strains and compete well with the natural amino acids for incorporation into a protein. The use of auxotrophic bacterial strains allows for suppression of synthesis of the particular natural amino acid and improves analog incorporation levels. Proteins have been labeled successfully in this way, and it provides a useful alternative to the naturally reactive amino acids by directly introducing functionalities capable of being further modified, such as the alkyne and azide chemical moieties.[119]

1.2.7.4. Enzymatic Conjugation

Beyond the scope of more traditional chemical modifications are the techniques of enzymatic modification. The advantage with many enzymes is that they often require a recognition sequence, which makes them much more specific to a particular location. These enzymes either recognize sequence motifs or residues to modify a protein by adding lipid chains, sugar units, and other peptides.

One such enzyme, transglutaminase, will catalyze the hydrolysis of glutamine side chains and, in the presence of suitable amine donors, transfer amines onto the side chain of the glutaminyl residue (Figure 1.6). Amide linkages are thus generated under mild conditions, with high specificity, between the γ-carboxamide of Gln and with low specificity from the ε nitrogen of Lys. The lowered specificity to the Lys residue has allowed for the modification of Gln with functionalized Lys residues.[120]

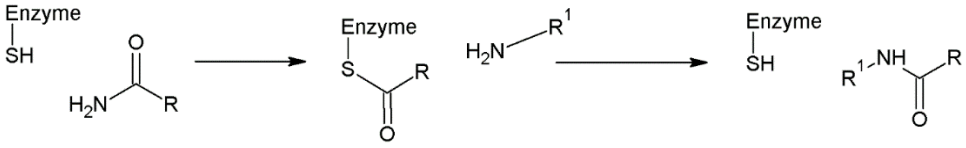

Figure 1.6: The enzymatic mechanism for transglutaminase showing a Gln residue (R) as an acyl donor to acylate the enzyme. The acyl acceptor (R^1) enters the active site and becomes acylated by the enzyme, which conjugates the donor to the acceptor and generates an isopeptide.

1.2.7.5. Non-covalent Affinity Interactions

Non-covalent interactions are a very important aspect in biological systems, often permitting more dynamic interactions that can be controlled. There are many biological non-covalent examples, such as coiled-coil helix interactions, DNA cognate pairs, metal coordination, aptamers, and hydrophobic and electrostatic sticky patches.[121-124] Non-native affinity interactions can be generated by techniques like phage display, which has been a tremendous source of short peptide sequences with high affinity for protein, organic, and inorganic substrates.[125] The addition of these affinity ligands can often be through established molecular genetic techniques at the C or N terminus of proteins, or as an added loop to proteins with relative ease.[126]

1.3. The Ferritin Superfamily

1.3.1. Sequence Identity

The research in our laboratory has involved the exploration of the multiprotein complex bacterioferritin (Bfr) from *Escherichia coli* (*E. coli*) as a cage protein that is potentially useful in novel nanomaterials development. Bfr is a spherical cage protein complex composed of 24 identical protomers. Its primary function is to oxidize Fe^{II} and store it as solid Fe^{III} (Figure 1.7).[127] Ferritins essentially act as a primitive type of organelle that stores excess iron. Bfr is a member of the ferritin family of proteins, which include eukaryotic ferritin, bacterioferritin, and Dps (DNA-binding protein from starved cells).[128] The amino acid sequence identity between Bfr and other ferritins is less than 20%, but despite the low sequence identity there is a high degree of structural conservation.[129] Since the sole function of ferritins is to deposit oxidized iron as a core, the residues that participate in iron oxidation (called the ferroxidase

centre) are highly conserved in each ferritin subfamily.[128] The ferroxidase centre will be discussed below.

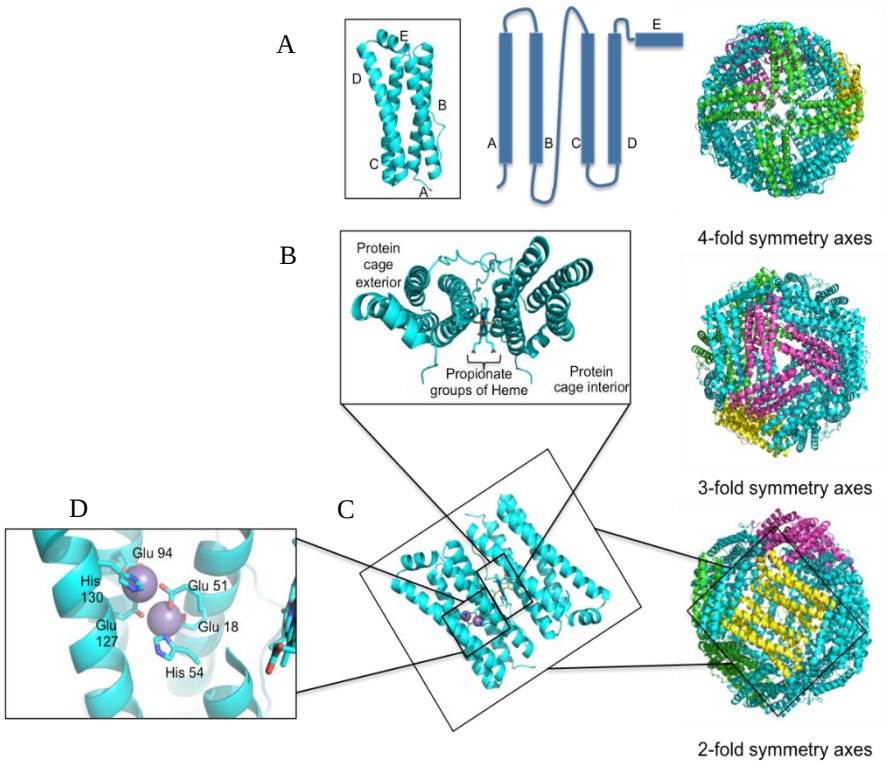

Figure 1.7: Overview of the structural data on Bfr and the ferroxidase centre found on the interior surface of each protomer. The four α-helical bundle of Bfr with the helices labelled is the base structural unit (A). The heme group is coordinated by two Met52 residues (B). The functional unit of Bfr is the dimer and it contains a maximum of a single heme, and two ferroxidase centres (C). The ferroxidase centre coordinates two iron atoms with 4 Glu, and 2 His residues, and allows for the reduction of molecular oxygen into water to facilitate the deposition of an iron core from the inner surface site (D). Images generated using Pymol (PDB ID: 1BFR) and Microsoft Powerpoint.

1.3.2. Ferroxidase Center

Ferritins function as storage molecules for iron in the cells of the majority of species on Earth because of the essential need for iron in cellular processes, such as in the electron transport chain. Due to the Fenton reaction and the production of harmful hydroxyl radicals, soluble iron levels need to be controlled.[130] All ferritins contain a dinuclear iron (ferroxidase) center found in intra-subunits for ferritins and Bfr, or formed by inter-subunit interactions for Dps.[131,132] The ferroxidase centre in Bfr is composed of two iron binding sites per subunit, each composed of four glutamate residues (18, 51, 94, 127) two of

which bridge the two Fe^{2+} (51, 127), and two histidine residues (54, 130) (Figure 1.7).[133] This centre functions to bind incoming Fe^{2+} entering through pores in the protein shell. Different from the ferritins, bacterioferritin contains a maximum of twelve heme groups each sandwiched between two adjacent subunits. The role of heme was, until recently, unknown and few kinetic studies had been performed to better characterize its function. Now, heme has been shown to be important in core removal, and kinetically important for core formation as well.[134]

1.3.3. Structural Composition

Ferritin, Bfr, and Dps of the ferritin superfamily have highly conserved tertiary structures, and for ferritin and Bfr, quaternary structures. Ferritins and Bfr are discussed in two contexts: one is with concern of the 24-mer intact quaternary structure (α_{24}), and the other is the dimer (α_2), which is considered the functional unit of the ferroxidase center. The amino acid length of each *E. coli* Bfr protomer is 158 amino acids, with a molecular weight (MW) of 18.5 kDa, and the multiprotein complex has a MW of 443.9 kDa. For all three subfamily members the protomer consists of a square, left-handed, four α-helical bundle, and in the case of ferritin and Bfr a fifth C-terminal helix is present. The fifth helix in ferritin and Bfr sits almost perpendicular to the plain of the helical bundle.[135]The helices are labeled as A through to E, AB being antiparallel to CD with one large loop connecting helix B to C. Bfr and ferritins form a 24-mer dodecahedron cluster with the same overall symmetry as a cube (octahedral) with 2-, 3-, and 4-fold symmetry (Figure 1.7). Pores are found at the 3- and 4-fold symmetry axes and the B-channel at the interface between dimers to facilitate iron movement into and out of the interior space (Figure 1.7).[136] The Bfr complex is approximately 12 nm in outer diameter, and the interior cavity is approximately 8 nm in diameter, with an interior volume of 2144 nm^3. The N-termini are situated such that they face the exterior of the protein cage, and the C-termini are situated to face the interior of the cage.

Each protomer is involved in binding interactions at each of its four interfaces. Structural experiments have been performed to elucidate the factors contributing to complex formation focusing on the role of the E helix, and improvements to complex stability. Since Dps lacks the E helix, a study was reported which attempted to evaluate the importance of the E-helix to the structure of these family members. A swapping experiment was performed between Bfr and Dps. Analysis of the data indicated that the E helix is essential for Bfr complex stability, and that it may be important in differentiating the 12-mer and 24-mer states.[137] There has also been an investigation to improve the stability of the Bfr complex by mutagenizing Asn residues at one interfacial water pocket. Removal of this water pocket with either introduction of Phe or Trp resulted in temperature stability increases for the protein of up to 20°C, and stability increases in guanidinium HCl dependent unfolding by approximately 1M.[138] The temperature stability of Bfr has been determined to be stable up to approximately 85°C.

One of the major distinctions between Bfr and other ferritin family proteins is the presence of 12 heme cofactors. A binding pocket exists between the dimer interface, where a methionine from each protomer coordinates the heme iron. The propionate groups of heme face the interior of the protein cage and thus there are 24 propionate groups on the interior. Based on the crystal structure of *E. coli* Bfr the propionate groups associate electrostatically with the side chain amine on a Lys residue, but no function has been assigned to this possible interaction. Heme, until recently, was debated as to its role in ferric iron core formation. Heme has been shown to not be absolutely required for iron core formation or for the liberation of free iron from the core. Since eukaryote ferritin functions without a heme cofactor, it was hypothesized that heme might have been a vestigial cofactor, and not important in iron homeostasis. In addition, heme was demonstrated to not be essential for proper structural formation either. These facts appeared to demote heme to a functionless cofactor. In more recent papers heme has been assigned a role in the increased rates of iron core formation in Bfr.[139] In addition to kinetic analysis, structural

data from *Pseudomonas aeruginosa* revealed a ferredoxin accessory protein involved in electron transfer through the heme moiety to the iron core to free iron.[81] It appears that heme is more likely central in the regulation of iron release and formation of iron cores.

1.4. Motivations for Pursuing Protein Based Nano-devices

The purpose of the experiments presented in this thesis are to further develop the field of self-assembling cage proteins as novel biomolecular platforms for control of host-guest interactions, and for development of advanced nanomaterials. Proteins are soft materials that form complex structures and geometric arrangements through genetic coding. Protein biochemistry has advanced such that there exists an immense repertoire of methodologies for monitoring and modifying these systems. Through structural data, genetic information, chemical bioconjugation, and detailed study of the function of proteins, the ability to repurpose or exploit functionalities has seen a growing number of examples in the literature. The reasons why protein cages have seen growing interest can be attributed to the nanometer size of the complexes. This scale remains difficult to control and generate new materials within. By using the already available proteins, design of new materials or devices at the nanometer scale is possible because of the exquisite controllability of protein scaffolds. Examples exist of the development of delivery vehicles, imaging agents, nanomaterial components, ferries/shuttles, and nano-sized reactors. The continued development of this field is important to expand leading-edge applications.

Investigation of Bfr entails two main approaches, one is to probe the limits of its use as a platform for encapsulation (host-guest interactions), and the second is to modify the native heme cofactor to provide an additional capability for encapsulation control. By exploring Bfr as a highly controllable nanomaterial one can envisage its usage in the fields of drug delivery and nanomaterial science, as has been recently demonstrated for other cage protein systems. Bfr has been chosen because of its more simple quaternary structure

(identical 24 protomers) and the presence of heme, a potentially novel and controllable element to this multiprotein system.[140]

2. Chapter 2: Encapsulation Studies

2.1. Introduction

This chapter will outline and discuss the methods for preparation and purification of bacterioferritin (Bfr) and Bfr mutants used in this research, and the encapsulation within Bfr of Streptavidin labelled with fluorescein (SF) and 1.8 nm and 5 nm gold nanoparticles (GNP). Some investigation on the nature of the assembly of 24mer Bfr with respect to the presence of heme will be discussed at the end of this chapter.

Four Bfr variants will be explored in this chapter: wild type (WT) Bfr, Hexahistidine tagged (His6-tag) Bfr, Methionine-less (BfrM), and S-tagged (S-Bfr). The WT and His6-tag Bfr were both used for encapsulation studies. The His6-tag Bfr contained a hexahistidine tag, which was genetically engineered onto the C-terminus of Bfr, designed by Dr. Uthaiwan Suttisansanee.[141] The C-termini of Bfr face the interior of the 24mer, and thus could act as a specific affinity label for encapsulating guest molecules decorated with nitrilotriacetic acid (NTA) functionalities (Figure 2.1). This non-covalent interaction has a Kd as low as 10 μM, which makes NTA-histidine interactions highly specific.[142] Previous work by Dr. Uthaiwan Suttisansanee.[141] had explored the encapsulation of a small molecular dye with an NTA functionality, ProQ® sapphire 365 oligohistidine stain. The dye was shown to be encapsulated, and some of the research discussed in this chapter was a continuation of this previous work.

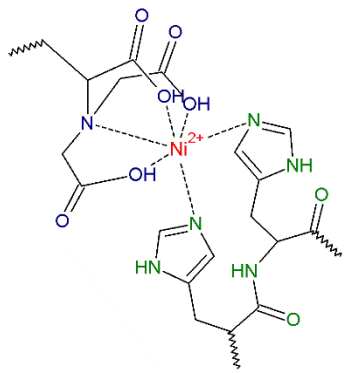

Figure 2.1: A nitrilotriacetic acid (NTA) functionality coordinating a nickel atom (red) with two histidine residues. This affinity interaction was utilized for encapsulation of two large guest molecules within Bfr.

The main topics of this chapter revolve around encapsulation of non-native guest molecules within Bfr. In addition to this main theme, auxiliary projects were pursued to develop Bfr as a bionanomaterial. One such project was the generation of a methionine-less mutant construct, BfrM. BfrM had five of the seven methionines mutated to lysine. The two methionine residues left were the initiator methionine, and the heme coordinating methionine M52. This construct required that a total of five mutations be made: M31L, M86L, M119L, M120L, and M144L. The molecular weight of BfrM was calculated as 19470 Da; higher than WT Bfr molecular weight because it also contained a hexahistidine tag on the C-terminus. This construct was made for the purpose of introducing unnatural methionine analogs into Bfr. With only the heme iron coordinating methionine remaining, methionine substitutions could be made to modulate heme electrochemistry. By modulating the electronic environment around the heme iron with methionine analogs the heme redox potential may be fine-tuned to alternative values. This type of electrochemical modification was performed in a previous study using methionine analogs to modulate the redox potential of a Cu^{2+} metal centre in an azurin protein.[143]

The second construct made was S-Bfr, which was an N-terminal extension of His6-tag Bfr. The N-terminus can be viewed in crystal structures as lying on the exterior face of the 24mer Bfr structure.[144] The S-tag is derived from RNase A, which is composed of S-protein and S-peptide, both of which

are necessary for the function of RNase A.[145] Residues 1-15 of the S-peptide have been determined as the minimum length necessary for function of RNase A; these 15 residues are the S-tag. The S-tag has been shown to not interfere with folding of host protein, and the dissociation constant between S-tag and protein-S can be regulated by mutagenizing the S-tag at specific locations.[145,146] In addition to this feature, which could be of future benefit to affinity purification studies, by adding the S-tag to the N-terminus it was hypothesized that the Gln on the S-tag would be more exposed than native Gln residues, and better suited for labelling by a transglutaminase. Transglutaminases form an epsilon-(gamma-glutamyl)-lysine cross linkage through proteins, and are regularly used in the food industry as a crosslinking agent in meat processing.[147] It has also been demonstrated that transglutaminase can label Gln residues with unnatural donor molecules modified with other chemical functionalities.[148,149] It had previously been shown that addition of an S-tag to a protein could improve cross linking by microbial transglutaminase (MTG) from *Streptomyces mobaraensis.*[150] S-tag contains both lysine and glutamine, the native substrates for transglutaminases, which afforded the opportunity to use both of these amino acids as separate, and specific labelling points on the surface of Bfr. This strategy will be further described in a chapter 4.

The encapsulation studies explored two types of guest molecules: SF, and two sizes of GNPs. SF was a commercially available fluorescently labelled streptavidin (Appendix 2), which is a tetrameric protein of the avidin family of proteins taken from the bacterium *Streptomyces avidinii.*[151] Streptavidin was chosen as a guest protein to probe the capabilities of Bfr to encapsulate large multimeric proteins, and to develop the methodologies to encapsulate complex biological guests. Streptavidin has an approximate size of 5-6 nm [152], which is large when compared to the 8 nm interior diameter of WT Bfr. Streptavidin has one of the highest known non-covalent association constants with its native ligand, biotin, Kd of 10^{-14} M.[153] Streptavidin is also a well-studied protein in molecular biology and in biotechnology, and was an ideal choice as a biological guest. A derivatized biotin was used in this research with an NTA functionality

synthesized onto the carboxylic acid on biotin. Thus, biotin-XNTA was the mediator between the high affinity interaction with streptavidin and the NTA metal dependant interaction with the hexahistidine tag found on Bfr. Three methods would be utilized to confirm the encapsulation of the SF guest within the host Bfr: chromatography, fluorescence quenching, and transmission electron microscopy (TEM).

Fluorescence quenching was used to confirm encapsulation by determining whether or not the fluorophore on streptavidin was protected by the protein shell of the host Bfr. This would be accomplished by titrating in a quenching molecule to the free and encapsulated SF and monitoring the change in fluorescence. This methodology was not unlike other experiments that have monitored tryptophan exposure in proteins with quenching.[154]

In addition to fluorescence measurements, TEM was pursued to characterize encapsulated SF. The methodology employed was negative staining of the samples in a heavy atom stain.[155] The negative stain does not specifically associate with proteins, it merely creates a layer in which protein can embed itself. Some of the stain is displaced by the protein, which generates contrast, and thus features can be distinguished. As is known of the ferritin family of proteins, the structures contain pores that are requisite for their native function as iron storage units. The pores are large enough to allow the passage of atoms and small molecules to the interior, and by the same means atomic stains may also pass to the interior volume of Bfr.[156] From this, it was hypothesized that determining the presence of encapsulated proteins within Bfr could be done with approaches utilizing negatively stained TEM. If there was a guest consisting of light atoms in the interior of Bfr it would exclude stain from the interior void, and this absence of stain could be visualized. TEM would be used for the determination of encapsulated GNP as well. Encapsulated GNP would be visualized clearly with TEM since the contrast between the highly electron dense GNP and the less electron dense protein would be high. Since the GNP

was not fluorescent, this would be a highly revealing method to verify encapsulation of GNP within Bfr other than chromatography.

Nanoparticles have been gaining interest in many fields. There has been particular interest in GNPs for their use in nanotechnology because of their biocompatibility, localized surface plasmon resonance properties, and optical properties.[157,158] Not only GNPs, but other nanoparticles have very interesting optical and catalytic properties that may be utilized in the development of optical probes or nano-reactors. By providing a unique environment for these nanoparticles within protein shells, like Bfr, they are protected from environmental contaminants and reaction, and the internal environment can be specifically controlled while the exterior of the Bfr host could be modified to direct this type of probe to various cellular or synthetic surfaces. By studying GNPs they may serve as a benchmark for the encapsulation of other nanoparticles, such as quantum dots.

In addition to the development of Bfr as a nano-platform, insight into the self-assembly characteristics of Bfr were explored. The mechanism of assembly from subunits to a fully formed 24mer in ferritins is still not a completely understood process. There are two clear states known, the dimer and the 24mer state, but intermediates between these two are uncharacterized.[137,159] Some differential scanning calorimetry studies have been performed on ferritins, but only on individual units rather than full complexes.[160] There seems to be an inherent equilibrium between the dimer and 24mer state, which is observed as two well separated protein peaks when pure ferritin is run on size exclusion columns. Some researchers have explored directed mutagenesis with Bfr to define important interfacial residues and improve resistance to temperature and pH changes.[137,161,162] These studies have focused largely on the role of interfacial residues and the e helix, but not of the role of heme in Bfr. Understanding the phenomenon of self-assembly is of importance because it will allow researchers to control the states that multimeric proteins occupy. For instance, ferritin has an equilibrium between dimer and 24mer. If one could force the equilibrium towards dimer formation, when desired, and then trigger complex formation then this would lend much more control to the system. Such a technique would be of great interest for studies of encapsulation, since they would no longer require harsh chemical or physical disruption to modulate the presence of certain assembly states.

2.2. Materials and Methods

2.2.1. Materials

Streptavidin FITC (Life Technologies, Frederick, MD, USA), dabsyl chloride (Sigma-Aldrich, Bellefonte, Pennsylvania, USA), Biotin-X NTA (AnaSpec, Fermont, CA, USA) Black Hole Quencher® 10 (BHQ®-10; Biosearch Technologies, Novato, CA, USA), and Ni-NTA-Nanogold™ (Nanoprobes, Yaphank, NY, USA) used for encapsulation studies. Formvar-Carbon 400 mesh, Cu Grids (Canemco-Marivac, Gore, QC, Canada), Molybdic acid ($(NH_4)_6Mo_7O_{24}$) (Sigma-Aldrich, Saint Louis, MO, USA), Phosphotungstic

acid ($H_3PW_{12}O_{40}$) (Sigma-Aldrich, Saint Louis, MO, USA), and Uranyl acetate ($UO_2(CH_3COO)_2$) (generously donated by Dale Weber of the department of Biology in the University of Waterloo) for TEM. Plasmids (Novogen, Mississauga, ON, Canada), and primers (Sigma-Genosys, Oakville, ON, Canada) were used for genetic work. All buffers were made with Milli-Q™ water with a resistivity of 18 MΩ·cm and filtered through a membrane with a 0.45 µm cut-off.

2.2.2. Safety Statement

All bacterial samples were handled in accordance to level 1 safety laboratory facilities. After use, all bacterial samples were bleached or autoclaved to sterilize the media before disposal. All uranyl acetate used with TEM was disposed of properly through the waste management facility. The safety of the experimenters and others was of the utmost importance throughout experimentation.

2.2.3. Purification of Bfr and Bfr mutants

The Bfr genes on selectively inducible vectors were transformed into and overexpressed in *E. coli* BL21 cells using standard expression techniques. In brief, a pET-22b vector was used to express WT and His6-tag Bfr, whereas a pET-29b vector was used for the S-Bfr expression, and a pGS-21a vector for BfrM expression. All vectors contained the lac operon, which was used to induce expression of Bfr with the addition of 1 M isopropyl β-D-1-thiogalactopyranoside (IPTG) to a final concentration of 1 mM in 1.5 L of media while cells were in mid-log phase growth. Cells were harvested using a Beckmann JA10 centrifuge at 5000 rpm for 20 minutes. Pellets were collected and re-suspended in 20 ml of 50 mM Tris 100 mM NaCl buffer at pH 8.0. The re-suspended cells were homogenized on an Avestin Emulsiflex-C5 (Mannheim, Germany) at a pressure of 17000 psi, and then centrifuged at 15000 rpm in a Beckmann JA25.5 rotor for 20 minutes. Supernatant was collected and heat shocked at 70 °C for 10 minutes and then left to cool to room temperature. This was again centrifuged using a Beckmann JA25.5 rotor at 15000 rpm for 20

minutes. The supernatant was collected to be further purified using chromatographic techniques.

Purification of WT Bfr was performed using anion exchange and size exclusion resins. A Bio-Rad Uno Q1™ anion exchange resin, which had a resin volume of 1.3 ml, and a binding capacity of 180 mg/ml. The column was run with an equilibration buffer of 50 mM Tris, 100 mM NaCl at pH 8.0, and elution buffer of 50 mM Tris, 2M NaCl at pH 8.0. Fractions were analyzed for the presence of WT Bfr using a 15% SDS-PAGE gel, and fractions containing WT Bfr were pooled and concentrated using an Amicon concentrator with a 10 kDa cut off. WT Bfr was then run on a GE Sephacryl™ S-400HR size exclusion column with a resin bed of 402.2 ml. The flow rate was 0.5 ml/min and fractions were collected every minute. Fractions were analyzed using a 15% SDS-PAGE gel and fractions containing pure WT-Bfr were pooled and concentrated, as before. If the ratio of 260/280 was above 1.0 then a Bio-Rad type II ceramic hydroxyapatite® column was used to separate contaminating DNA from WT Bfr. The equilibration buffer used was 10 mM potassium phosphate dibasic buffer at pH 6.8, and 400 mM potassium phosphate dibasic buffer at pH 6.8 was used as an elution buffer. Fractions were examined on a 15% SDS-PAGE gel, and fractions containing pure WT Bfr lacking DNA were pooled, as before. WT Bfr was analyzed with MS. An electrospray ionization quadrupole time of flight mass spectrometer (Waters, Micromass Masslynx) was used to analyze the mass of protein samples.

His6-tag Bfr, BfrM, and S-Bfr all contained his6-tags, and were all purified using the same methods. His6-tag containing Bfr was purified using a 1 ml GE HisTrap™ affinity column. Equilibration and elution buffers were 50 mM Tris, 100mM NaCl, and 20 mM imidazole at pH 8.0, and 50 mM Tris, 100mM NaCl, and 300 mM imidazole at pH 8.0, respectively. Elute was analyzed on 15% SDS-PAGE gels. Fractions were pooled and concentrated on an Amicon with a MW cut-off of 10 kDa. His6-tag containing Bfr were confirmed by MS, as before.

His6-tag and WT Bfr were reconstituted fully with heme. The insertion method was followed from previous reporting on heme reconstitution into Bfr[163]. Hemin was suspended in a solution of 0.1 M NaOH to make a 10 mM solution of hemin. This was diluted with 0.2 M MES buffer at pH 6.5 to a final concentration of 1.5 mM hemin. This solution was then added to Bfr in excess of two equivalents at 80 °C in 0.2 M MES, 1M NaCl buffer at pH 6.5 for 10 minutes, and then left to cool to 23°C. Bfr was run on a GE Sephadex™ G-25 Fine desalting column with 50 mM Tris, 100 mM NaCl buffer at pH 8.0 to remove free hemin and MES buffer.

2.2.4. Encapsulation of SF and GNP

A molar equivalent of SF (0.1 mg, 1.89×10^{-9} mol) was pre-incubated with biotin-XNTA (0.021mg, 2.93×10^{-8} mol, 8.0 equiv.) and nickel sulfate (4.5×10^{-6}g, 2.93×10^{-8} mol, 8.0 equiv.) in 50 mM Tris, 100 mM NaCl buffer at pH 8.0 for 10 min at 23 °C. SF pre-incubated with biotin-XNTA and nickel sulfate was added to Bfr (1.89×10^{-9} mol, 1.0 equiv.) in 8 M GndHCl buffered with 50 mM Tris, 100 mM NaCl at pH 8.0 for 90 minutes at 5 °C. This was then dialyzed against 4 L of 50 mM Tris 100 mM NaCl buffer at pH 8.0 for 24 hours. The sample was concentrated with a Pall Nanosep® spin column with a 10 kDa cut off to a volume of 0.5-1 ml. Free SF was separated from encapsulated SF using a GE Sephacryl™ S-300HR resin, void volume of 99.05 ml, running with a flow rate of 0.5 ml/min collecting fraction volumes of 0.5 ml. The running buffer was the same as the dialysis buffer. The first peak was collected and concentrated to 1 ml as before.

The 1.8 nm GNP (1.0×10^{-9} mol) was pre-mixed with nickel sulfate (1.0×10^{-7} mol, 100 equiv.) in 50 mM Tris, 100 mM NaCl buffer at pH 8.0 for 10 minutes at 23 °C. Pre-incubated 1.8 nm GNP mixed with nickel sulfate was stirred in with Bfr (0.5 mg, 1.0×10^{-9} mol, 1 equiv.) in 8 M GndHCl for 90 minutes and then dialyzed into 4 L of 50 mM Tris, 100 mM NaCl buffer at pH 8.0 for 24 hours at 5 °C. This was purified in the same manner as described for encapsulated SF.

The 5 nm GNP ($1.0x10^{-10}$ mol) was pre-incubated with nickel sulfate ($2.0x10^{-8}$ mol, 200 equiv.) in 50 mM Tris, 100 mM NaCl buffer at pH 8.0 for 10 minutes at 23 °C. Pre-incubated 5 nm GNP was mixed with Bfr (0.1 mg, $2x10^{-10}$ mol, 2 equiv.) at 70 °C for 90 minutes. After 90 minutes, the solution was left to cool to 23 °C. The sample was purified in the same manner as described for encapsulated SF.

2.2.5. Quenching Experiments

Quenching agents were iodide, Dabsyl-glutamate, and BHQ®-10. Dabsyl-glutamate was prepared from Dabsyl-Cl following a previously reported procedure[164]. Syntheis was monitored by MS (Appendix 1). The stock solutions of iodide, Dabsyl-glutamate, and BHQ®-10 utilized were 0.1 M, 0.27 mM, and 0.4 mM, respectively. Each of these quenchers was titrated into a small volume cuvette (Hellma 45 μl) with 0.3 cm path length in one or two microliter volume increments. After addition of the quencher, the solution was vigorously mixed to ensure homogenous distribution of quencher. The emission scan was recorded over a range of 500-550 nm with a fixed excitation wavelength of 495 nm. Slit widths for incoming and emission light were set to 1 mm. All fluorescence quenching experiments were performed on a PTI fluorimeter A-1010B. Additional components attached were a LPS-220B lamp power supply, a SC-500 shutter control, MD-5020 motor driver, and 814 photomultiplier detection system using a maximum excitation wavelength determined from the excitation spectrum.

2.2.6. TEM Preparation and Imaging

Transmission electron microscopy was performed on a CM10 Philips microscope modified with an Advanced Microscopy Techniques image capturing CCD camera. The accelerating potential was set to 100 keV for imaging in bright field mode. Preparation for TEM imaging for both encapsulated SF and GNP was performed using 400 mesh copper grids with a carbon-formvar coating. Two negative stains were used to generate the contrast needed to visualize protein: Molybdic acid ($(NH_4)_6Mo_7O_{24}$), and Uranyl acetate

($UO_2(CH_3COO)_2$). Molybdic acid, uranyl acetate, and phosphotungstic acid ($H_3PW_{12}O_{40}$) stains were prepared and used as both 1.0 % and 0.5 % solutions.[155,165] Encapsulated Bfr samples were prepared to a concentration of approximately 0.1 mg/ml, and buffered exchanged into water using a spin column to remove unwanted salts. Grids were prepared by placing a 20 µl sample droplet, two 20 µl droplets of water and one droplet of stain on Parafilm®. Using ultra-fine tweezers, the grid was placed on top of the sample droplet for one minute. The grid was then removed, dabbed with a piece of Whatmann No 1 paper such that almost all of the liquid was removed except for a thin glassy layer of solution coating the grid. This was then washed by placing in two the two subsequent water droplets as in the previous step without the minute wait time. The final step was to dip the grid onto the stain solution and then dab away excess stain until a thin glassy layer of solution was left on the grid. This was left, covered, at room temperature to dry for 24 hours.

2.2.7. MS Preparation and Operation

All protein samples were buffer exchanged for water using Pall Nanosep® 10 kDa cut-off spin columns and then diluted to a final concentration of 1-5 µM in a 50 µl solution of 1:1 water:MeCN with 0.2% formic acid. Protein samples were run on a Waters Micromass MassLynx nanospray electrospray ionization quadrupole time of flight (ESI-QToF) mass spectrometer. Spectrum was collected between 100-2500 m/z, and the protein mass was deconvoluted using the supplied MaxEnt-1 MassLynx software. Native MS was attempted with protein suspended in 20 mM ammonium acetate pH 7.0, as previously reported.[166,167] The collision energy and cone voltage were lowered to 10 eV and 2.0 V, and sample in ammonium acetate was directly injected into the mass spectrometer. A Thermo Scientific Q-Exactive™ was used when the QToF was down. The samples were prepared in the same fashion, except re-suspended in 1:1 water:MeOH with 0.1% formic acid.

2.2.8. EMAN2 Image Processing

Images were imported into the EMAN2 workflow GUI to appropriately prepare particles for analysis[168]. The methodology used was based on the several tutorials on the EMAN2 wiki, but the general procedure will be outlined here. In general, EMAN2 was used in a more rudimentary fashion to organize and obtain many images and to utilize the averaging features. It was not intended to be used as a means to generate 3D reconstructions, as it is more frequently used in cryogenic electron microscopy. TEM images were imported with the correct accelerating voltage of 100 kV, molecular weight of 440 kDa, Å/pixel, and microscope Cs values. Single particles were selected using the "interactive boxing" function. The appropriate box size was determined based on the number of pixels that made up the diameter of the particles. An appropriate size was chosen to allow significant background to be included to accommodate the processing functions. Box sizes were based on the list of appropriate sizes on the EMAN2 wiki. These stacks of images were saved as bdb files for further processing. Stacks were iteratively run through the "automated fitting", "interactive tuning", and "generate structure factor" functions until the defocus and B-factor matched well. Typically this took two or three iterations due to the lower resolution of the negatively stained images. These stacks were opened in the "Build particle set" function as wiener filtered images. "Bad particles" were manually removed before the reconstruction. "Bad particles" were arbitrarily defined as obscure, incomplete, or off center images that would likely be detrimental to the final reconstruction. Finally, the "generate classes function" was executed to generate a reference free class average. Here the phase flipped-hp data was chosen for the reconstruction, the class number was set to 10, and 8-15 refinement iterations were performed. Again, more information is available on the EMAN2 wiki.[169]

2.3. Results and Discussion

2.3.1. WT Purification

All of the Bfr proteins were expressed and purified in the Honek laboratory. The genes for WT and His6-tag Bfr were previously generated by Dr. Uthaiwan Suttisansanee in the Honek laboratory.[141] In brief, the WT Bfr gene was inserted into a pET 22b vector using *Nde*I and *Bam*HI cut sites, and was transformed into an *E. coli* BL21 cell line for over expression. The pET 22b vector contained the Lac operon, which allowed for the use of IPTG to induce overexpression of desired proteins. Before expression, WT Bfr was sent for sequencing to confirm the sequence (Table 2). After cell lysis steps the protein was purified using two or three column types.

Table 2: Sequencing results for the WT Bfr, His6-tag Bfr, BfrM, and S-Bfr. The gene is highlighted in bolded, and the associated protein translations are shown below in italics with the methionine residues highlighted in bold.

WT Bfr	NNNNNgNNcgtaNcaTTcCnCTCTaganaTAATTTTGTTtaACTTTAAGAAGGAGATATACAT**ATGAAAGGTGAT ACTAAAGTTATAAATTATCTCAACAAACTGTTGGGAAATGAGCTTGTCGCAATCAATCAGTACTTTCTCCAT GCCCGAATGTTTAAAAACTGGGGTCTCAAACGTCTCAATGATGTGGAGTATCATGAATCCATTGATGAGAT GAAACACGCCGATCGTTATATTGAGCGCATTCTTTTTCTGGAAGGTCTTCCAAACTTACAGGACCTGGGCAA ACTGAACATTGGTGAAGATGTTGAGGAAATGCTGCGTTCTGATCTGGCACTTGAGCTGGATGGCGCGAAG AATTTGCGTGAGGCAATTGGTTATGCCGATAGCGTTCATGATTACGTCAGCCGCGATATGATGATAGAAAT TTTGCGTGATGAAGAAGGCCATATCGACTGGCTGGAAACGGAACTTGATCTGATTCAGAAGATGGGCCTG CAAAATTATCTGCAAGCACAGATCCGCGAAGAAGGTTGA**GGATCCGAATTCGAGCTCCGTCGACAAGCTTG CGGCCGCACTCGAGCACCACCACCACCACCACTGAGATCCGGCTGCTAACAAAGCCCGAAAGGAAGCTGAGT TGGCTGCTGCCACCGCTGAGCAATAACTAGCATAACCCCTTGGGGCCTCTAAACGGGTCTTGAGGGGTTTTTT GCT ***M****KGDTKVINYLNKLLGNELVAINQYFLHAR****M****FKNWGLKRLNDVEYHESIDE****M****KHADRYIERILFLEGLPNLQDLGK LNIGEDVEE****M****LRSDLALELDGAKNLREAIGYADSVHDYVSRD****MM****IEILRDEEGHIDWLETELDLIQK****M****GLQNYLQ AQIREEG*
His6-tag Bfr	NNNatgNGNcGtaNcNATTCCCCTCTAgAnaTAATTTTGTTtaACTTTAAGAAGGAGATATACAT**ATGAAAGGT GATACTAAAGTTATAAATTATCTCAACAAACTGTTGGGAAATGAGCTTGTCGCAATCAATCAGTACTTTCTC CATGCCCGAATGTTTAAAAACTGGGGTCTCAAACGTCTCAATGATGTGGAGTATCATGAATCCATTGATGA GATGAAACACGCCGATCGTTATATTGAGCGCATTCTTTTTCTGGAAGGTCTTCCAAACTTACAGGACCTGGG CAAACTGAACATTGGTGAAGATGTTGAGGAAATGCTGCGTTCTGATCTGGCACTTGAGCTGGATGGCGCG AAGAATTTGCGTGAGGCAATTGGTTATGCCGATAGCGTTCATGATTACGTCAGCCGCGATATGATGATAGA AATTTTGCGTGATGAAGAAGGCCATATCGACTGGCTGGAAACGGAACTTGATCTGATTCAGAAGATGGGC CTGCAAAATTATCTGCAAGCACAGATCCGCGAAGAAGGTCTCGAGCACCACCACCACCACCACTGA**GATCC GGCTGCTAACAAAGCCCGAAAGGAAGCTGAGTTGGCTGCTGCCACCGCTGAGCAATAACTAGCATAACCCCT TGGGGCCTCTAAACGGGTCTTGAGGGGTTTTTTGCTGAAAGGAGGAACTATATCCGGATTGGCGAATGGGAC GCGCC ***M****KGDTKVINYLNKLLGNELVAINQYFLHAR****M****FKNWGLKRLNDVEYHESIDE****M****KHADRYIERILFLEGLPNLQDLGK LNIGEDVEE****M****LRSDLALELDGAKNLREAIGYADSVHDYVSRD****MM****IEILRDEEGHIDWLETELDLIQK****M****GLQNYLQ AQIREEGLEHHHHHH*
BfrM	NNNNNNNNNNNNNNatTCCCCTCTAgaataATTTTGTTTAACTTTAAgaAGGAGATataCAT**ATGAAAGGTGAC ACGAAAGTCATTAACTATCTGAACAAACTGCTGGGCAACGAACTGGTCGCCATCAATCAATACTTCCTGCAC GCACGCCTGTTTAAAAACTGGGGCCTGAAACGTCTGAATGATGTCGAATACCATGAAAGTATCGATGAAAT GAAACACGCCGACCGTTACATTGAACGCATCCTGTTCCTGGAAGGTCTGCCGAACCTGCAGGATCTGGGCA AACTGAATATTGGTGAAGACGTTGAAGAACTGCTGCGTAGCGATCTGGCACTGGAACTGGACGGCGCTAA AAACCTGCGCGAAGCGATCGGTTATGCCGATAGCGTGCATGACTACGTTTCTCGTGATCTGCTGATTGAAAT CCTGCGCGATGAAGAAGGCCACATTGACTGGCTGGAAACCGAACTGGACCTGATCCAAAAACTGGGTCTG CAAAACTACCTGCAAGCACAAATCCGTGAAGAAGGCCTCGAGCACCACCACCACCACCACTGA**GATCCGGC TGCTAACAAAGCCCGAAAGGAAGCTGAGTTGGCTGCTGCCACCGCTGAGCAATAACTAGCATAACCCCTTGG GGCCTCTAAACGGGTCTTGAGGGGTTTTTTGCTGAAAGGANGAACTATATCCGGATTGGCGnAATGGGACGC GCCCTGTAGCGGCNCATTAAGCGCGGCGGGTGTGGTGGTNACNCGCAGCGTGACNGCTACACTTGNNANC GCCNTANCGNNNGCN ***M****KGDTKVINYLNKLLGNELVAINQYFLHARLFKNWGLKRLNDVEYHESIDE****M****KHADRYIERILFLEGLPNLQDLGKL NIGEDVEELLRSDLALELDGAKNLREAIGYADSVHDYVSRDLLIEILRDEEGHIDWLETELDLIQKLGLQNYLQAQIRE EGLEHHHHHH*
S-Bfr	ATAATTTTGTTTAACTTTAAGAAGGAGATATACAT**ATGAAAGAAACCGCTGCTGCTAAATTCGAACGCCAGC ACATGGACAGCCCAGATCTACATATGAAAGGTGATACTAAAGTTATAAATTATCTCAACAAACTGTTGGGA AATGAGCTTGTCGCAATCAATCAGTACTTTCTCCATGCCCGAATGTTTAAAAACTGGGGTCTCAAACGTCTC AATGATGTGGAGTATCATGAATCCATTGATGAGATGAAACACGCCGATCGTTATATTGAGCGCATTCTTTTT CTGGAAGGTCTTCCAAACTTACAGGACCTGGGCAAACTGAACATTGGTGAAGATGTTGAGGAAATGCTGC GTTCTGATCTGGCACTTGAGCTGGATGGCGCGAAGAATTTGCGTGAGGCAATTGGTTATGCCGATAGCGTT CATGATTACGTCAGCCGCGATATGATGATAGAAATTTTGCGTGATGAAGAAGGCCATATCGACTGGCTGGA AACGGAACTTGATCTGATTCAGAAGATGGGCCTGCAAAATTATCTGCAAGCACAGATCCGCGAAGAAGGT CTCGAGCACCACCACCACCACCACTGA**GATCCGGCTG ***M****KETAAAKFERQH****M****DSPDLH****M****KGDTKVINYLNKLLGNELVAINQYFLHAR****M****FKNWGLKRLNDVEYHESIDE****M****K HADRYIERILFLEGLPNLQDLGKLNIGEDVEE****M****LRSDLALELDGAKNLREAIGYADSVHDYVSRD****MM****IEILRDEEGHI DWLETELDLIQK****M****GLQNYLQAQIREEGLEHHHHHH*

Originally, WT Bfr was purified using an anion exchange column and a size exclusion column, but this was later adapted to an anion exchange column and a hydroxyapatite column. The anion exchange column used was a Bio Rad Uno^{TM}-Q1 column. To this column, volumes of supernatant from the homogenized cells were injected at 1 ml increments. Fractions were then examined on an SDS-PAGE gel to determine the purity of the protein (Figure 2.2). Bfr protein was observed in both the flow through and the eluted fractions. Only the eluted fractions were collected since there was less contamination. These fractions were collected and concentrated using an Amicon stirred cell pressure concentrator with a Millipore Ultrafiltration membrane with a 10 kDa cut off. This collected protein was loaded onto a GE Sephacryl^{TM} S-400 HR column. These fractions were analyzed with SDS-PAGE to examine the purity of the WT Bfr (Figure 2.3). The R_f for the 24mer and dimer peaks on this column were 0.88 and 0.73, respectively, with a void volume of 253.68 ml. There appeared to be fractions that contained pure WT Bfr protein. These fractions were concentrated as before, and then the correct molecular weight of 18495 Da was determined with the use of an ESI-QTOF mass spectrometer (Figure 2.4). The deconvoluted spectrum revealed a peak with a molecular weight of 18494 Da, whereas the calculated weight was 18495 Da. Deviation of a single mass unit can be expected in lower resolution mass spectrometry. In addition to purifying WT Bfr, re-incorporation of heme into Bfr was performed. As is discussed below, heme was expected to be favourable in promoting the formation of the 24mer. The heme was reconstituted back into Bfr using a previously derived method, and subsequently used for encapsulation studies.[163]

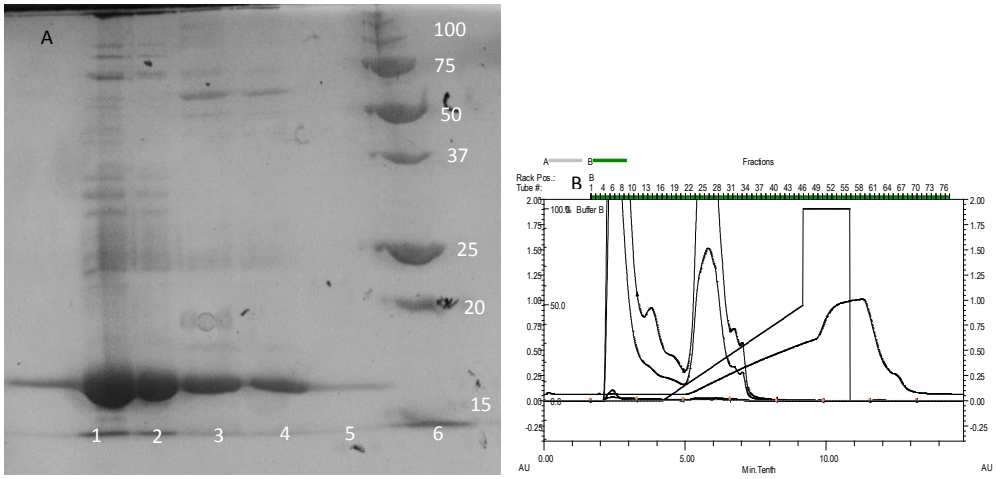

Figure 2.2: SDS-PAGE of WT Bfr fractions (A) from a Bio-Rad Uno™-Q anion exchange resin (B). The lanes listed from left to right were fractions 6B, 8B, 25B, 26B, 33B, and the Precision Plus Protein™ ladder from Bio-Rad. The largest bands above the 15 kDa marker were WT Bfr. Fractions from and between lanes 3, 4, and 5 were pooled and concentrated for the next step

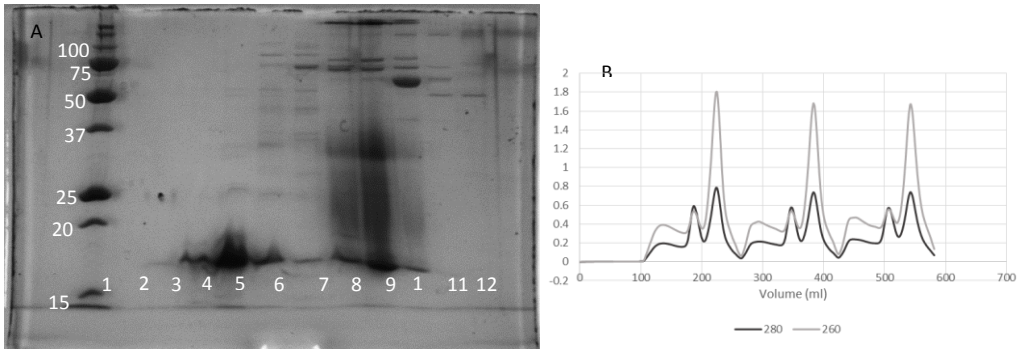

Figure 2.3: SDS-PAGE of WT Bfr (A) fractions from a GE Sephacryl™ S-300 HR size exclusion chromatography, which had three samples injected sequentially (B). Lanes from left to right were Bio-Rad Procession Plus Protein™ ladder, fractions 63A, 70A, 77A, 85A, 89A, 2B, 7B, 16B, 20B, and 27B. Fractions from 77A to 85A (volumes 150-210 ml, 330-370 ml, and 480-530 ml) were collected and analysed with MS.

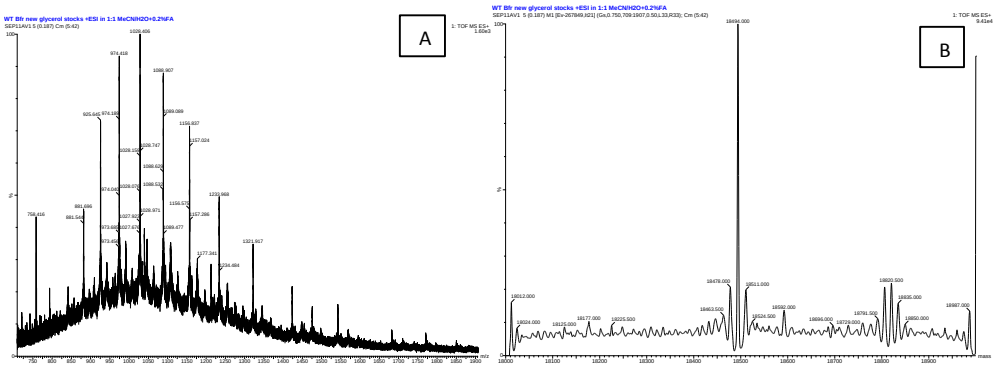

Figure 2.4: Mass spectrum of WT Bfr obtained from a Waters Micromass nanospray ESI-QTOF. The raw spectrum (A) showed a Gaussian distribution of multiply charged WT Bfr. The processed spectrum (B) was deconvoluted using the MaxEnt 1 tool supplied with the MassLynx software. The deconvoluted mass was measured as 18494 Da, one mass unit off of the correct mass of 18495 Da.

After a series of WT Bfr purifications, an increasing nucleotide contaminant was observed. The nucleotide contaminant was identified by a high 260/280 ratio of 1.60, and a fluorescent band was visible when running an agarose gel (Figure 2.5).To remedy this issue, several attempts were made to remove this contaminant by filtration. After dialysis for over 24 hours, and buffer exchanging with an Amicon concentrator with 500 ml of fresh buffer the 260/280 ratio remained the same. Use of a third column was entertained to try and selectively bind either the nucleotide or the protein. A Bio-Rad CHT^{TM} ceramic hydroxyapatite type II resin was used, which was reported to bind DNA. The nucleotide contaminated WT Bfr from the size exclusion Sephacryl^{TM} S-300 HR column was used to test the hydroxyapatite column. Fractions were examined on SDS-PAGE, and then on ESI-QTOF MS to determine the mass of WT Bfr (Figure 2.6). It was determined that the protein was pure and absent of nucleotide contamination by the low 260/280 ratio of 1.03. In subsequent purifications of WT Bfr the size exclusion step was removed entirely, and only the anion exchange column and hydroxyapatite columns were used. This greatly reduced the preparation and run time for purification. The origin of the nucleotide contaminant was not investigated.

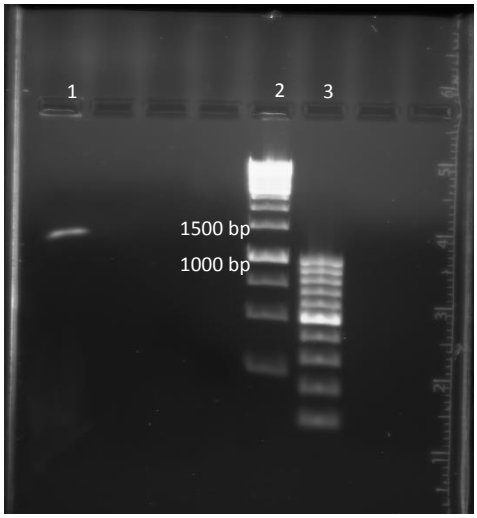

Figure 2.5: Agarose gel of a purified WT Bfr protein prep showing nucleotide contamination. Lanes from left to right were the contaminated WT Bfr sample, 1kbp Fermentas GeneRuler^{TM}, and 100 Bp Fermentas GeneRuler^{TM}.

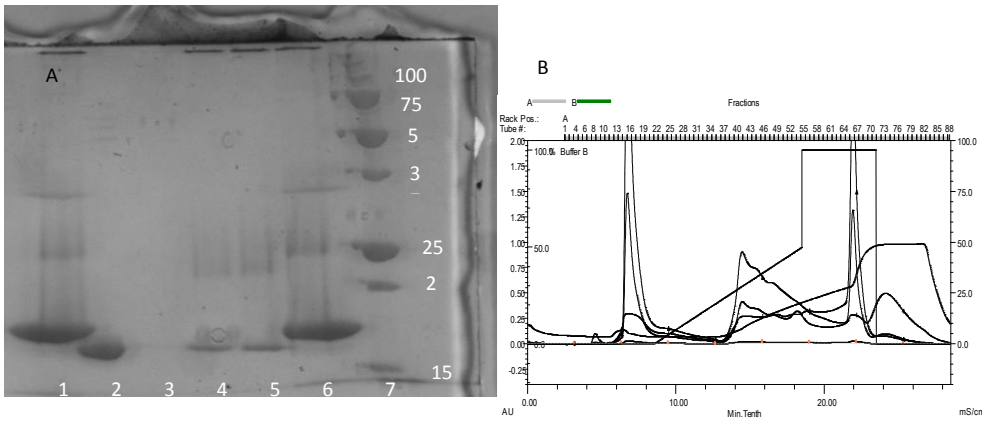

Figure 2.6: SDS-PAGE of WT Bfr (A) fractions from a Bio-Rad CHT™ ceramic hydroxyapatite type II resin (B). Lanes, from left to right, were pure His6-tag Bfr, fractions 54A, 68A, 73A, 74A, pure His6-tag Bfr, and Bio-Rad Procession Plus Protein™ ladder. Fractions from lanes 4 and 5 were collected and analyzed with MS.

3.3.2. S-Bfr Purification

The S-Bfr construct was designed for the purposes of labelling the exterior of Bfr. S-Bfr was designed with an S-tag on the N-terminus, which faces the exterior surface. By making this N-terminal extension, a Gln residue on the tag would become externally exposed. It was hypothesized that this Gln would be available for enzymatic labelling with a transglutaminase (TGase). In order to generate an S-tag onto His6-tag Bfr Anthony Petrie, of the Honek laboratory, designed primers to add a *Bgl*II cut site at the N-terminus of Bfr. A *Bgl*II cut site would enable the correct, in-frame, placement of the His6-tag Bfr gene into a pET29b vector containing an N-terminal S-tag. In addition to the S-tag, a His6-tag was kept on the C-terminus to simplify downstream purification procedures. In order to generate this cut site a point mutation was made upstream of the original initiator codon, and in consequence four additional residues, PDLH, were added after the S-tag. In total, there were 20 amino acids added, which increased the molecular weight to 21884 Da. Anthony Petrie made this mutation and prepared the gene in a pET29b vector. The correct gene was confirmed by Anthony Petrie through sequencing of the plasmid. This was transformed into *E. coli* BL21 cells and expressed, as before, using IPTG. Cells were lysed and the supernatant treated with a 70 °C heat shock step, which S-Bfr stable to. S-Bfr was purified using a GE HisTrap^{TM} column, using the same method as the His6-tag Bfr purification procedure. This resulted in pure S-Bfr protein, which was concentrated and analyzed on ESI-Orbitrap MS to confirm the correct mass. A single mass of 21883.6 kDa was observed, signifying the expression and purification of the correct protein (Figure 2.7). Fragmentation of S-Bfr was observed after leaving a solution of S-Bfr at 4 °C for a week. It was suspected that the fragmentation was a result of a trace amount of contaminant protease. Two protease inhibitors were examined by a student under my supervision, Hawa Gyamfi of the Honek laboratory. The inhibitors were ethylenediaminetetraacetic acid (EDTA), and phenylmethanesulfonyl fluoride (PMSF), tp determin if there was either a metalloprotease, or serine protease, respectively. The concentrations used were 1 mM and 5 mM for EDTA and

PMSF, respectively. After incubating at room temperature, 23 °C, for five days the inhibitor-less control showed fragmentation, similar to S-Bfr with PMSF inhibitor. BfrM with EDTA lacked fragmentation, which indicated that it was likely a metalloprotease (Figure 2.8).

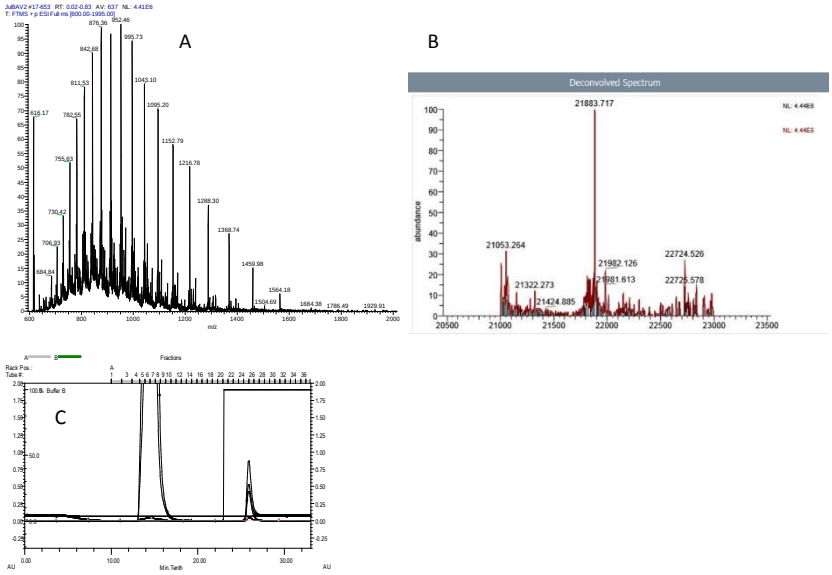

Figure 2.7: MS of purified S-Bfr from a GE HisTrap™ column using a Thermo Scientific Q Exactive™. The raw spectrum (A) was deconvoluted (B) and revealed a mass of 21883.7 Da, which was close to the calculated mass of 21884.7 Da. The elution profile from a GE HisTrap™ column was similar to that seen with His6-tag Bfr elution (C).

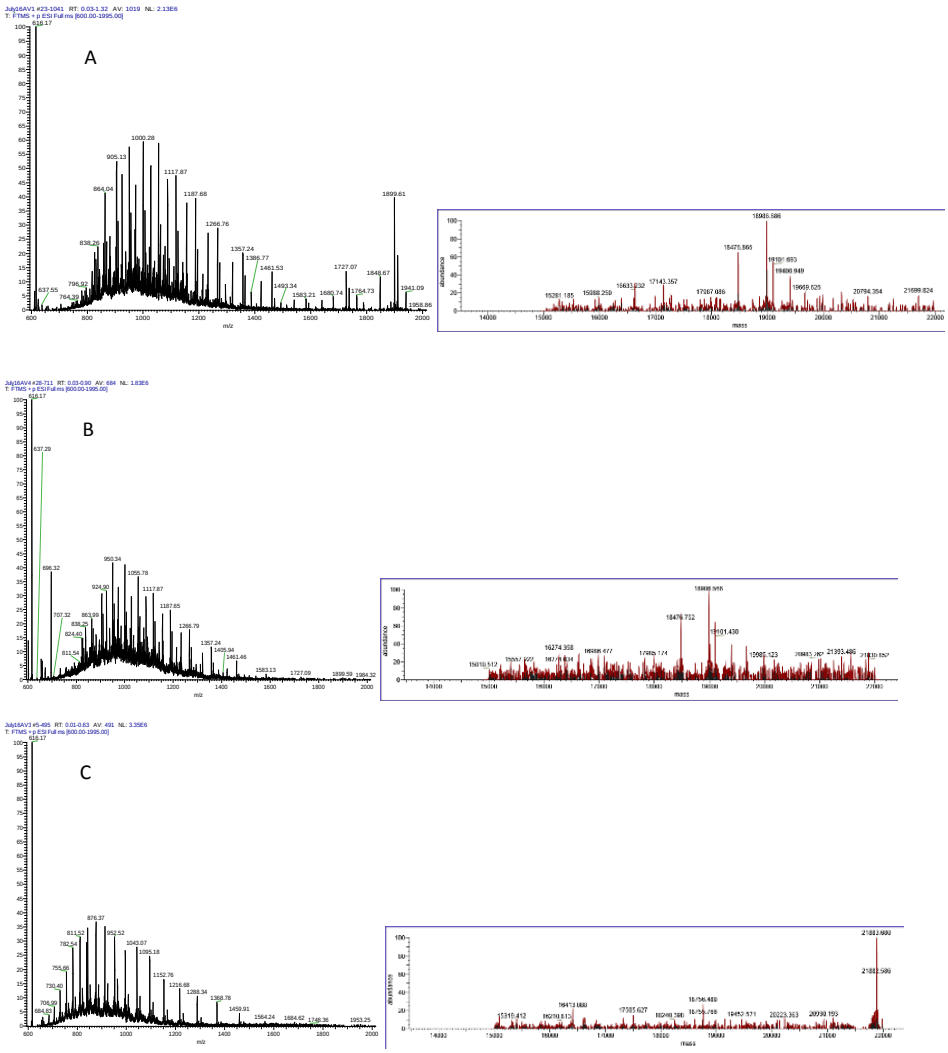

Figure 2.8: MS of S-Bfr with PMSF and EDTA protease inhibitors. An inhibitor-less control (A), along with two inhibitors: PMSF (B), and EDTA (C) were used. It was observed after a week of incubation at 23 °C that the control and PMSF trial showed a high level of fragmentation, whereas the EDTA trial showed no fragmentation, as can be observed by analysis of the deconvoluted spectrums.

3.3.3. Streptavidin Encapsulation within Bfr

Initial conditions for encapsulation of SF were explored by monitoring the ratio of peaks on size exclusion chromatography. The peak ratio was based on the measured absorbance value at 495 nm, which was the absorption maxima for SF, of the eluted peaks on a GE Sephacryl^{TM} S-300 HR size exclusion column. Free SF would elute where the observed "second peak" would elute after an encapsulation trial, which corresponded to unsuccessfully encapsulated SF. The first peak, therefore, should have corresponded to the encapsulated SF, which eluted at the same time point as 24mer Bfr. By dividing the first peak by the second the peak ratio was obtained, which was used as an indicator for the amount of SF that was encapsulated within Bfr. Two conditions were explored when encapsulating SF: the effect of the ratio of His6-tag to WT Bfr, and the concentration of guanidine hydrochloride (GndHCl). Since the tag on His6-tag Bfr was facing the interior it was likely that this would decrease the inner diameter, as shown previously in computer simulations.[141] By modulating the ratio between WT and His6-tag, it was possible to optimize encapsulation conditions, trading off between crowding and the number of affinity interactions. Upon declustering of the self-assembled units, it would be possible to generate a hybrid of WT and His6-tag Bfr upon reformation of the cage structure.

SF encapsulation was analyzed with varying ratios of His6-tag to WT Bfr, which were separated on a GE Sephacryl^{TM} S-300 HR column (Figure 2.9). The R_f of the first and second peak were 0.47 and 0.70, respectively, with a void volume of 99.05 ml. There was a subtle difference between the 80/20, 60/40, and 50/50 mixtures of His6-tag/WT, with peak ratios of 0.76, 0.80, and 0.81, respectively. Although the 80/20 and 50/50 were very similar in the ratio of the eluted peaks, 60/40 was chosen as the ideal ratio. The encapsulated SF peak ratios for 40/60 and 20/80 His6-tag/WT were 0.63 and 0.54, respectively. A control was also run with SF and His6-tag Bfr, which did not contain any biotin-XNTA. It was observed in this control that only a single peak eluted from

the GE Sephacryl™ S-300 HR column at the same time as free SF and the observed second peak in the encapsulation trials.

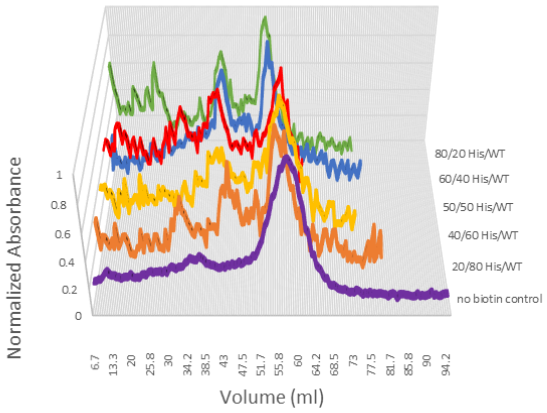

Figure 2.9: Varying ratios of His6-tag/WT Bfr with encapsulated SF run on a GE Sephacryl™ S-300 HR resin. The elution was monitored with four wavelengths, 280 nm, 260 nm, 418 nm, and 495 nm. Displayed here is the 495 nm monitored wavelength, which corresponded to the fluorescein on SF.

Concentrations of GndHCl to decluster 24mer His6-tag/WT Bfr were varied in order to examine the amount that was necessary for proper encapsulation of SF. If less GndHCl was required for encapsulation, then it might be more advantageous to perform encapsulation experiments in less harsh conditions. Several concentrations of GndHCl were used to evaluate the importance of using this chemical disruptant for exposure of the inner surface of Bfr by declustering. All of these trials were performed using a 60/40 ratio of His6-tag to WT, with SF, Biotin-XNTA, and nickel sulfate. Five concentrations were explored, 8 M, 4 M, 2 M, 1 M, and 0 M, keeping the conditions otherwise identical between these trials (Figure 2.10). The no biotin-XNTA control was also included in this graph as a point of comparison to the rest of the data. As was observed with the elution pattern, even total absence of GndHCl seemed to yield some amount of encapsulated SF. This was interesting because it was thought that the His6-tag would largely be unexposed in buffered aqueous solution. This was likely due to some of the inherent equilibrium between the 24mer and the dimer state of Bfr. Dimer Bfr would have had an exposed His6-tag, and would have been able to interact with the Biotin-XNTA. This process

was, however, not as efficient at encapsulation as the in the presence of GndHCl. Peak ratios were 0.70, 0.64, 0.60, 0.60, and 0.49 for 8 M, 4 M, 2 M, 1 M, and 0 M GndHCl, respectively. It was possible to encapsulate in all of these conditions, but it seemed to be more favourable to do so in higher amounts of GndHCl. This seemed to indicate that the interaction between His6-tag Bfr and SF was favourable enough that even under non-declustering conditions some SF would become encapsulated. The use of 60/40 His6-tag/WT conditions with 8 M GndHCl were scaled up by five times, and it was observed in some cases to encapsulate quantities of SF that had peak ratios as high as 1.20 (Figure 2.11).

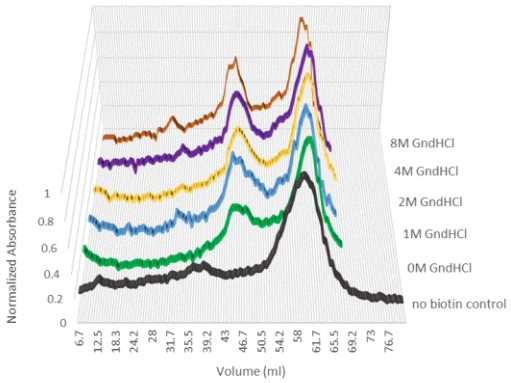

Figure 2.10: Varying concentrations of GndHCl during encapsulation of SF within His6-tag/WT Bfr. The samples were run on a GE Sephacryl™ S-300 HR resin while monitoring the 495 nm wavelength, specific for the SF marker.

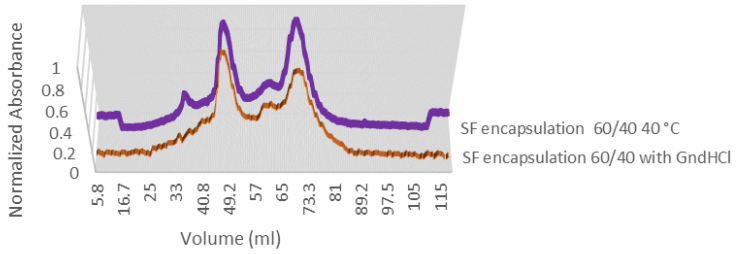

Figure 2.11: Encapsulation of SF within 60/40 His6-tag/WT Bfr using two declustering agents: GndHCl and a 40 °C temperature change. These samples of encapsulated SF used 60/40 His6-tag/WT Bfr and were run on GE Sephacryl™ S-300 HR resin. The wavelength monitored, 495 nm, was specific for the fluorescein label found on SF.

An absence of GndHCl during the encapsulation procedure resulted in some small levels of SF being encapsulated. It was suspected that an alternative, possibly less severe, conditions could be utilized for encapsulation. Since both Bfr and SF are known to be heat stable, a temperature based method to decluster Bfr was attempted. Using a hot water bath at 40 °C the mixture of host, guest, and linker was left for 90 minutes. Instead of needing to dialyze excess GndHCl out, it was left at room temperature to cool and was then run on size exclusion (Figure 2.11). The peak ratio for the 40 °C temperature based encapsulation trial was 0.96, which was very comparable to some of the other 8 M GndHCl trials. This demonstrated that it was possible to use another method to encapsulate the SF guest molecule, which may prove to simplify preparation time. The encapsulated samples prepared here were used for future experiments with TEM and fluorescence quenching.

2.3.2. GNP Encapsulation within Bfr

Two commercial gold nanoparticles (GNP) were investigated as inorganic guest particles to encapsulate in Bfr. The sizes of these nanoparticles were 1.8 and 5 nm, each of which had NTA ligands attached to the surface through a proprietary polymer linker. The 1.8 and 5 nm linker distances were 0.7-1 nm and 1.5 nm, respectively. This made the final diameter of the 1.8 and 5 nm nanoparticles 2.8 and 8 nm, respectively. For these nanoparticles, 2.8 nm was well within the size limitations of the interior 8 nm core of Bfr, whereas 8 nm was at the very extreme of allowable sizes. The 1.8 nm GNP was explored first by a student under my supervision, Robert Taylor, as it was suspected to be a better candidate for encapsulation within Bfr. This GNP appeared brown-red in colour and had a reported absorption maxima at 420 nm. This maxima, unfortunately, overlapped with the heme present in Bfr reconstituted with heme. Thus, for these experiments His6-tag and WT bfr were utilized in the absence of heme in their structure. Therefore any signal at 420 nm on chromatograms should have been a result of the presence of the 1.8 nm GNP. The first step was to determine the optimal ratio of His6-tag to WT for encapsulating 1.8 nm GNP.

Robert Taylor explored the ratios of His6-tag and WT to optimize the conditions for 1.8 nm GNP encapsulation. The method for encapsulation used 8 M GndHCl to decluster the 24mer Bfr to expose the interior His6-tag. This was then incubated in the presence of the 1.8 nm GNP and nickel sulfate and then dialyzed into 50 mM Tris, 100 mM NaCl buffer at pH 8.0. This procedure mirrored that which was used for the encapsulation of SF in the previous experiment. Before the encapsulation trial was performed, absorption spectra for both 1.8 and 5 nm GNP were taken (Figure 2.12). Curiously, the absorption spectra for the 1.8 nm GNP did not contain a distinctive peak at 420 nm, as was stated in the specifications for the product. Whereas, the 5 nm GNP clearly contained a 518 nm absorption peak. Both GNPs, however, exhibited high absorption in the UV range. For future experimental identification, 518 nm wavelength was used to specifically identify the 5 nm GNP, but 420 nm could not be used for the 1.8 nm GNP. The 1.8 nm GNP encapsulation was examined

with several ratios of His6-tag and WT Bfr to optimize conditions. Ratios of His6-tag/WT Bfr explored were 0/100, 10/90, 50/50, 70/30, and 100/0. Each of these trials used GndHCl to decluster as described before, and solutions were dialyzed into 50 mM Tris, 100 mM NaCl buffer at pH 8.0 for 24 hours, and then eluted through a GE Sephadex^{TM} S-300 HR column (Figure 2.13). The first peak in this chromatogram was attributed to the 24 mer Bfr, the second to the free 1.8 nm GNP, and the third to dimer Bfr. This equilibrium between fully formed 24mer and dimer Bfr had been observed previously.[159,170] Examining Figure 2.13 seemed to suggest that Bfr was more in the 24mer state when the His6-tag/WT ratios were 10/90 and 0/100. As the ratios were shifted to higher His6-tag Bfr content the dimer peaks appears to dominate in the chromatograms. As a reference, the pure 1.8 nm GNP was run by itself and seemed to elute slightly earlier than the dimer peak observed for Bfr. These trial runs were also examined with TEM to visualize the presence of encapsulated 1.8 nm GNP in Bfr.

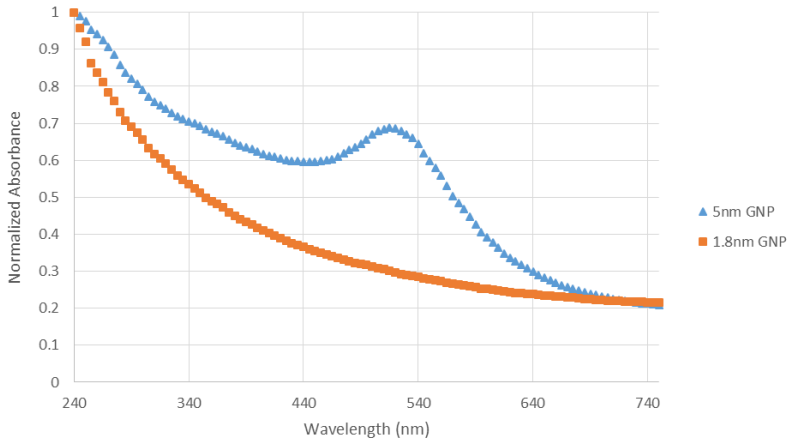

Figure 2.12: UV-Vis absorption spectrum of 1.8 and 5 nm GNP in aqueous buffer. The 5 nm GNP showed a clear absorption peak at the manufacturer specified absorption maxima of 518 nm. The 1.8 nm GNP, however, showed no observable 420 nm absorption peak, contrary to manufacturer specification.

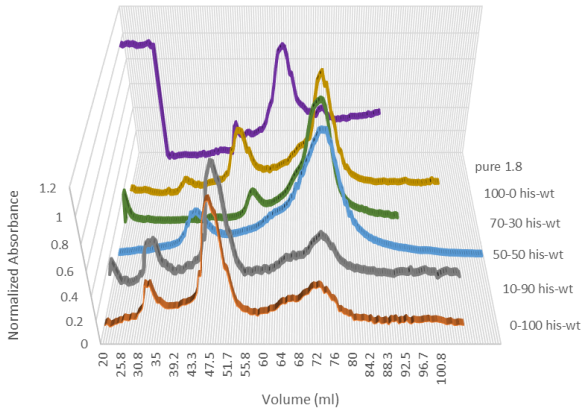

Figure 2.13: Encapsulation trials of 1.8 nm GNP with varying ratios of His6-tag/WT Bfr. The trials were run on a GE Sephacryl™ S-300 HR with the monitored wavelength of 280 nm.

In addition to these initial trials, further experiments were conducted altering the conditions for encapsulation. Encapsulation in the absence of GndHCl at varied temperatures were examined to rule out the possibility that GndHCl was negatively affecting association between 1.8 nm GNP and Bfr, and to explore alternative means of encapsulation. Three temperatures, 4, 25, and 50 °C were used to encapsulate 1.8 nm GNP in the absence of GndHCl using a ratio of His6-tag/WT Bfr of 50/50 (Figure 2.14). In these trials the previously observed dimer peak appeared to virtually disappear. This very dramatic change in elution profile may have resulted because the conditions were less disruptive. Using temperature as a strategy for encapsulation could potentially be advantageous as a future encapsulation methodology since it was very easy to regulate, and may be less disruptive.

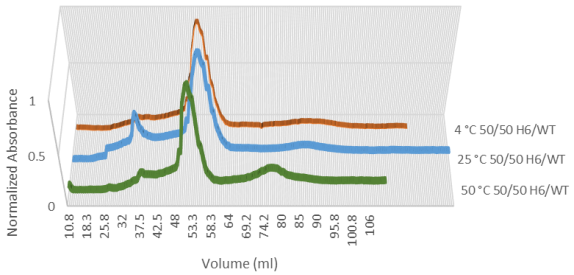

Figure 2.14: Encapsulation of 1.8 nm GNP under varying temperatures. The encapsulated 1.8 nm GNP was run on a GE Sephacryl™ S-300 HR resin, with a monitored wavelength of 280 nm. The three temperatures used were 4, 25, and 50 °C, each using a 50/50 His6-tag/WT ratio.

A control trial for 1.8 nm encapsulation was performed without any nickel sulphate present. In the absence of Ni^{2+} no coordination site on the surface of the 1.8 nm GNP would be available for the histidine groups on the inner surface of Bfr. (Figure 2.15). It was quite clear that there was a shoulder within the dimer peak of the control run. This shoulder was attributed to the free 1.8 nm GNP, which was not coordinated by any Bfr. The pure 1.8 nm GNP had an elution time identical to this shoulder on the dimer peak of the control.

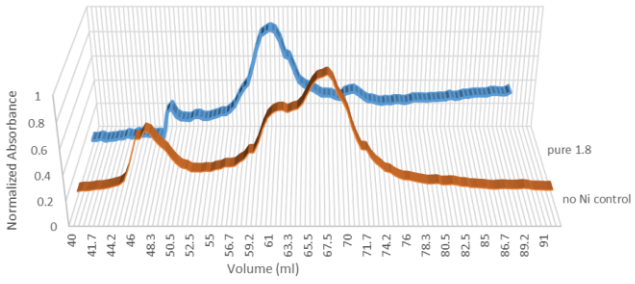

Figure 2.15: Negative control of encapsulated 1.8 nm GNP in Bfr. The samples were run on GE Sephacryl™ S-300 HR column, and the monitored wavelength was 280 nm. The control underwent the same encapsulation conditions as previously, but without the presence of nickel sulfate.

After much trial and analysis with attempts to encapsulate 1.8 nm GNP there was no clear evidence of successful, or proficient encapsulation within Bfr.

Subsequently, the 5 nm GNP candidate was explored briefly to attempt encapsulation of a GNP. The approach taken was meant to quickly assess whether it was possible or not to encapsulate this extremely large guest particle. The first attempt was with GndHCl as the declustering agent, and with a 60/40 ratio of His6-tag/WT Bfr, as has been shown previously to be optimal for both SF and ProQ® Sapphire 365 oligohistidine gel stain.[141] Attempts were also made to encapsulate without GndHCl, but with temperature increase, as with the 1.8 nm GNP. After encapsulation trials using GndHCl and temperature change the resulting solutions were separated on a GE Sephadex™ S-300 HR column (Figure 2.16). It was observed that the elution of the 5nm GNP was slightly earlier when using temperatures changes, which suggested that the GNP was associating with Bfr. Although it was thought that encapsulation of the larger 5 nm GNP would be less likely, it appeared to interact favourably with Bfr. TEM experiments would later confirm that there was indeed proper encapsulation, an interesting difference since the smaller 1.8 nm GNP did not appear to encapsulate.

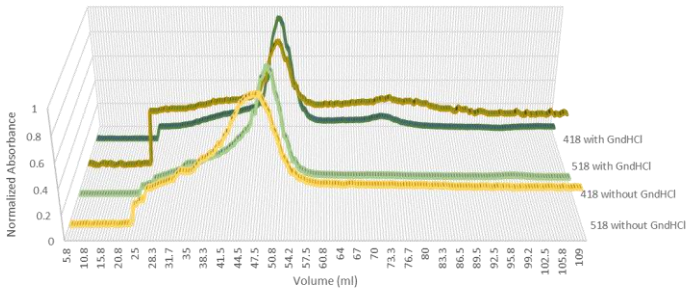

Figure 2.16 Encapsulation of 5 nm GNPs in Bfr separated on a GE Sephacryl™ S-300 HR resin. Two conditions were used, one with GndHCl as the declustering agent, one without. Each trial was monitored at the wavelengths of 418 nm and 518 nm, which corresponded to the heme in Bfr absorption maxima, and the 5 nm GNP absorption maxima, respectively. There was a slight shift in the elution time of 5 nm GNP to an earlier time point when no GndHCl was used.

In addition to the encapsulation conditions explored above, two control experiments were also conducted. One control was performed with 100% His6-tag Bfr, and another with 100% WT Bfr (Figure 2.17). Here a subtle, but observable shift in the elution times between the 100% His6-tag and the 100%

WT was observed. There was a clear shift in the 5 nm GNP elution between the two. The WT control had a 5 nm GNP elution time that was very similar to the elution time of the pure 5 nm GNP. The elution of the 100% His6-tag Bfr, as indicated by the 420 nm monitored wavelength, mirrored that of the encapsulated 5 nm GNP. TEM experiments would confirm encapsulation of GNP with the His6-tag Bfr control, but not with the WT control, which is elaborated on below. The efficiency of encapsulation of the 5 nm GNP was calculated using the extinction coefficient at 518 nm of 1.0×10^7 $M^{-1}cm^{-1}$, and the concentration of Bfr using the heme extinction coefficient of 1.09×10^5 ($M^{-1}cm^{-1}$) and extrapolating the Bfr concentration from this.[134] The yield was calculated to be approximately 13%, or one GNP encapsulated in every seven-eight Bfr cages. Use of 100% His6-tag Bfr appeared to be the optimal ratio for 5 nm GNP encapsulation.

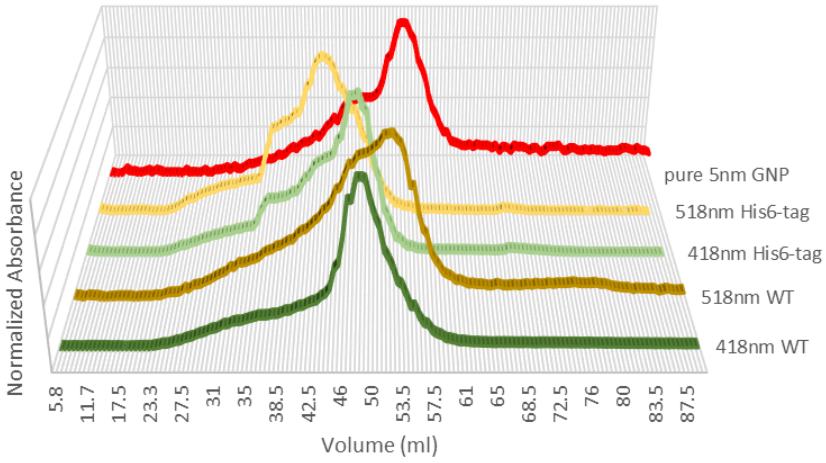

Figure 2.17: Encapsulated 5 nm GNP with a negative control separated on a GE Sephacryl™ S-300 HR resin. The elution was monitored with wavelengths 418 nm and 518 nm, corresponding to heme in Bfr, and 5 nm GNP, respectively. Two controls were run, one with 100% His6-tag Bfr, and one with 100% WT Bfr. The 100% His6-tag Bfr trial showed a clear shift in the elution time of the 5 nm GNP.

2.3.3. Fluorescence Measurements of Encapsulated SF

Streptavidin, a large tetrameric protein, was chosen as a guest protein to probe the capabilities of Bfr to accommodate entire proteins. By encapsulating SF it would aid develop of methodologies to encapsulate other complex and large guest molecules. Streptavidin has an approximate size of 5-6 nm [152], which was thought to be within the capabilities of the 8 nm interior diameter of Bfr to contain. A fluorescent label on streptavidin was used to permit fluorescence quenching measurements to determine the degree of protection of streptavidin from the external environment.

A commercially available fluorescein-labelled streptavidin, SF, was utilized to track and analyze encapsulation within Bfr (Figure 2.18). The first eluted peak from size exclusion chromatography exhibited an absorbance corresponding to the absorption maxima of both fluorescein (495 nm) and Bfr (418 nm) (Figure 2.19). Control experiments without Biotin-XNTA did not reveal the same absorption peaks. Analysis of these results indicated that SF was indeed associating with Bfr, and that both the His6-tag and Biotin-XNTA were essential for this association.

Figure 2.18: Streptavidin, a tetrameric beta barrel protein, has four biotin binding sites, which were utilized for the affinity mediator biotin-XNTA to encapsulate SF. Each beta-barrel is presented in a different colour, and the biotin molecules are displayed as red spheres. Image generated using PDB ID 3RY1 in pymol.

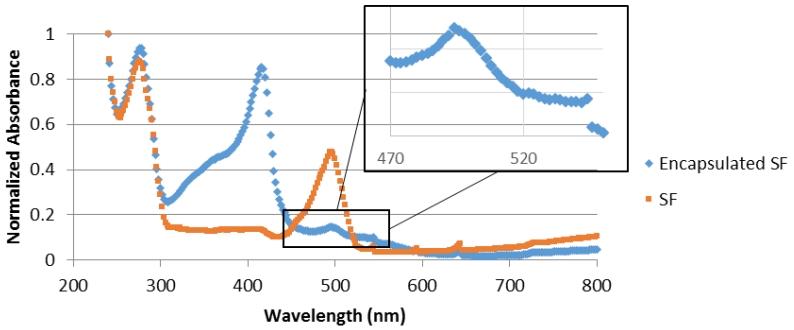

Figure 2.19: Absorption spectrum of encapsulated SF and free SF. There was an absorption peak at 495 nm in the encapsulated spectra, which corresponded to the absorption maxima of the fluorescent label of SF. This suggested that SF had been encapsualted within Bfr.

Each SF encapsulated sample was evaluated using fluorescence quenching studies. A lack of quenching would provide evidence that SF was protected by a protein-cage barrier, *i.e.* Bfr. Three quenching agents were used to evaluate encapsulation: iodide, dabsyl-glutamate, and black hole quencher® 10 (BHQ®10). Iodide is a static quencher[171], while dabsyl-glutamate and BHQ®10 both quenched based on Förster resonance energy transfer.[172,173] Dabsyl chloride was labelled with glutamate to ensure that it would not react with free amines on either of the proteins in solution. Experimental and theoretical data were used to calculate a theoretical FRET distance for both dabsyl-glutamate and BHQ®10 with SF. Using a model derived in the Visser lab, a theoretical FRET distance was calculated for both dabsyl-glutamate and BHQ®10.[174] FRET distances were approximately 4 and 5 nm for dabsyl-glutamate, and BHQ®10, respectively. The dipole orientation factor, refractive index of the medium, and the quantum yield were all approximated to 0.667, 1.4, and 0.5, respectively. Analysis of the x-ray structure of Bfr[135] provided an estimation of the protein shell width to be between 2.5 and 3 nm without solvation radius, electrostatics, or other factors considered. Both quenchers showed potential to quench fluorescence at this distance, though not all parameters were considered in this theoretical evaluation.

Both encapsulated and non-encapsulated SF were titrated with quencher and again separately with buffer to control for dilution effects.

Iodide, dabsyl-glutamate, and BHQ®10 were plotted with both the encapsulated and exposed SF (Figure 2.20). Encapsulated SF exhibited almost total absence of quenching over the course of titration of iodide, whereas Dabsyl-glutamate showed some quenching over titration, and BHQ®10 showed essentially complete quenching. When compared to the theoretical FRET distances and the quenching trend observed for Dabsyl-glutamate and BHQ®10 it is reasonable to expect that more quenching should be observed for BHQ®10 due to its predicted larger FRET distance. Therefore the quenching affect with BHQ®10 should not necessarily indicate exposure of SF.

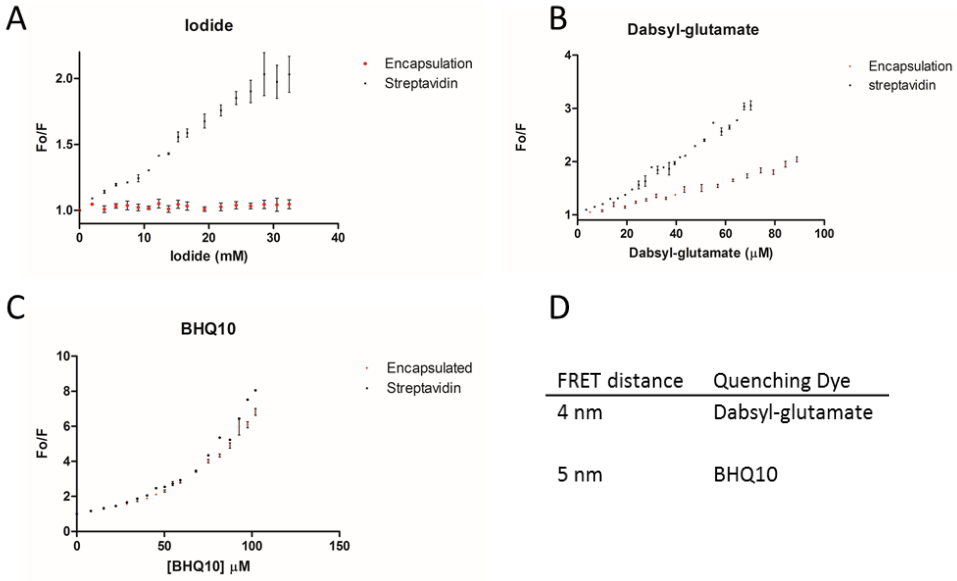

Figure 2.20: Titrations of quencher into solutions of free SF and encapsulated SF were transformed into Stern-Volmer plots. Titration of three different quenchers were used to validate encapsulation of SF in Bfr. Iodide (A) showed an apparent total absence of quenching, whereas dabsyl-glutamate (B) and BHQ10 (C) showed some level of quenching. The expected reason for increased quenching between dabsyl-glutamate and BHQ10 was that the two FRET based quenchers had FRET distances larger than the protein shell (D).

2.3.4. TEM Conditions and Trials

Confirmation of SF encapsulation was made by employing transmission electron microscopy (TEM). This technique had been successfully utilized to visualize encapsulated guest molecules within virus-like particles, but had not previously been employed for Bfr.[175,176] Three TEM stains were used: uranyl acetate, molybdic acid, and phosphotungstic acid to highlight Bfr and determine the presence of internalized guest molecules within.[177] Due to the intrinsic pores found in the structure of Bfr, it was hypothesized that atom sized stains would be able to penetrate the core, as evidenced with pores on viruses.[13,15,124] SF was large enough to consume most of the interior space in Bfr and thus any stain would be largely excluded from the interior. A lack of stain in the interior would indicate the encapsulation of SF, as monitored by TEM.

Analysis of commercial apo-ferritin and apo-Bfr by TEM showed obvious stain penetration with both uranyl acetate and molybdic acid into the interiors of these multisubunit proteins (Figure 2.21). The penetration of stain confirmed that single atom stains were small enough to transit across the native pores found in intact Bfr. In addition to these preliminary trials a new image processing technique was explored. This processing technique is called single particle analysis, and the software used to explore this technique was called EMAN2.[178] This technique was first evaluated with apo-Bfr without encapsulated materials, and improved TEM-obtained image quality (Figure 2.22). The measured size of apo-Bfr matched well with crystal data, giving an outer diameter of 11.7 nm and inner diameter of 4.8 nm.

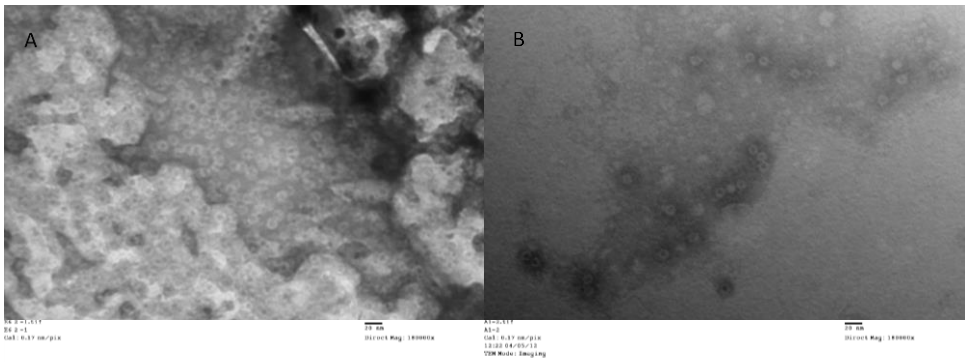

Figure 2.21: Negatively stained TEM images of horse apo-ferritin and apo-Bfr. The stain used with apo-ferritin (A) was uranyl acetate, and molybdic acid was used with apo-Bfr (B). The stain clearly penetrated the interior of apo-Bfr, which made Bfr appear as a donut shaped 2-D object.

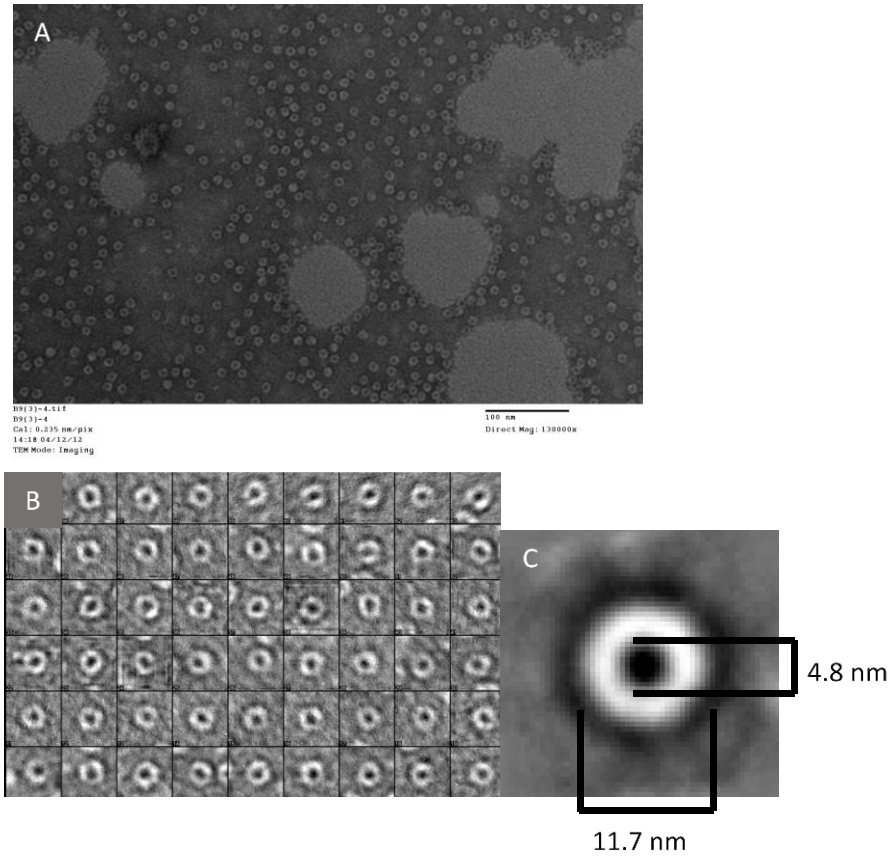

Figure 2.22: A negatively stained image of apo-Bfr using 0.5 % molybdic acid (A). Multiple images were used, and hundreds of single particles gathered (B) were used to generate a reference free class in EMAN2 (C). Measurement of this final image matched the expected size of apo-Bfr based on crystallographic data[179].

This staining technique was used further to probe the presence of encapsulated SF within Bfr. After many staining trials, single particle analysis was utilized to help clarify images.[168] Multiple single images of encapsulated SF in Bfr were averaged to try and obtain a clarified picture. A total of 479 particles from multiple images were analyzed to generate a conserved average image of encapsulated SF in Bfr (Figure 2.23). In this case the outer diameter remained similar to the native Bfr with a diameter of 11.6 nm, while the inner cavity contained a particle of approximately 3 nm in diameter. The expected size of SF was larger than this, but image processing may have resulted in some reduction of the diameter. Some unprocessed images (Figure 2.23B) showed an explusion zone on the interior of Bfr that measured around 4.5 nm, much closer to the SF diameter. The unprocessed images for encapsulated SF showed largely covered surfaces (Figure 2.23) with potentially exposed regions. These exposed regions could also be a result of the non-native conditions of the TEM imaging grids. Despite possible incomplete coverage, there was clear evidence of the interaction between host and guest molecules. Protection of the guest molecule from the external environment as shown by TEM is consistent with conclusions drawn from the fluorescence quenching results.

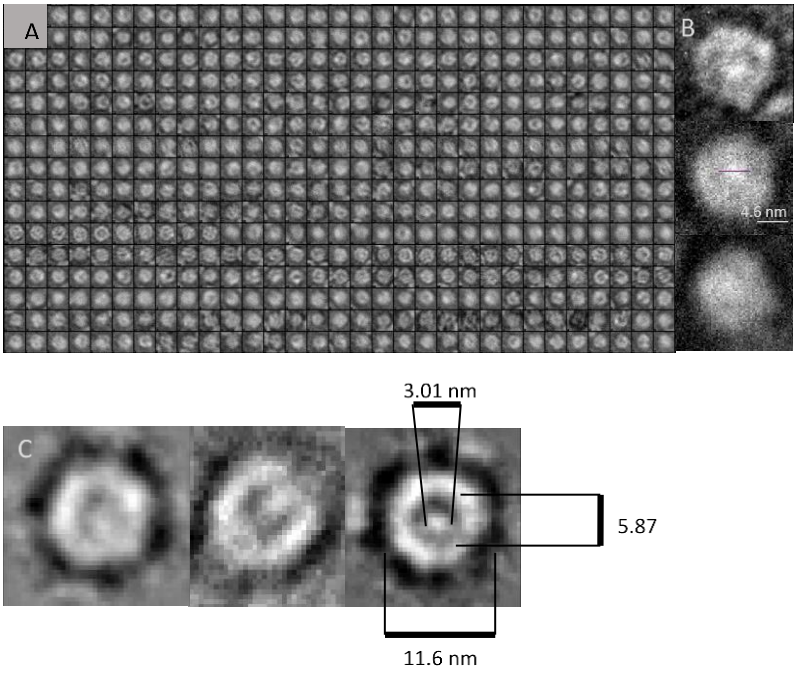

Figure 2.23: Single particle analysis of encapsulated SF in Bfr. Over 400 single particles (A) were collected and then averaged into three classes. Individual particles selected from the pool of 400 images that showed to be especially well resolved with a zone of excluded stain in the interior with a diameter of approximately 4.5 nm (B). These three classes (C) seem to have an excluded area of stain in the interior of approximately 3 nm.

One TEM grid condition used in the investigation of encapsulated SF resulted in interesting formation of two-dimensional crystals. This may be of future importance for study of structural aspects of the Bfr platform. By forming two-dimensional crystals one may be able to extract more precise structural data by electron beam scattering patterns. A technique of this nature would require an equipped electron microscope to collect the diffracted signal. Interestingly, crystals were observed using solution conditions with only eight times higher concentration of protein than was previously used, and no other additives (Figure 2.24).

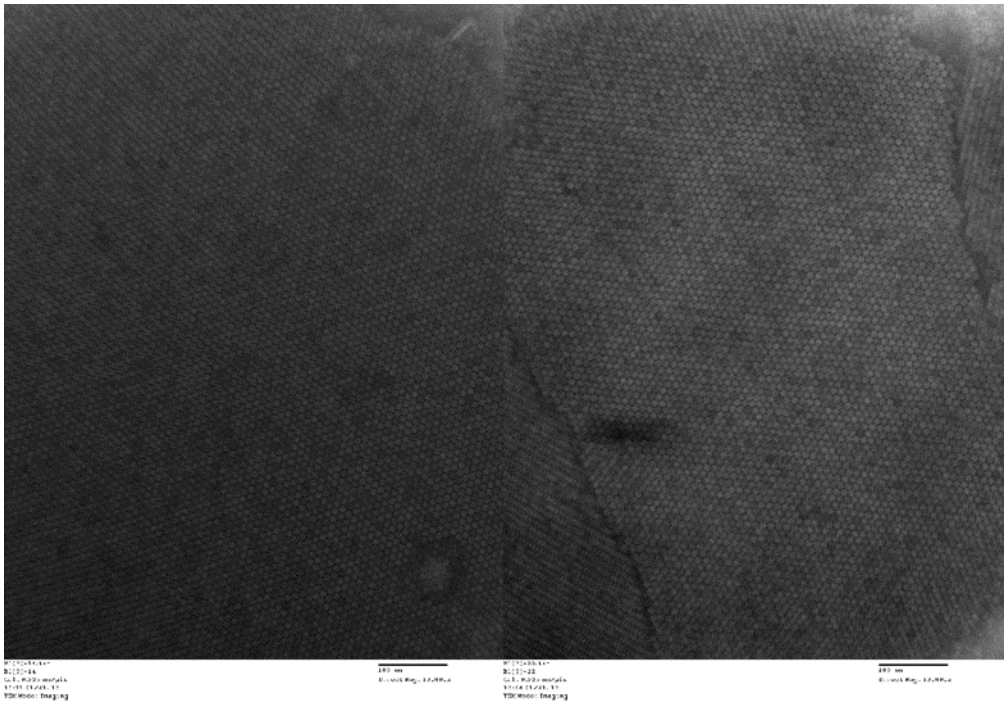

Figure 2.24: Formation of two dimensional crystals of SF encapsulated in 60/40 His6-tag/WT Bfr in TEM imaging. Using eight times the concentration of encapsulated SF with 60/40 His6/WT Bfr it was possible to generate two dimensional crystals. The image was stained with 0.5 % molybdic acid, as before.

In addition to a large biological molecule, the encapsultion of inorganic 1.8 and 5 nm GNP were also investigated. Commercially available NTA-surface modified GNPs were studied as paradigms for encapsulation of inorganic nanoparticles. TEM was performed on both encapsulated and free 1.8 and 5 nm GNP. Free GNP was investigated to determine how the polymer coating surrounding the GNP would appear in images. Since the polymer decorating the GNP with NTA functionalities was organic it would appear as a shell surrounding the GNP in a negatively stained image on TEM. This polymer coating might have falsely been perceived as Bfr protein coating the GNP. TEM analysis of free 5 nm GNP clearly demonstrated that the surrounding polymer was not as thick as the protein shell of Bfr (Figure 2.25). When measured, the protein layer of Bfr was 3-4 nm in width while the polymer on GNP was only detectable on the highest resolved images with a width of approximately 1.5-2 nm. The 1.8 nm GNP approached the imaging limitations, and seemed to vary in diameter (Figure 2.26). It was challenging to acquire images of acceptable quality with the 1.8 nm GNP, explainable by a dramatic difference in the number of gold atoms found in the 1.8 nm particle. In addition to the difficulty associated with imaging, the 1.8 nm GNPs had high variability in size, with particles larger than 1.8 nm by almost two times.

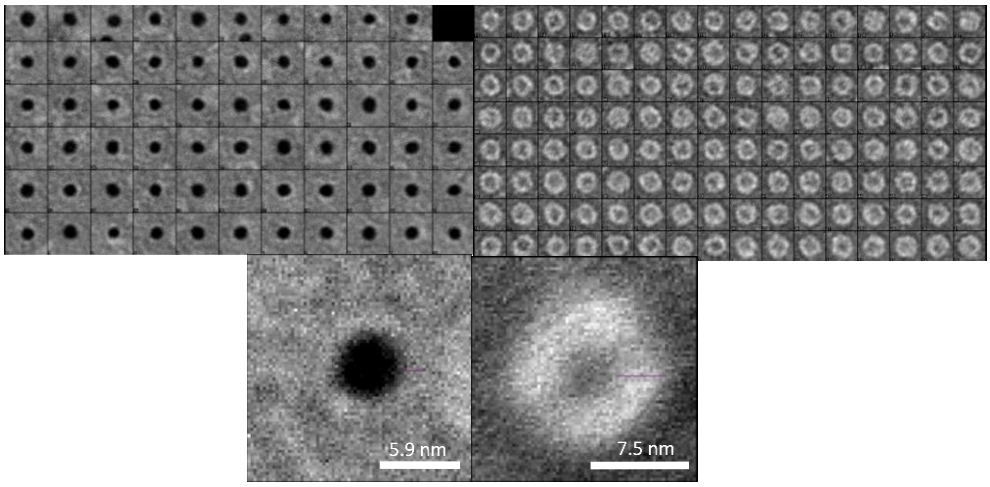

Figure 2.25: Comparative TEM images of free 5 nm GNP (A), and empty Bfr (B). There was an observable shell around the 5 nm GNP, which was the polymer containing the NTA functionality. When measured, this polymer was no larger than 1.8 nm, whereas the thickness of the protein shell of Bfr could be as large as 4 nm when measured.

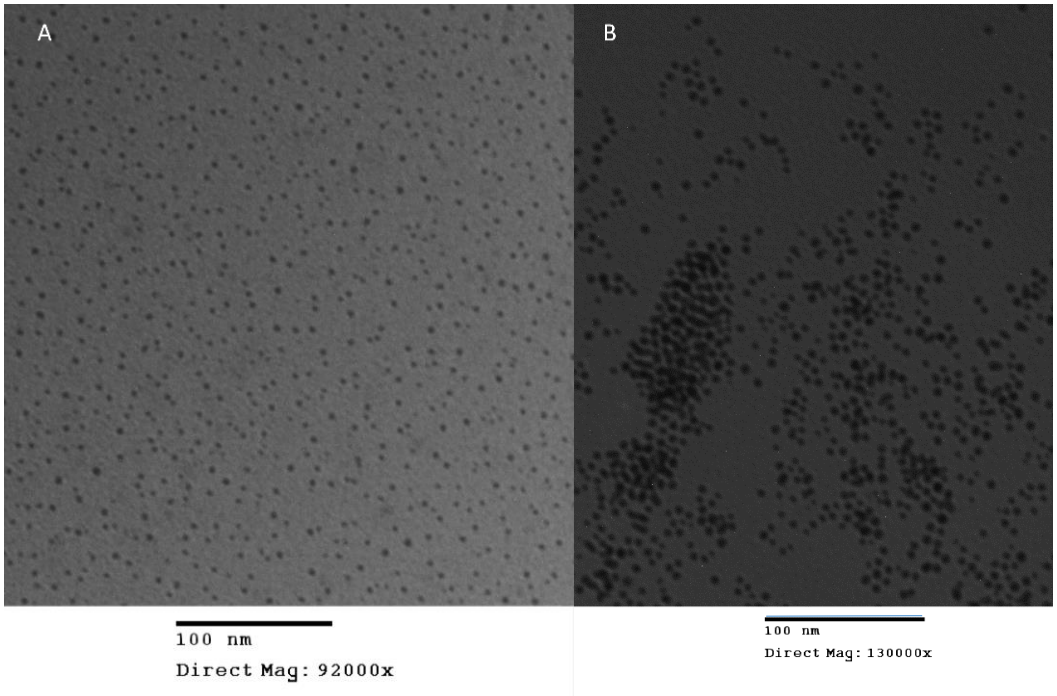

Figure 2.26: TEM images of free 1.8 nm (A) and 5 nm (B) GNP without any negative stain. The 1.8 nm GNP was measured between 1.8 and 3 nm in diameter, and the 5 nm GNP was measured more uniformly around 5 nm in diameter.

The 1.8 nm GNP was the first nanoparticle investigated for encapsulation within apo-Bfr. The optimal ratio for encapsulation was determined previously by Robert Taylor of the Honek laboratory to be 50/50

His6-tag/WT Bfr. Trials with 50/50 His6-tag/WT Bfr using 8 M GndHCl as a declusterant were imaged after being separated on a GE Sephacryl^{TM} S-300 HR resin (Figure 2.27). Although there were a select few encapsulated 1.8 nm GNPs, the fraction of encapsulation was extremely small. Some particles highlighted were as large as 5 nm and ranged within 1.8 to 3 nm. Those particles that where 1.8 nm were the most challenging to differentiate in the TEM image due to their poor contrast. Thus, further imaging trials were pursued to obtain more definitive proof of encapsulation.

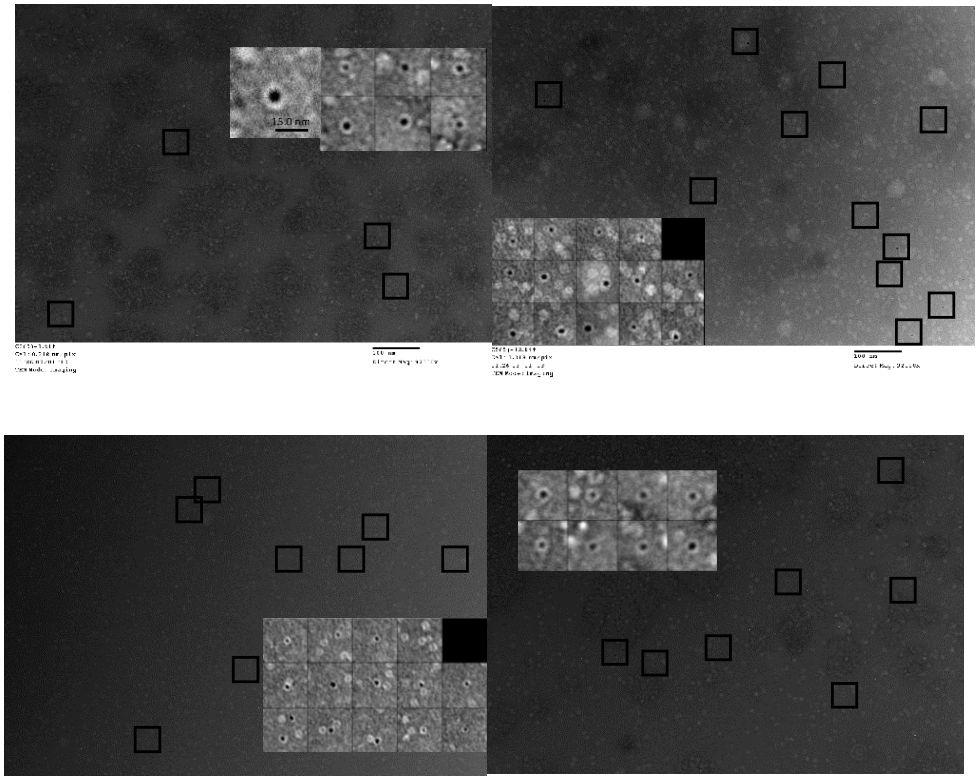

Figure 2.27: TEM images of the encapsulated 1.8 nm GNP in apo-Bfr. Highlighted in the boxes are the images that have been enlarged in the insert. There were clearly highly electron dense guest molecules in the centre of Bfr. This was attributed to GNP because it was more electron dense than the background stain.

In order to circumvent the issue of contrast with the small 1.8 nm GNP, another staining technique was employed when imaging the

encapsulated 1.8 nm GNP. By using the comparatively larger phosphotungstic acid ($H_3PW_{12}O_{40}$) negative stain, it was hypothesized that the stain would be unable to penetrate the core of Bfr through the native pores. To prove this, His6-tag Bfr without any encapsulated guests was imaged in the presence of phosphotungstic acid (Figure 2.28). These images clearly demonstrated Bfr without the previously observed stain penetration of the interior. This was a highly advantageous technique to probe 1.8 nm GNP encapsulation because any electron dense spot in the centre of Bfr would be the result of encapsulated GNP and not just a stain artifact. In addition, stain exclusion would improve the contrast of small GNP within Bfr. Attempts were made to image under these conditions using the same methodology to prepare encapsulated 1.8 nm GNP as before (Figure 2.29). These images, however, revealed no encapsulated GNP. It was decided that the declusterant used to disrupt the Bfr shell should be examined for its effectiveness. A series of incubation temperatures were used and examined on TEM with the phosphotungstic acid negative stain. After analyzing the TEM images it was clear that there was not an improvement in the efficiency of encapsulation (Figure 2.30). Unfortunately, it was not possible to get better encapsulation yields than what was observed here. This was especially odd in light of the success of the much larger 5 nm GNP images. It seemed to be contrary to logical reasoning that a smaller particle would be far less favourable for encapsulation.

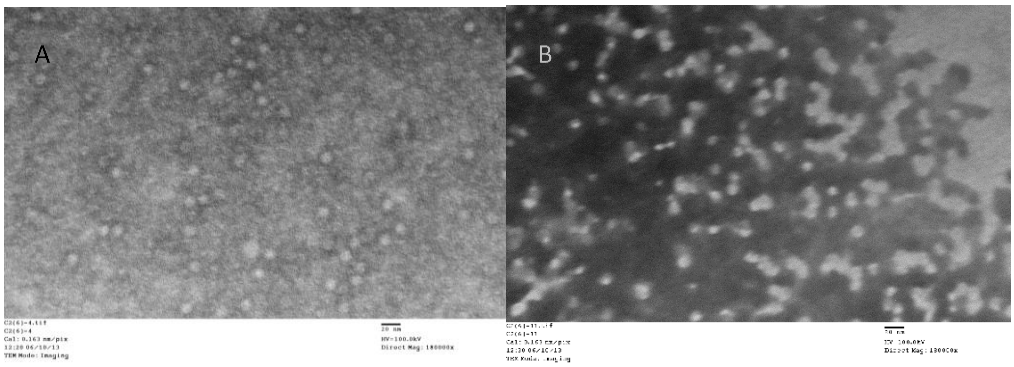

Figure 2.28: TEM image of apo-Bfr using phosphotungstic acid as a negative stain. Both images were generated using 0.5 % phosphotungstic acid. Image B had much more contrast than A, but both were generated using the same stain concentration, and importantly both lacked stain penetration to the interior.

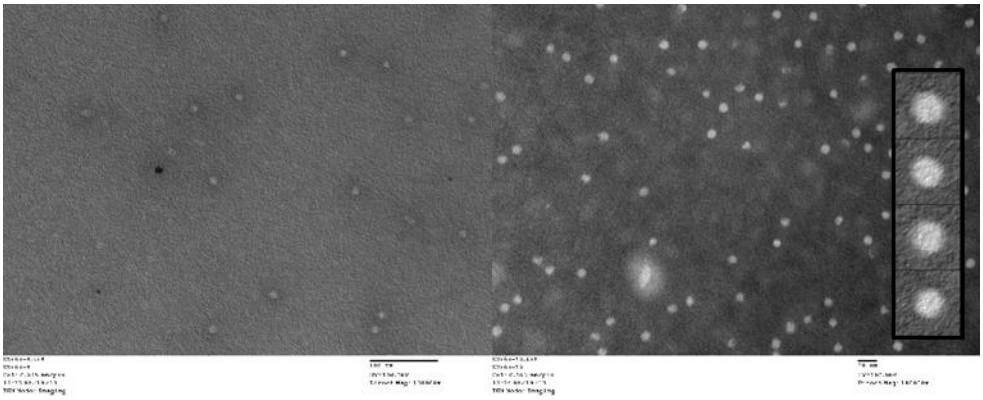

Figure 2.29: TEM images of 1.8 nm GNP encapsulated in Bfr using phosphotungstic acid. Although the encapsulation conditions were similar to previous conditions, the images did not reveal any encapsulated 1.8 nm GNP. The insert showed that there was clearly no stain penetration.

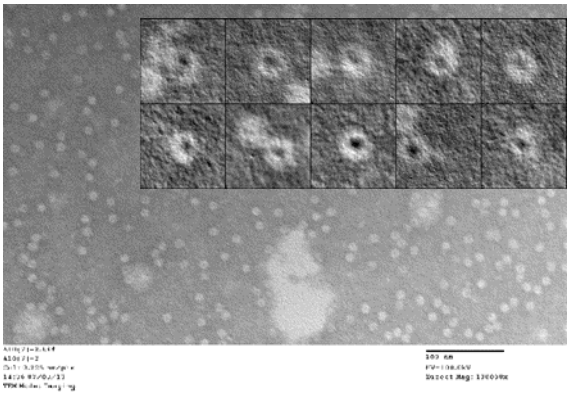

Figure 2.30: TEM images of encapsulated 1.8 nm GNP in Bfr stained with phosphotungstic acid. There were scarcely any 1.8 nm GNP encapsulated in Bfr. The insert showed some potential evidence for encapsulated 1.8 nm GNP in Bfr.

The encapsulated 5 nm GNPs were analyzed under TEM using molybdic acid after being separated on GE Sephacryl^{TM} S-300 HR resin. The encapsulated 5 nm GNP images exhibited a clear protein coat fully covering the surface (Figure 2.31). In addition, all the GNPs present in these images were clearly encapsulated. When compared, the width of the protein coat matched the width of the measured shell of apo-Bfr. Analysis with the EMAN2 program was performed as before, and it was possible to derive an averaged measurement for the radius of the host-guest complex (Figure 2.32). Slight increases in diameter were observed with an increase of approximately 2-3 nm based on the averaged image. Such increases suggested conformational changes to the protein coat structure to accommodate this large guest molecule. Stable conformational changes appeared to be allowable as a result of the compensatory number of multiple affinity interactions between host and guest. For the SF encapsulation study tetrameric SF had a maximum of four possible affinity interactions, whereas the gold nanoparticle had several NTA affinity ligands. The GNP was 5 nm in diameter with an approximate 1.5 nm extension in thickness of the shell due to the addition of a polymer terminated with NTA linkers. Based on the diameter of a sphere of 5 nm the absolute maximum number of affinity tags can be approximated to 130. It was likely much lower than 130, but this still gives a sense of the difference in number of affinity interaction between SF and 5 nm GNP.

To address the question of why the 1.8 nm GNP was less successful than the 5 nm GNP for encapsulation within Bfr, it could be theorized that the GNP was acting more as a scaffold for Bfr rather than a passive guest. The 5 nm GNP was of a similar size and shape to the native interior volume of Bfr, and could have built the Bfr shell around it. Whereas the 1.8 nm GNP was significantly smaller than the internal volume of Bfr, and may have not been an ideal template to complement the native self-assembly of Bfr. In the case of the 1.8 nm GNP, fewer affinity ligands may have been more ideal. Many affinity ligands on 1.8 nm GNP may have dominated the interaction between GNP and Bfr over Bfr-Bfr subunits. If a single affinity ligand existed between 1.8 nm

GNPs and Bfr, self-assembly of Bfr may have instead been dominated by the native interaction energy between subunits. Future nanoparticle encapsulation should take into consideration this effect in choosing the size of guest and the number of affinity interactions it possesses (Figure 2.33).

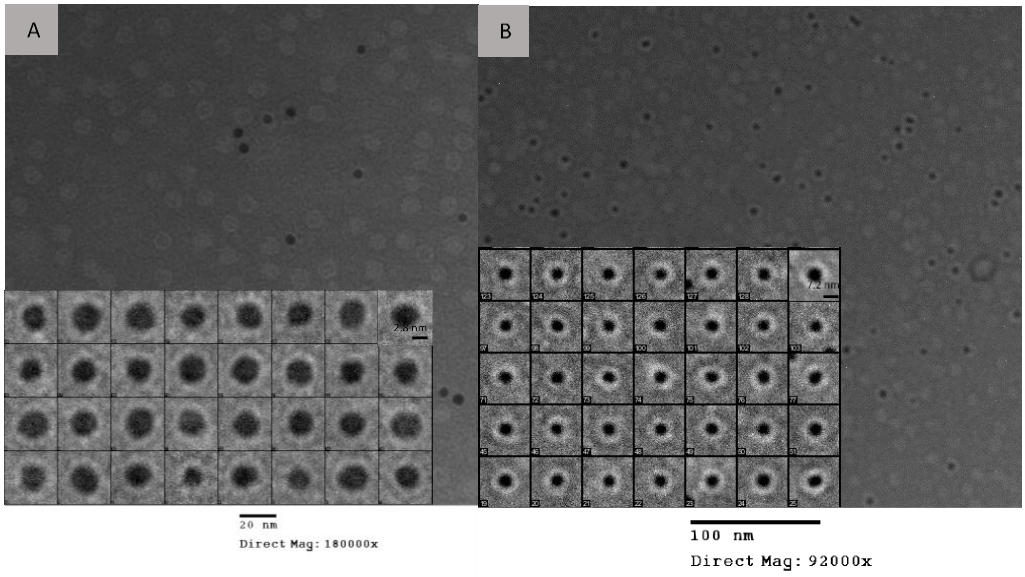

Figure 2.31: TEM images of free and encapsulated 5 nm GNP in 100% His6-tag Bfr. A WT Bfr negative control (A) revealed 5 nm GNPs not encapsulated, as highlighted in the insert. A thin polymer coating of an approximate width of 1.5 nm. The 5 nm GNP was encapsulated within 100% His6-tag Bfr, as was evidenced by the extremely electron dense interior within Bfr, and the width of the protein shell. The protein shell was measured as approximately 3.7 nm, similar to the width of native Bfr observed with TEM.

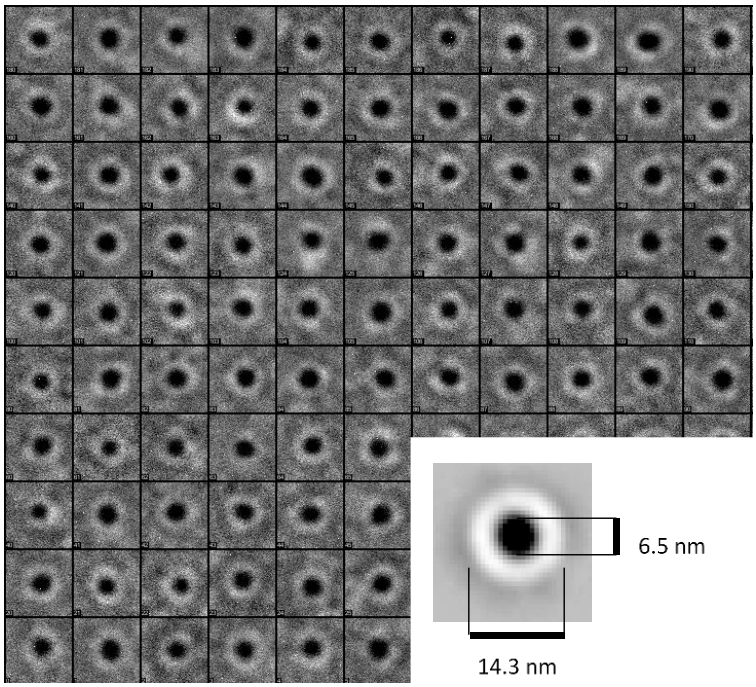

Figure 2.32: Single particle analysis of 5 nm GNP encapsulated within 100% His6-tag Bfr. The reference free class of these images generated a particle with sizes slightly larger than previously seen. The interior diameter appeared to be closer to the size of the GNP, and the exterior diameter had grown by two nanometers to approximately 14 nm.

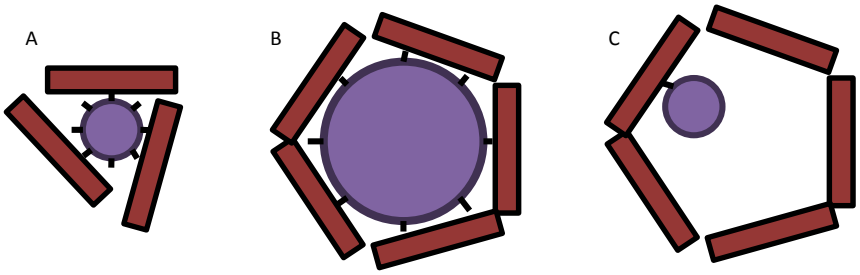

Figure 2.33: Geometrical factors and the number of affinity interactions determined the success and failure of 5 nm and 1.8 nm GNP encapsulation. By having multiple affinity ligands on the 1.8 nm GNP it did not act as an ideal scaffold for Bfr to build onto (A). The 5 nm GNP, however, matched the native internal size of Bfr, appropriately, and thus was a good scaffold to build Bfr onto (B). If instead only one affinity interaction was available between Bfr and the 1.8 nm GNP, then the self-assembly of Bfr might not be disrupted by competing affinity interactions.

2.3.5. Structural Investigation of the Dimer-24mer Equilibrium, and the Significance of Heme

Investigation into the self-assembly of 24mer Bfr was an ongoing side project during the fulfilment of this M.Sc. degree. As has been stated, Bfr and ferritins have been documented as existing in equilibrium between two states: a fully formed 24mer, and a dimer. Not much is known of the intermediate forms occupied between these two states. In the process of performing experiments and controls, it was noted that in both size exclusion chromatography and native PAGE the presence of heme in the Bfr structure increased the population of 24mer (Figure 2.34). Heme alone seemed to be contributing to the stabilization of the 24mer structure. This was curious because heme is found at the interface between dimers. It was not expected that a missing element between dimers would strengthen the full 24mer species. Differential scanning calorimetry was attempted to evaluate the claim that the complex was strengthened by the presence of heme. MS was approached, as well, as a method to examine this claim, both of which were unsuccessful. The data from the size exclusion and native PAGE suggest that heme strengthened the 24mer state, which would make heme an important structural factor for Bfr.

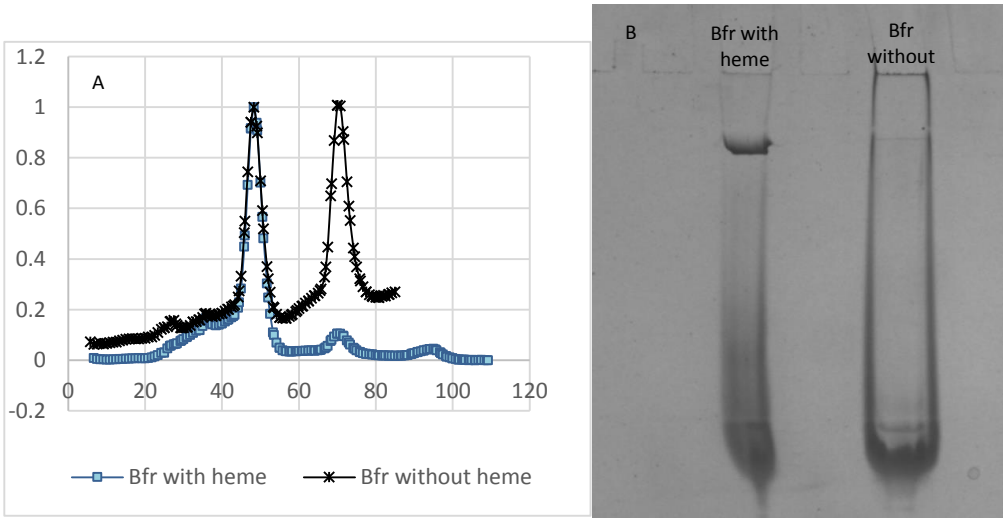

Figure 2.34 : Analysis of the effects of heme with respect to the equilibrium of Bfr between dimer and 24mer states. Bfr with and without heme was run on a GE Sephacryl™ S-300 HR size exclusion resin (A). When the heme containing Bfr was run on a native PAGE (B) it would run with a high molecular weight band and low molecular weight band, whereas the Bfr without heme ran as only one lower molecular weight band.

Differential scanning calorimetry was performed on Bfr, but a distinct transition temperature was undetectable. This was not wholly unexpected since there would be a litany of individual unfolding events taking place at varied temperatures. This likely helped to obscure the overall reading, and little information was gathered from this technique. MS was explored as well to try and utilize some previously derived experimental conditions for observing native conformations of proteins.[166] Proteins were suspended in 200 and 20 mM ammonium acetate solutions before running on an ESI-QTOF MS. His6-tag Bfr with heme re-incorporated was run in these native conditions. Some success was made in generating lower charge state peaks in the spectrum (Figure 2.35). Low charge state ions are expected for the native structures of proteins in the gas phase.[180] There was a clear shift to these ions from the typical spectrum generated. The spectrum range would likely have to be extended greatly to accommodate the large mass of multimeric proteins. It was not possible to scan with the same range that other experimenters have used, reaching a maximum range of 4000 m/z, which may have not have been enough to capture larger complexes.[166] In addition, the nanospray ESI-Q-TOF was not modified in the exact fashion as in these previous experiments.[166] However, these initial results suggested that it is highly likely to examine Bfr in a non-denatured form with MS.[167] Unfortunately, the instrument used to run these experiments was under repairs shortly after obtaining these results, and follow up experiments could not be performed.

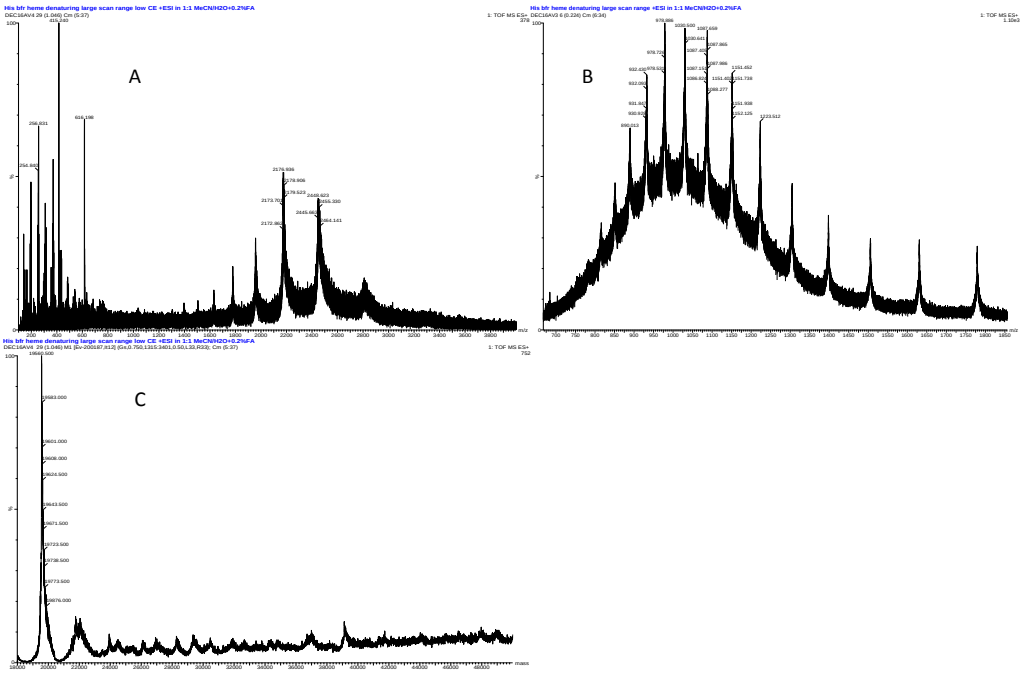

Figure 2.35: Native protein MS trials using heme containing Bfr. Bfr with heme was exchanged into a 20 mM ammonium acetate solution and run on a nanospray ESI-QTOF mass spectrometer (A). When run in denaturing conditions the spectrum contained higher charge state ions, as was usual (B). When the native spectrum was deconvoluted it revealed a protein mass of 19560 Da, as was expected for the monomeric protein.

2.3.6. Conclusion

By demonstrating the encapsulation of protein and nanoparticle guest molecules Bfr was evaluated as a platform to encapsulate foreign guests. Through chromatographic, fluorescent, and TEM, SF was able to be characterized as encapsulated within Bfr. The 1.8 nm and 5 nm GNPs were evaluated, and only the 5 nm GNP was able to be encapsulated, as confirmed with chromatography and TEM. It was curious that the 1.8 nm GNP did not encapsulate within Bfr, whereas the much larger 5 nm GNP was encapsulated to a high degree. It has been hypothesized that the reason for this discrepancy might be due to both the size and the number of affinity interactions. The 5 nm GNP complimented the interior diameter of Bfr, and may have acted as a scaffold. The 1.8 nm GNP too acted as a scaffold, but with disproportionate geometry to the Bfr interior. If the 1.8 nm GNP could be synthesized with one or two affinity ligands it might act less like a scaffold. This balance between size and number of affinity ligands displayed will play an integral aspect in the

decision for future guests. Larger guests that may cause minor perturbations in the native structure of Bfr may be compensated for by numerous affinity interactions. With both SF and the 5 nm GNP it was demonstrated that the affinity interaction was critical for the specific encapsulation of the guest particle within the host Bfr. Preliminary results were also presented that suggest that the heme cofactor was important for the formation of the 24mer complex. This was shown with size exclusion and with native PAGE. The factors that heme had on the formation of 24mer Bfr are unknown, but the evidence does suggest that it contributes to a shift in the equilibrium between the dimer and 24mer state.

3. Chapter 3: Cofactor Modification

3.1. Introduction

In the ferritin superfamily of proteins, Bfr is the only family member that contains heme cofactors. Heme is protoporphyrin IX, which is protoporphyrin with an iron atom in the centre of the porphyrin ring. In the context of Bfr, the heme cofactors are coordinated by two methionines, M52, from separate protomers (Figure 3.1). As is observed, the heme binding pocket is on the inner face of Bfr with propionate groups exposed and pointing to the inside of the cage protein. It was hypothesized that by modifying the propionate groups little would be altered in hemes ability to be coordinated by Bfr. Heme propionate groups exposed in this nature provided a unique opportunity for adding an array of functionalities and ligands to heme, and thus to Bfr. In addition, increased complexity of heme labelling could be obtained by individually modifying propionate groups[98] (Figure 3.2). These factors make heme an important and ideal cofactor to explore for further development of Bfr as a platform for bionanotechnology.

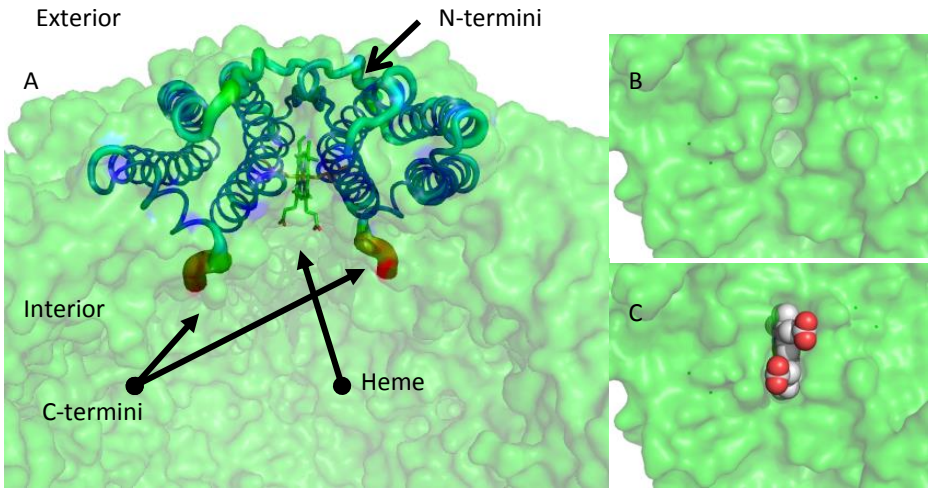

Figure 3.1: A crystallographic image of the heme binding pocket of Bfr displaying the heme propionates facing the interior space, and the C and N termini are shown facing the interior and exterior, respectively (A). The heme binding pocket (B) clearly is on the interior face, and the propionate groups are solvent exposed (C).

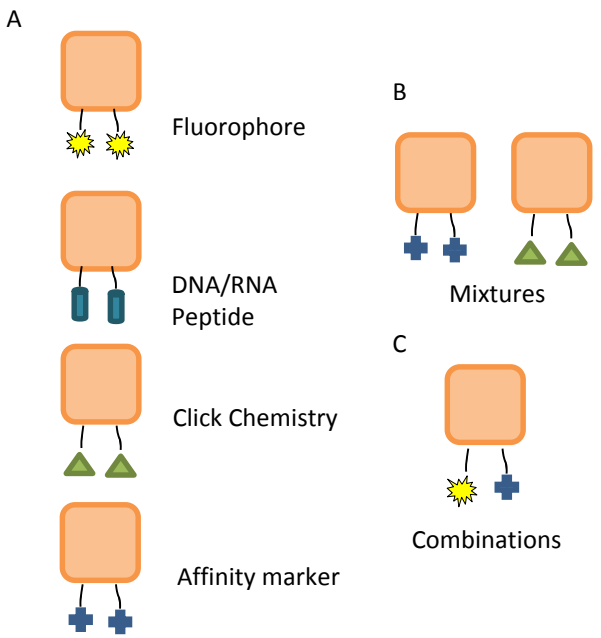

Figure 3.2: Potential labels for heme propionate groups (A). Alternatively labeled hemes could be mixed within the same Bfr 24mer to add additional complexity (B). Alternatively, two alternate labels could also be combined on a single heme (C).

In this chapter heme modification of the propionate groups will be explored with a variety of functionalities. Heme modification was primarily examined with fluorescent labels to develop a proof of principle for the ability to label heme with large fluorescent molecules and then incorporate them into Bfr. Modifications of the propionate groups of heme have been made and successfully incorporated back into myoglobin in previous studies[95], and so there is precedence for functionalizing heme in this way. The fluorophores explored were Lucifer yellow (LY), a coumarin derivative (DCCH), and two fluorescein derivatives (FSTC, AAF) (Figure 3.3). Two non-fluorescent molecules were also labelled onto heme: N-butylamine (NBA) and an NTA derivative (Lysine-NTA) (Figure 3.3).

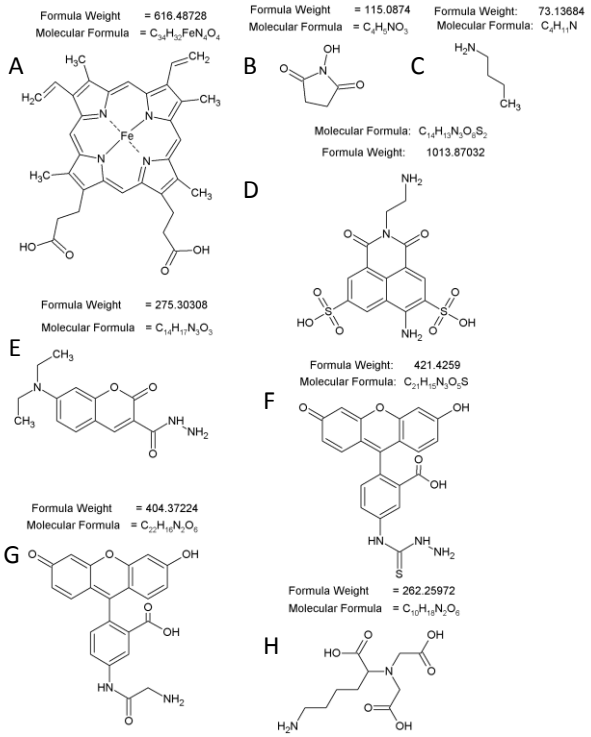

Figure 3.3: Structures of heme (A), NHS (B), NBA (C), LY (D), DCCH (E), FSTC (F), AAF (G), and lysine-NTA (H).

The reaction used to label heme propionate groups followed an activation scheme where the propionates were reacted with a carbodiimide and an N-hydroxysuccinimide (NHS) producing heme-NHS. Heme-NHS served as a semi-stable intermediate, which could be used directly to label heme with molecules containing primary amines or hydrazides (Figure 3.4). In earlier work performed by Denise Lieuson of the Honek laboratory, hydroxybenzotriazole was used in combination with a carbodiimide, but eventually the heme-NHS preparation method was adopted for all heme labelling experiments. Heme was modified out of the protein environment, which was an advantage of this process, and then reinserted into the protein architecture. This allowed for stringent conditions to be used without the associated risks of damage to the protein. This chapter will explore the labelling, purification, and incorporation of modified heme (mod-hemes) into His6-tag Bfr.

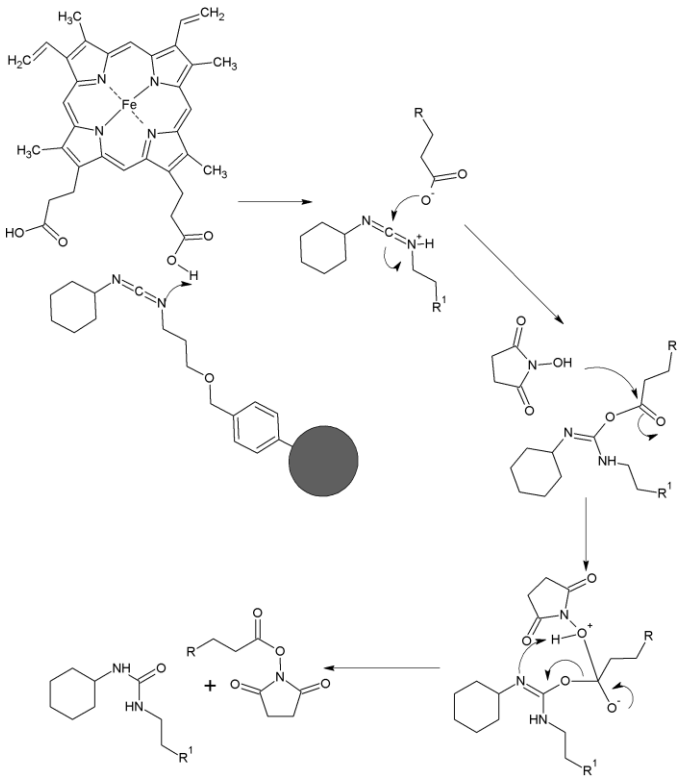

Figure 3.4: Reaction mechanism for the synthesis of heme-NHS using a polystyrene linked carbodiimide.

3.2. Materials and Methods

All materials and methods for this section of the thesis are listed below otherwise they have been listed in chapter 2.

3.2.1. Materials

Hemin (Sigma-Aldrich, Buchs, Switzerland), PS-carbodiimide (Biotage, Hengoed, United Kingdom), N-Hydroxysuccinimide (1-Hydroxy-2,5-pyrrolidinedione) (Sigma-Aldrich, Louis, MO, USA), 5-(Aminoacetamido)fluorescein (fluoresceinyl glycine amide) (Molecular Probes® Life Technologies, Eugene, OR, USA), 7-Diethylaminocoumarin (Molecular Probes® Life Technologies, Eugene, OR, USA), Nα,Nα-Bis(carboxymethyl)-L-lysine (Sigma-Aldrich, Buchs, Switzerland), N-butylamine (Spruce Street, Saint Louis, MO, USA), Fluorescein-5-Thiosemicarbazide (Molecular Probes® Life Technologies, Eugene, OR, USA), Lucifer yellow ethylenediamine (Molecular Probes® Life Technologies,

Eugene, OR, USA), Biotage® KP-C18-HS SNAP column (Charlotte, NC 28269 U.S.A), GE Sephadex™ LH-20 (GE Life Sciences Quebec, Canada), GE Sephadex™ G-25 Fine (GE Life Sciences Quebec, Canada), Corning® half-area black 96 well microplate (Corning®, Lowell, MA, USA), Dimethylformamaide from a Sure-Seal™ bottle was stored over dry 4 Å molecular sieves (Sigma-Aldrich, Sheboygan Falls, WI, USA), and Dimethyl Sulfoxide from a Sure-Seal™ bottle was stored over dry 4 Å molecular sieves (Sigma-Aldrich, Sheboygan Falls, WI, USA) were used for synthesis and purification.

3.2.2. Safety

All solvents were handled with appropriate glove wear, laboratory coats, googles, and in a fume hood. Chromatography using solvents was performed in a fume hood, and silica resins and TLC plates were disposed of correctly through the hazardous waste management facility. All biological substances, such as bacterial cultures, were handled in accordance to biological level 1 safety environments and either autoclaved or bleached overnight before disposed in a biohazardous waste container.

3.2.3. Heme Analogs

Heme-NHS was synthesized by adding hemin ((Chloro(protoporphyrin)iron(III); 200 mg, 0.307 mmols) and PS-carbodiimide (954mg, 2.8 equiv., 1.3 mmol/g) to 3.2 ml of anhydrous DMF with stirring at 23 °C for 10 minutes. NHS (88 mg, 2.5 equiv., 0.76 mmol) was added to this solution and stirred at 100 °C for an hour in a Biotage® Initiator microwave synthesizer (Scheme 1). After an hour, the solution was allowed to come to room temperature and the PS-carbodiimide was removed by running the solution through a column with glass wool packed at the bottom. The flow through solution was precipitated into 10 times the volume of chilled isopropanol and centrifuged at 5800 rpm for 10 minutes in a VWR clinical 100 centrifuge. The pellet was collected, dried in vacuo, and stored away from light exposure at -20 °C. The reaction was not further purified, which was performed

after downstream reactions. On silica plate thin layer chromatography (TLC) in dichloromethane:methanol 9:1 mobile phase, the heme-NHS product had two R_f values of 0.62 and 0.75.

Scheme 1: Heme-NHS synthesis from heme activated with PS-carbodiimide and reacted with NHS

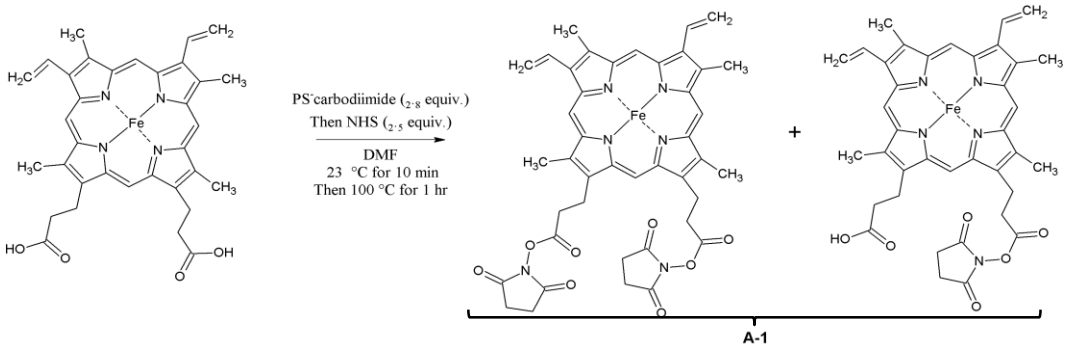

3.2.4. Reactions of Heme-NHS with NBA, LY, FSTC, Lysine-NTA, AAF, and DCCH

Heme-NBA was synthesized by mixing heme-NHS (3.4 mg, 4.2 µmol) and NBA (1.2 mg, 16 µmol, 4 equiv.) and stirring in 500 µl of anhydrous DMF for 40 minutes at 100 °C in a Biotage® Initiator microwave synthesizer (Scheme 2). Heme-LY was synthesized by mixing heme-NHS (4.3 mg, 5.3 µmol) and LY (6.2 mg, 11.9 µmol, 2.5 equiv.) together in 500 µl of anhydrous DMF and water (1:1 ratio) for 45 minutes at 100 °C in a Biotage® Initiator microwave synthesizer. Heme-FSTC was synthesized by mixing heme-NHS (1.12 mg, 1.38 µmol) and FSTC (3.09 mg, 7.33 µmol, 5 equiv.) in 500 µl of anhydrous DMF for 6 hours at 50 °C in a Biotage® Initiator microwave synthesizer. Lysine-NTA was dissolved in anhydrous DMSO by vigorously mixing at 23 °C to make 1 ml of a 10 mg/ml solution. Heme-lysine-NTA was synthesized by mixing heme-NHS (1 mg, 1.23 µmol) with DMSO dissolved lysine-NTA (1 mg, 3.81 µmol, 3 equiv.) in 500 µl of anhydrous DMF for 6 hours at 80 °C in a Biotage® Initiator microwave synthesizer. Heme-DCCH was synthesized by mixing heme-NHS (5.5 mg, 6.79 µmol) and 500 µl of a 10 mg/ml DMF solution of DCCH (4.67 mg, 16.97 µmol, 2.5 equiv.) into a total volume of 1500 µl of anhydrous DMF stirred at 50 °C for 6 hours in a Biotage® Initiator microwave synthesizer. Unreacted activated mono heme-DCCH was

reacted to completion by the addition of more free DCCH (1.1 mg, 4.07 µmol, 0.6 equiv.).Heme-AAF was synthesized by mixing heme-NHS (2.0 mg, 2.47 µmol) and 500 µl of a 5mg/ml solution of AAF (2.5 mg, 6.17 µmol, 2.5 equiv.) to 550 µl of DMF and stirred at 50 °C for 6 hours in a Biotage® Initiator microwave synthesizer.

Scheme 2: General reaction scheme for heme propionate group labelling.

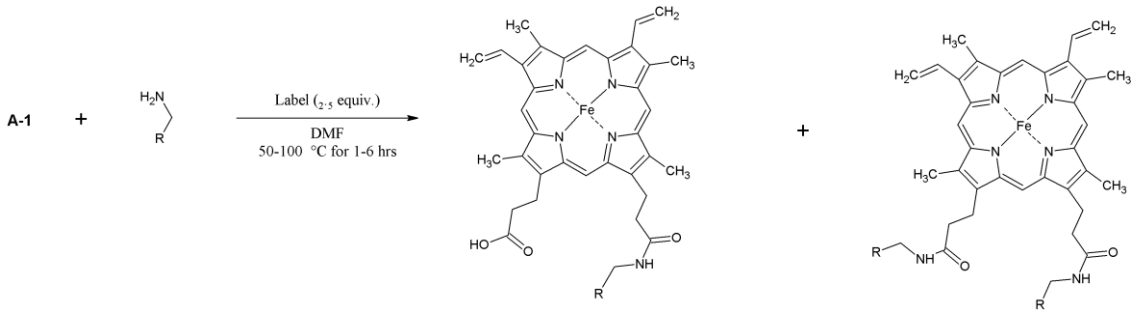

3.2.5. Purification of Modified-heme products

Bis heme-DCCH was purified on a Biotage® KP-C18-HS SNAP column with a Biotage® Isolera chromatography system. Reaction product was diluted from 500-1000 µl into 100x MeCN with 2% glacial acetic acid. This was then added to a Biotage® KP-C18-HS samplet (3 g) where a tight brown band would form at the top of the samplet. Once dry, the samplet was added to a KP-C18-HS column (30 g resin) that had been equilibrated with 100 ml of 7 mM potassium phosphate dibasic buffer at pH 7.0. The samplet was then washed with 50 ml of the same phosphate buffer. Two gradients were used, the first going from 100% phosphate buffer to 100% MeCN in 300 ml. The second gradient went from 100% MeCN to 50% MeOH in 1240 ml, and finally to 100% MeOH in 100 ml. Heme-AAF was purified using a GE Sephadex^{TM} LH-20 resin (8.6 ml of resin, column dimensions of 10 mm x 110 mm). The running solution was 100 mM potassium phosphate dibasic buffer at pH 8.0. Heme-AAF reaction product was added in 100-500 µl injection volumes and run at a flow rate of 40 ml/hr with fractions collected at 2 minute intervals. The first eluted peak was collected and used directly for incorporation within Bfr.

3.2.6. Insertion of Mod-heme into Bfr

Bis heme-DCCH in DMF ($3.5x10^{-8}$ mol, 1.0 equiv.) was added to His6-tag Bfr ($7.0x10^{-8}$ mol) and placed in a water bath at 80 °C for 10 minutes buffered with 0.2 M MES and 1.0 M NaCl at pH 6.5, as was outlined in previous research[139]. After 10 minutes of incubation the sample was left to cool to 23 °C on the bench. Unincorporated bis heme-DCCH was separated from incorporated bis heme-DCCH on a GE Sephadex™ G-25 Fine column using a buffered running solution of 50 mM Tris and 100 mM NaCl at pH 8.0. Heme-AAF ($2.6x10^{-8}$ mol, 2 equiv.) was taken directly from the GE Sephadex™ LH-20 column and mixed with His6-tag Bfr ($2.6x10^{-8}$ mol) at 80 °C for 10 minutes, and then cooled to 23 °C on the laboratory bench, as before. Heme-AAF incorporated in Bfr was separated on a GE Sephadex™ G-25 Fine column from unincorporated heme-AAF using a buffered running solution of 50 mM Tris and 100 mM NaCl buffer at pH 8.0.

3.2.7. MS Experimentation

Crude reaction samples were prepared by taking 5 µl of a 16 mM crude reaction and diluting into 50 µl of 1:1 MeCN:H_2O with 0.2% formic acid, and then taking 5 µl of that dilution and further diluting into 50 µl of the same solution. This was run on a Waters Micromass MassLynx nanospray electrospray ionization quadrupole time of flight mass spectrometer. MS/MS experiments were performed by selecting the ion of interest and increasing the collision energy to 40-60 eV.

3.2.8. Anisotropy Measurements

Anisotropy was measured on a Molecular Devices Spectramax M5 fluorescence plate reader using the pre-set basic anisotropy protocol. Sucrose from a 60% stock in 50 mM Tris, 100 mM NaCl buffer at pH 8.0 was added in 3% increments to a final concentration of 30% sucrose to the mod-heme incorporated Bfr in a Corning® half-area black flatbottom 96 well microplate with 50 µl of sample in each well and a 50 µl buffer blank well, which also had sucrose added to it during the reading.

3.3. Results and Discussion

3.3.1. Heme Preparation and Modification

3.3.1.1. Heme Activation with NHS

The first work with heme was performed by an undergraduate student in the Honek laboratory, Denise Lieuson. She had started the work with heme labelling, and successfully developed a method for the synthesis of heme-NHS, labelling of heme with N-butylamine (NBA) and labelling with Lucifer yellow, but was unable to purify any of these products. This work laid the basis for future synthesis reactions, and to best document the progress of the mod-heme project, a terse overview of this previous work will be highlighted here for the sake of consistency.

Denise Lieuson worked on several methodologies with carbodiimides to try and activate the propionate groups for functionalization with amine and hydrazide containing labels. Heme in its solid form is hemin, which is identical to heme with the exception that a chloride coordinates the heme iron, and is only soluble in dimethylformamide (DMF). Therefore all reactions were carried out in anhydrous DMF. The method that was eventually developed and used for much of the labelling experimentation to follow was mixing of hemin with a polystyrene bead linked carbodiimide (PS-C) (2.8 equiv.) and NHS (2.5 equiv.) in DMF. The product, Heme-NHS, would form both mono and bis heme-NHS products, quantities of which varied between reactions (Figure 3.5). The mono heme-NHS product was not separated from the bis product because purification would be performed downstream after functionalizing heme with desired labels. Heme appeared to react until completion, as monitored by MS with no detectable presence of free heme, and formed largely the bis heme-NHS product. Evaluation of the ratios of products by MS required the assumption that the mono and bis products would ionize to the same degree without supressing ionization of the other. Since these were highly similar molecules it was perceived as a qualitative method to analyse reaction completion and evaluate mono and bis product ratios qualitatively.

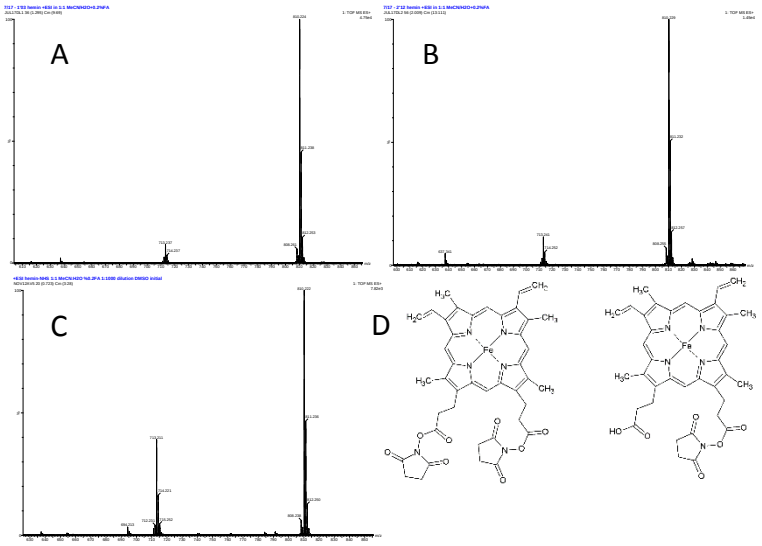

Figure 3.5: Three alternate reactions of heme with NHS (A, B, and C) demonstrating the varying quantities of mono and bis substituted heme-NHS. The mono heme-NHS had a calculated molar mass of 713.56 g/mol, and the bis heme-NHS had a calculated molar mass of 810.63 g/mol. Structures are also displayed (D).

3.3.2. Heme Modification with Functional Labels

3.3.2.1. Heme Reaction with N-Butylamine

The first attempted label was a small ligand, N-butylamine (NBA), which established the ability to label heme with a simple ligand. Heme-NHS was mixed with NBA in anhydrous DMF for 40 minutes at 100 °C. This resulted in the formation of predominantly bis heme-NBA, with some of the mono labelled heme (Figure 3.6). This established that heme was able to be labelled with a simple molecule containing an amine using this particular reaction scheme. The labelled heme produced was primarily the bis product, this was likely due to the size of the ligand, having little steric hinderance on bis product formation. As will be discussed, the larger fluorescent ligands showed less bis product formation than the smaller NBA. Denise Lieuson, with my supervision, attempted to incorporate this modified heme into His6-tag Bfr. The Heme-NBA product was soluble in DMSO, which was used to incorporate into His6-tag Bfr. DMSO was not an ideal solvent since it was observed to cause some precipitation of Bfr. This likely led to the low levels of heme within His6-tag Bfr. A spectral shift in the Soret peak of heme to 418 nm, indicative of heme incorporation into His6-tag Bfr was observed. However, this was the only

evidence of re-insertion, and no further proof was obtained since this molecule was not easily distinguished within the protein milieu.

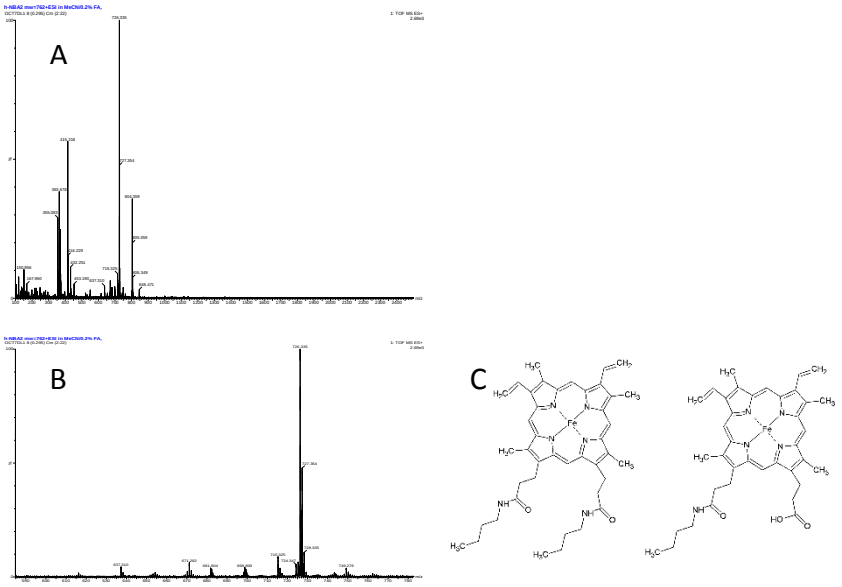

Figure 3.6: The heme-NHS reaction with NBA label, a small alkane containing an amine, monitored with MS. This small label was substituted primarily as the bis product, which had a calculated molar mass of 726.73 g/mol. The mono could be observed as a small peak with a calculated molar mass of 671.61 g/mol. The full spectrum (A) and an enhanced region of the spectrum highlighted the mono and bis heme-NBA peaks (B), with the structures of the mod-heme (C).

3.3.2.2. Heme Reaction with Lucifer Yellow

By labelling heme with a fluorescent agent it would be possible to characterize the incorporation of mod-heme in Bfr, and any effects that might arise with localization of multiple fluorophores within the restricted space of Bfr. Lucifer yellow (LY) was the first fluorophore chosen to explore for labelling of heme (Figure 3.3). It was chosen because of its water solubility, which was expected to improve solubility of the final product. Increased aqueous solubility of product would likely enhance the ease of mixing and incorporation into Bfr. This dye was non-soluble in DMF, however, which was the crux of some of the issues associated with synthesizing heme-LY in high quantities. Upon performing these reactions there was clearly less heme-LY present (Figure 3.7). Unfortunately, this product was never produced in high enough quantities for incorporation into Bfr. In the mass spectrum there was a second peak observed, which had a mass of 1038 g/mol, 27 mass units higher

than the expected mono product. This was later determined to likely be the result of a porphyrin modification from the hydrazide functionality of LY, explained below. The issue of LY solubility in DMF resulted in synthesis issues, which was also observed to be somewhat limiting with the synthesis of heme-lysine-NTA. As a consequence of the poor reactant solvent compatibilities experienced here two alternative dyes were explored.

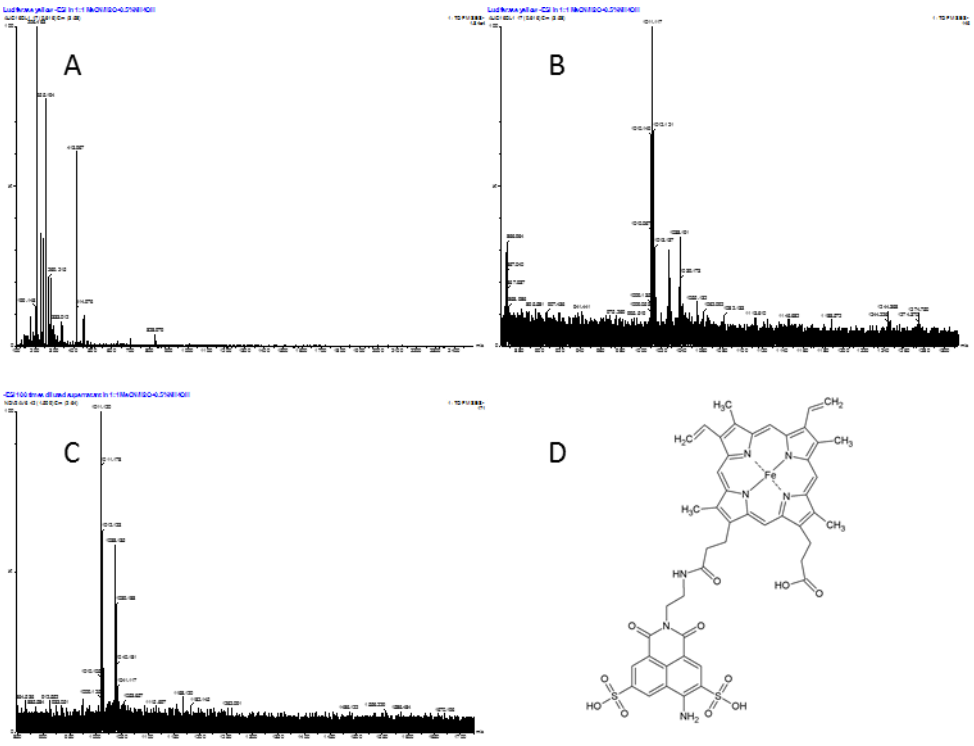

Figure 3.7: The synthesis of heme-LY as monitored by MS. Here the full spectrum (A) showed that the mono heme-LY peak was almost within the background, and only upon closer examination of the expected region of the spectra where the heme-LY product would lie (B, C) can one observe the mono heme-LY product with a molar mass 1013.8 g/mol, which was two mass units higher than the observed mass. A second product peak 27 mass units higher than the expected mono heme-LY mass was observed. The labeled mod-heme structure is displayed as well (D).

3.3.2.3. Heme Reaction with 7-Diethylaminocoumarin-3-Carboxylic Acid, Hydrazide

A coumarin derivative, 7-Diethylaminocoumarin-3-Carboxylic Acid, Hydrazide (DCCH) (Figure 3.3), was used as a proof of principle to show that heme could be fluorescently labelled and then incorporated back into His6-tag Bfr. This dye was chosen because it was soluble in DMF, and

therefore would remediate the suspected solvent solubility issues encountered with LY. The excitation and emission wavelengths for DCCH in MeCN are 420 nm, and 468 nm, respectively.

The reaction with heme proceeded similarly to the previous reactions with NBA and LY, where heme-NHS was mixed in anhydrous DMF with DCCH. Reaction completion was monitored with MS, as before (Figure 3.8). There were three product species observed in the mass spectrum of the reaction mixture after synthesis: an 873.77, 970.84, and 1131.03 g/mol peak corresponding to the mono, mono activated, and bis labelled heme DCCH, respectively. The mono activated heme contained one dye and one NHS group, which was able to be further reacted to bis labelled heme by the addition of free DCCH until all mono activated heme was converted to bis heme-DCCH (Figure 3.9).

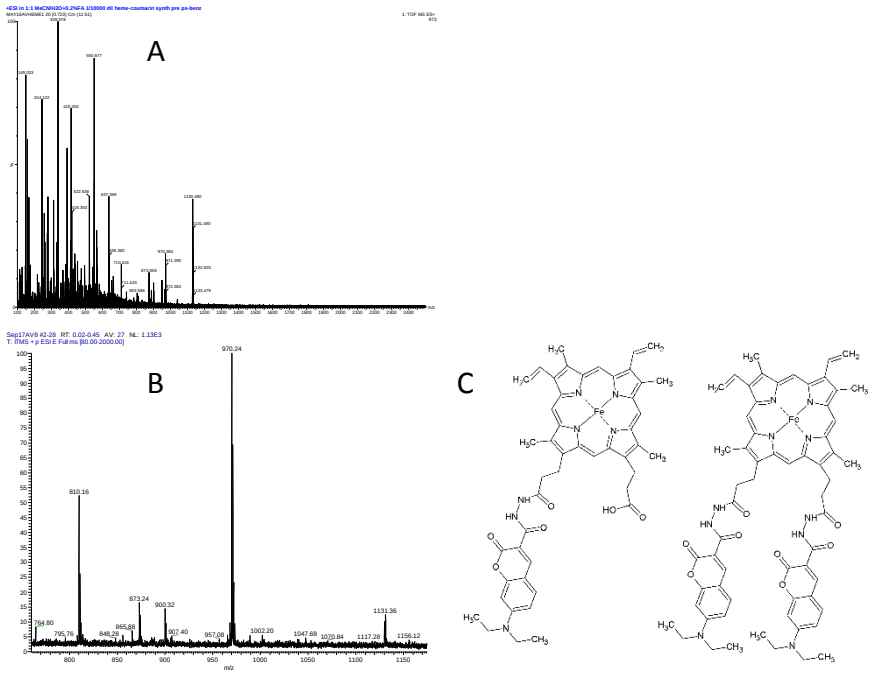

Figure 3.8: Synthesis of heme-DCCH with the full spectrum (A), and an enhanced area of the spectrum showed the ions of interest (B). The mono heme-DCCH had a molar mass of 873.77 g/mol, and the bis heme-DCCH had a molar mass of 1131.03 g/mol.

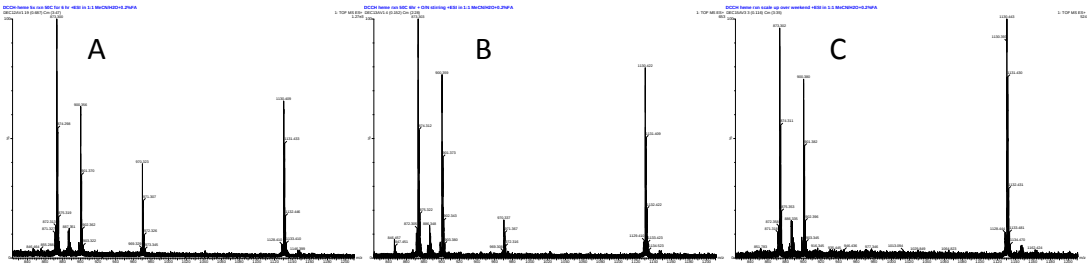

Figure 3.9: Addition of free DCCH dye reacted with mono-activated heme-DCCH at 0 hours (A), overnight (B), and after three days (C). The disappearance of the mono-activated peak can been observed as time progressed.

In addition to the expected labelled peaks of heme there was an additional peak observed that was slightly larger than the mono heme-DCCH. This peak was 900 mass units, which was an increase of 27 mass units from the mono heme-DCCH. To explore the potential of this ion belonging to a heme side reaction, MS/MS experiments were performed (Figure 3.10). When the 900 peak was analyzed in MS/MS with a collision energy of 50 eV the peak fragmented to a 882 peak, signifying the loss of water from the parent 900 peak, and thus that the second carboxylic acid on heme was unmodified. This same 18 mass unit decrease was observed for the 873 peak during MS/MS experiments. This indicated that the modification could have been an addition to the porphyrin ring. Confirmation of this was seen with the lack of a 557 peak, which was observed when the mono heme DCCH was fragmented. This 557 peak was also seen with the heme fragmentation, but was not observed with the 900 peak. There was, however, a 584 peak, which was 27 mass units larger than the 557 peak observed with both heme and mono heme-DCCH fragments. This further confirmed that the likely modification was on the porphyrin ring. The potential source of this modification was explored. In the reaction mixture there were few components that could have contributed to this side product: heme itself, the DCCH dye, the DMF dolvent, or liberated NHS. It was noticed that the expected mass for DCCH, 275, was not observed in the spectrum after the reaction, and instead a 244 peak was observed. This peak was 32 mass units less than the expect mass, which was possibly a result of the loss of the hydrazide functionality (Figure 3.11). The hypothesis of

hydrazide loss was bolstered by results in the FSTC work, discussed below. The mechanism and exact nature of this modification was not further explored because it was neither the main interest of this research nor critical for the continuation of this research. Exploration of optimal conditions for the synthesis of bis heme-DCCH and lower quantities of the heme side product were explored by examining various reaction temperatures (Figure 3.12). The optimal conditions with the highest bis heme-DCCH and lowest heme side product were determined to be 50 °C. This temperature was used throughout the rest of the synthesis to attempt to limit the amount of side product formation. Vinyl side reaction was likely since it has been shown in nature that the vinyl groups are reactive towards amino acids.[181]

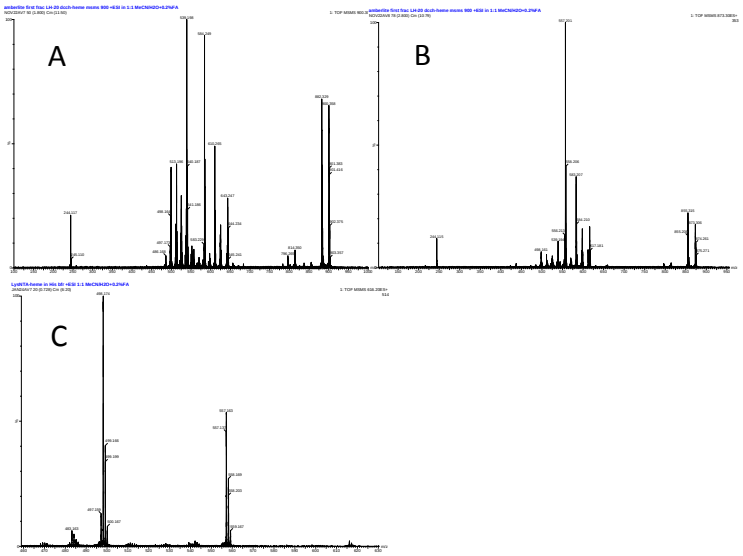

Figure 3.10: MS/MS experiments with the 900 peak (A), the mono heme-DCCH 873 peak (B), and with heme 616 peak (C). Both the 900 peak and mono heme-DCCH 873 peak showed an 18 mass unit loss, which is typical of water loss from carboxylic acids. This indicated that both ions likely contained a free carboxylic acid functionality. Both mono heme-DCCH and heme showed a 557 fragment peak, which corresponded to the loss of four oxygens from the protoporphyrin propionate functionalities. The 900 peak had a fragment peak 27 mass units higher than this, which indicated that there was likely a modification to the porphyrin ring of mono heme-DCCH.

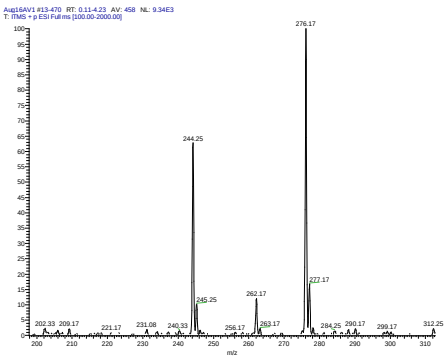

Figure 3.11: Free DCCH fragmented by MS/MS showing a 244 ion peak, which was seen in the spectra from reacted DCCH instead of the expected 276 ion, a loss of 32 mass units.

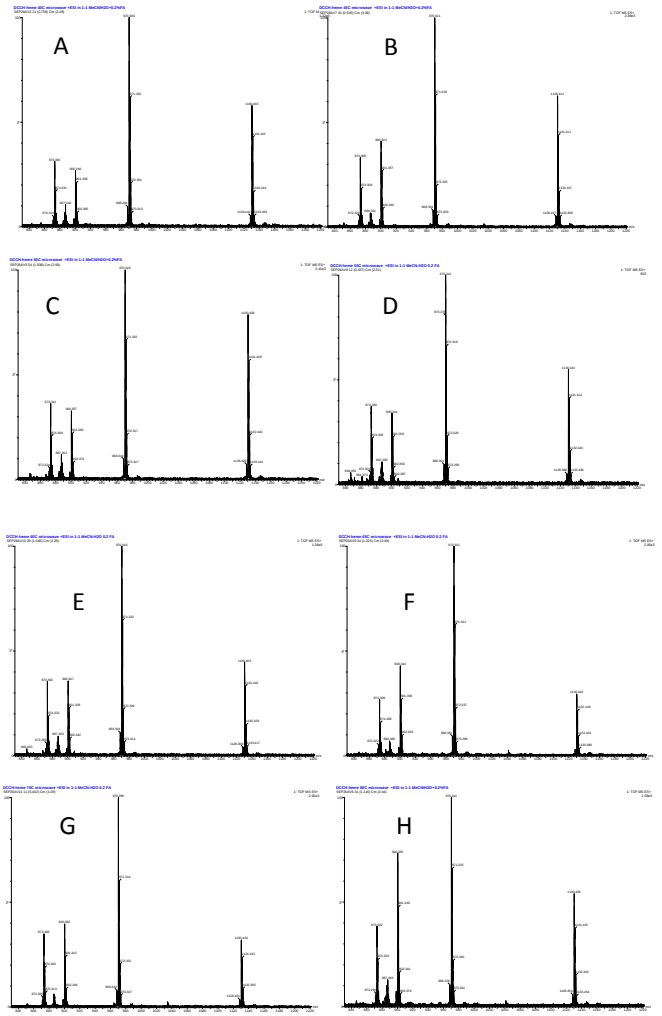

Figure 3.12: Temperature trials with heme-DCCH reaction using temperature of 40 (A), 45 (B), 50 (C), 55 (D), 60 (E), 65 (F), 70 (G), and 80 °C (H). The 80 °C reaction trial had a significant amount of the side reaction 900 peak. The optimal condition chosen was 50 °C, which seemed to have the least amount of the side reaction peak, and the most bis mod-heme.

3.3.2.4. Heme Reaction with Fluorescein-5-Thiosemicarbazide

A fluorescein derivative, Fluorescein-5-Thiosemicarbazide (FSTC) was also explored as a fluorescent molecule to functionalize heme (Figure 3.3). FSTC, along with many fluorescein derivatives, are ideal candidates because of the dual solubility in both DMF and H_2O when the pH is above pH 6. FSTC has a molecular weight of 421 Da, and excitation and emission wavelengths in water of 492 nm and 516 nm, respectively. Synthesis of heme-FSTC proceeded in the same fashion as with the synthesis of the previous mod-hemes. Heme-NHS was mixed in anhydrous DMF in the presence of FSTC. Unlike the DCCH reactions, there was no product observed. All the Heme-NHS remained unreacted, and it seemed that most of the FSTC had disappeared (Figure 3.13). Initially, this was unexpected, but after more careful consideration a pattern emerged that was similar to what was observed with DCCH synthesis. There was a 390 Da peak associated with the loss of 32 Da from free FSTC observed in the spectrum, as was seen with DCCH reactions. When the free FSTC was run there was no 390 Da peak, and so the free FSTC was fragmented using MS/MS (Figure 3.14). A 390 fragment arose from the MS/MS of the 422 FSTC peak. This was likely a result of loss of the hydrazine on FSTC rather than the sulfur from the thioketone since it was the same mass loss seen with DCCH. FSTC seemed to lose the hydrazine more vigorously than DCCH, which may be a result of the slight difference in chemistry since DCCH contained a ketone rather than a thioketone. This rapid loss of hydrazine resulted in none of the heme-NHS being labelled. Closer examination of the reaction spectra revealed that FSTC was modifying heme in the same way that DCCH did. A peak corresponding to mono heme-NHS with a 27 mass unit increase was observed (Figure 3.15). This side reaction must have been of the same mechanism as previously seen with DCCH, but fast enough such that no desired product could be formed. A second fluorescein

derivative was chosen to label heme-NHS with, which lacked a hydrazide and thioketone.

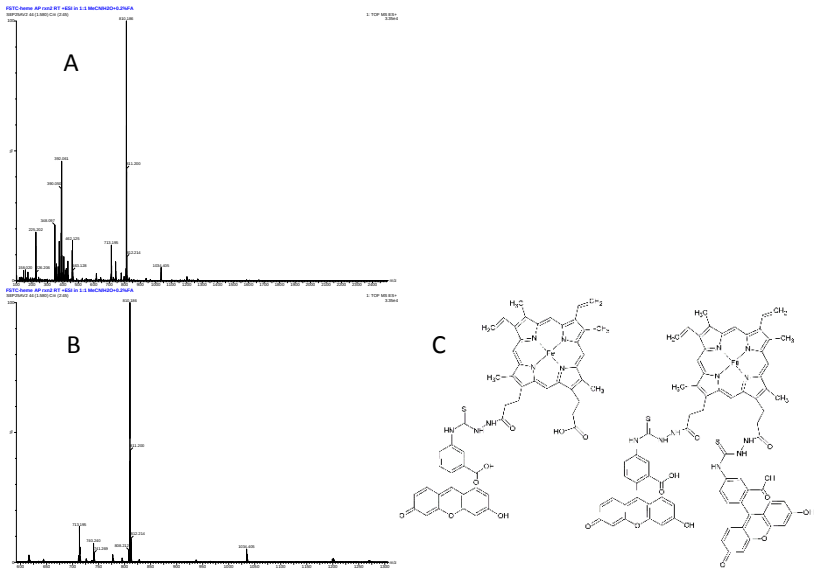

Figure 3.13: Initial reaction of FSTC with heme-NHS (A), and enhancing the area of spectra where there appeared to be the unreacted mono heme-NHS (713) and the bis heme-NHS (810) (B). The structure of the mod-heme is displayed as well (C).

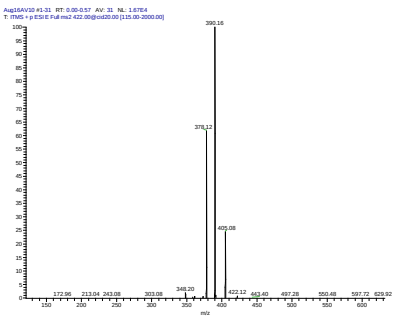

Figure 3.14: Free FSTC fragmented with MS/MS showed a 390 peak, which corresponded with the loss of 32 mass units from the original mass. This was similar to the mass loss of 32 Da from the fragmented DCCH dye.

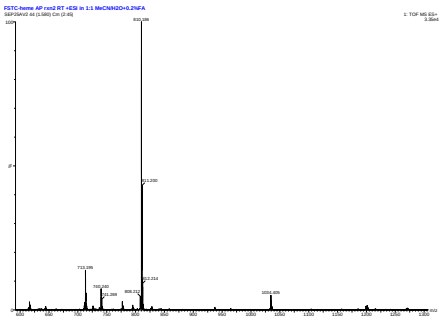

Figure 3.15: The side reaction to the mono heme-NHS reactionshowing a shift in mass of 27 Da was observed as a peak at 740. This was likely a result of the same chemistry seen with the DCCH reactions.

3.3.2.5. Heme Reaction with AAF

After lackluster synthetic results with FSTC, a new fluorescein derivative, 5-(Aminoacetamido)Fluorescein (AAF), with the same physical properties as FSTC was purchased (Figure 3.3). AAF has a molecular weight of 404 Da, and excitation and emission wavelengths in water of 491 and 515 nm, respectively. This new fluorescent molecule lacked the hydrazide functionality that was previously found in both DCCH and FSTC. AAF was added to heme-NHS in the same fashion as previously described which included mixing heme-NHS in anhydrous DMF with AAF. The resulting reaction showed that there was a mono, mono-activated, and bis substituted heme-AAF after reaction (Figure 3.16). Addition of additional AAF converted the remaining mono-activated heme-AAF to bis heme-AAF, and therefore the reaction proceeded to completion. With AAF there was no observed degradation of mod-heme or of the unreacted AAF. These synthesized products were later purified and then incorporated into Bfr.

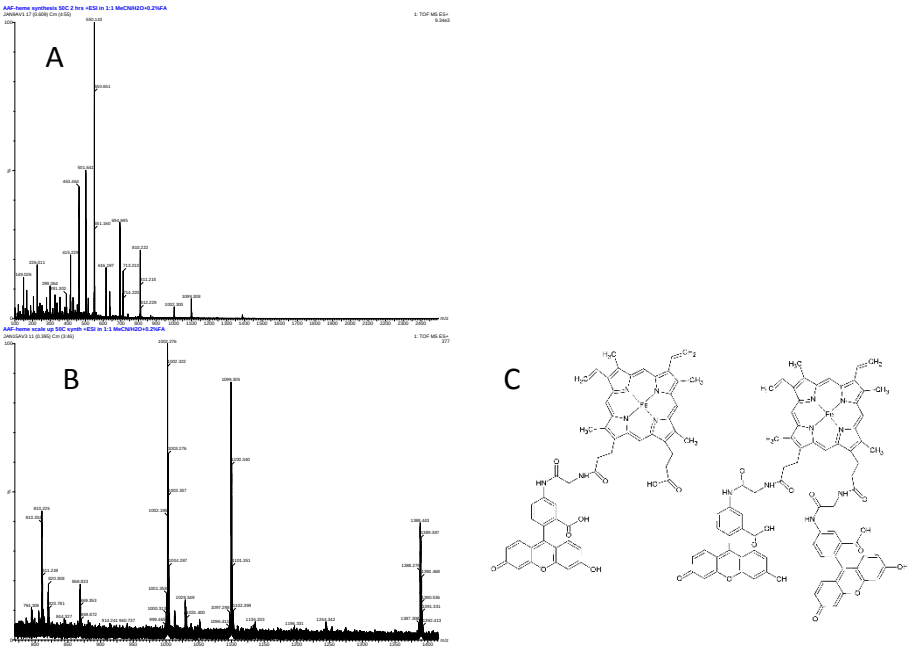

Figure 3.16: Synthesis of heme-AAF (A and B) showing the expected masses for mono, mono-activated, and bis products. There was no heme porphyrin side reaction, as observed before, and the AAF fluorophore did not degrade. The Structure is displayed as well (C).

3.3.2.6. Heme Reaction with Lysine-NTA

In addition to the fluorescent labelling of heme, an affinity ligand was explored to further functionalize the heme cofactor, N_{α},N_{α}-Bis(carboxymethyl)-L-lysine (lysine-NTA) (Figure 3.3). By generating this functional group on heme it would allow for the reversal of the host-guest affinity interaction that was explored in chapter two. Lystine-NTA was not soluble in DMF, but was partially soluble in DMSO. Lysine-NTA was first dissolved in anhydrous DMSO at a concentration of 10 mg/ml, which was then added to a solution of heme-NHS in DMF. The progress of the reaction was monitored by MS, as previously (Figure 3.17). The expected mass for the mono substituted heme-lysine-NTA was observed at 860 Da. There was also some free heme, 616 Da, but no side reactions with heme, nor any degradation of free lysine-NTA. The presence of free heme was not observed for any of the previous reactions with fluorophores, which might have been due to the presence of trace water in the reaction solution. Trace water might have hydrolyzed the heme-NHS to produce heme. Alternatively, the remaining stock of Heme-NHS used may have degraded

with time. Although mono heme-lysine-NTA was demonstrated to be synthesized, continued work with synthesis, purification and incorporation of this mod-heme are required. Due to the fact that lysine-NTA is a highly aqueous soluble molecule it should increase the solubility of the heme-lysine-NTA product. This should thus improve the incorporation into Bfr, as was seen with heme-AAF incorporation in Bfr outlined below.

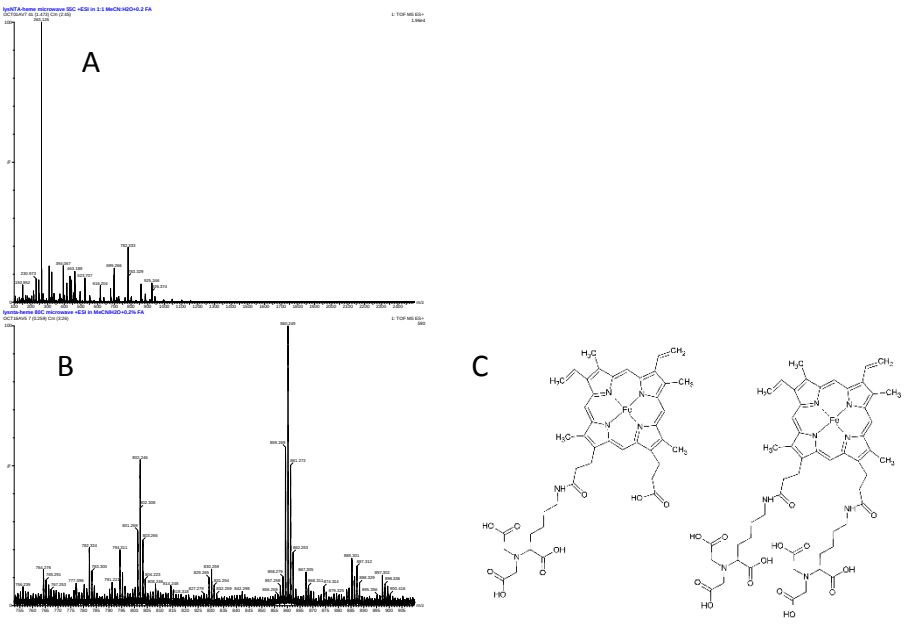

Figure 3.17: Synthesis of heme-lysine-NTA (A and B) with the expected mass of 860 g/mol for the mono heme-lysine-NTA product, but not the bis modified product. There appeared to be no heme side reaction being formed, and the unreacted lysine-NTA appeared to not be degraded. The structure of the mod-heme is displayed as well (C).

3.3.3. Mod-Heme Purification

3.3.3.1. Heme-DCCH Purification

The purification of bis heme-DCCH from the reactants and mono heme-DCCH product required exploration of many resin types, and many conditions. As it was found, it was less challenging to separate mod-heme from reactants, but much more challenging to separate the highly similar mono heme-DCCH from the bis heme-DCCH, which resulted in extremely low yields. The first column used was a GE LH-20 resin, which was described as useful for natural product separation by size, and was tolerant to almost all solvent types. This made LH-20 seem like an ideal candidate for the purification of bis heme-DCCH. The use of this column resulted in the partial separation of mono from bis heme-DCCH, but was unable to completely purify the bis heme-DCCH product (Figure 3.18). After several attempts to separate mono from bis product on LH-20 other resin types were explored.

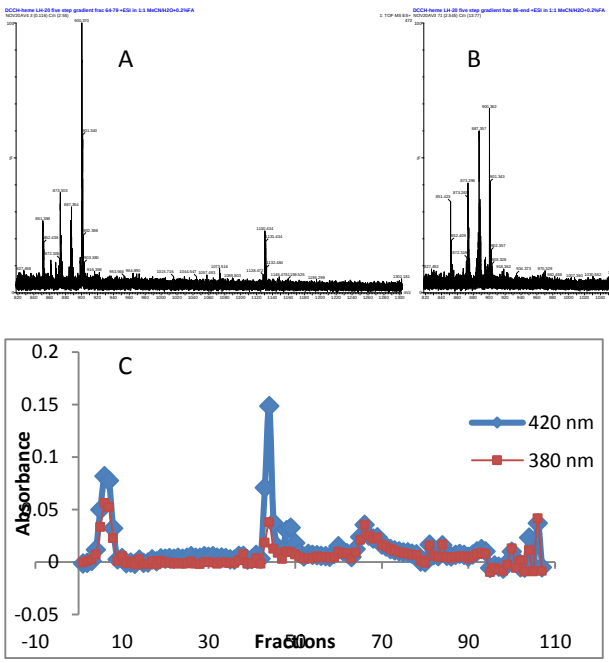

Figure 3.18: Bis heme-DCCH purification on a GE Sephadex™ LH-20 resin. Fraction 67-79 (A) and 86-end (B) show a shift in the ratios of mono heme-DCCH to bis heme-DCCH towards more bis heme-DCCH. Despite many trials and conditions these two products could not be fully separated from each other. The elution profile was monitored by examining the wavelengths at 380 and 420 nm, corresponding to the heme absorption and DCCH absorption maxima, respectively (C).

A series of macroreticular anion exchangers were used to try and bind the available carboxylic acid found on the mono heme-DCCH product in an attempt to purify bis heme-DCCH, which lacked any carboxylic acid functionality. Unfortunately, these resins were unable to make such separations. After continued failure to separate using anion exchanger resins a Biotage® SNAP KP-C18 column was chosen. In order to prepare the sample for running on a Biotage® SNAP KP-C18 column it was first placed on a samplet pre-column. When adding the product in DMF directly to a Biotage® samplet cartridge it would simply flow through. A dilution of the heme-DCCH product was made into 100x MeCN with 2% glacial acetic acid. This was added to the samplet, successively, which formed a tight brown band at the top of the samplet. By forming a tight band on the samplet the separation resolution was improved. Using MeOH as a running solvent, the C-18 column was able to separate the mod-heme from the free dye (Figure 3.19). This separation attempted to be improved upon by using solvents of decreasing polarity to better separate mono from bis product. The solutions used to wash the samplet were 7 mM potassium phosphate buffered to pH 7.0 to deprotonate the one carboxylic acid on mono heme-DCCH in order to create a larger polarity difference between mono and bis heme-DCCH. This was followed by an MeCN gradient to 100% MeCN, which was followed by a gradient to 100% MeOH. Within the MeOH gradient the products would elute as one large peak (Figure 3.20). It was observed that later fractions contained pure bis heme-DCCH, which were collected and rotary evaporated. This procedure was performed eight more times, and all the total collected bis product was pooled together and re-suspended in 300 µl of DMF. Calculating the percent yield gives an approximate yield of 3.1 %. This calculation was somewhat incorrect because the assumption was made that 100% of the heme-NHS was bis heme-NHS. This was known to not be true, as evidenced by MS. If it is assumed that the ratio of mono to bis heme-NHS was at worst 50%, bis heme-NHS the yield would be closer to 6.2%, which remained a poor yield. The primary issue with low yields was the extreme challenge of separating mono from bis product. Although the

reaction appeared to go to completion, upon separation much of the bis product was contaminated with the mono product. In the future a highly resolving technique may be more fruitful in obtaining bis heme-product, such as a C-18 HPLC column.

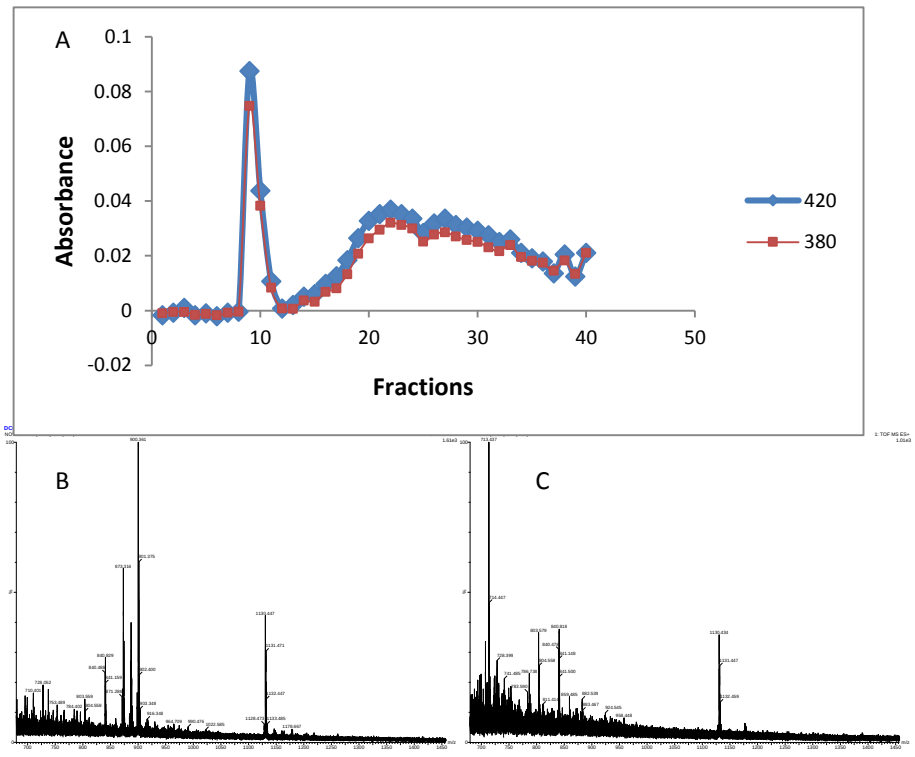

Figure 3.19: Heme-DCCH reaction separated on a Biotage® KP-C18-HS SNAP column using MeOH as a running solvent. There were three visible peaks (A). The second and third peaks were analyzed with MS. The second contained a mixture of mono and bis heme-DCCH (B), and the third peak appeared to contain no mono heme-DCCH (C).

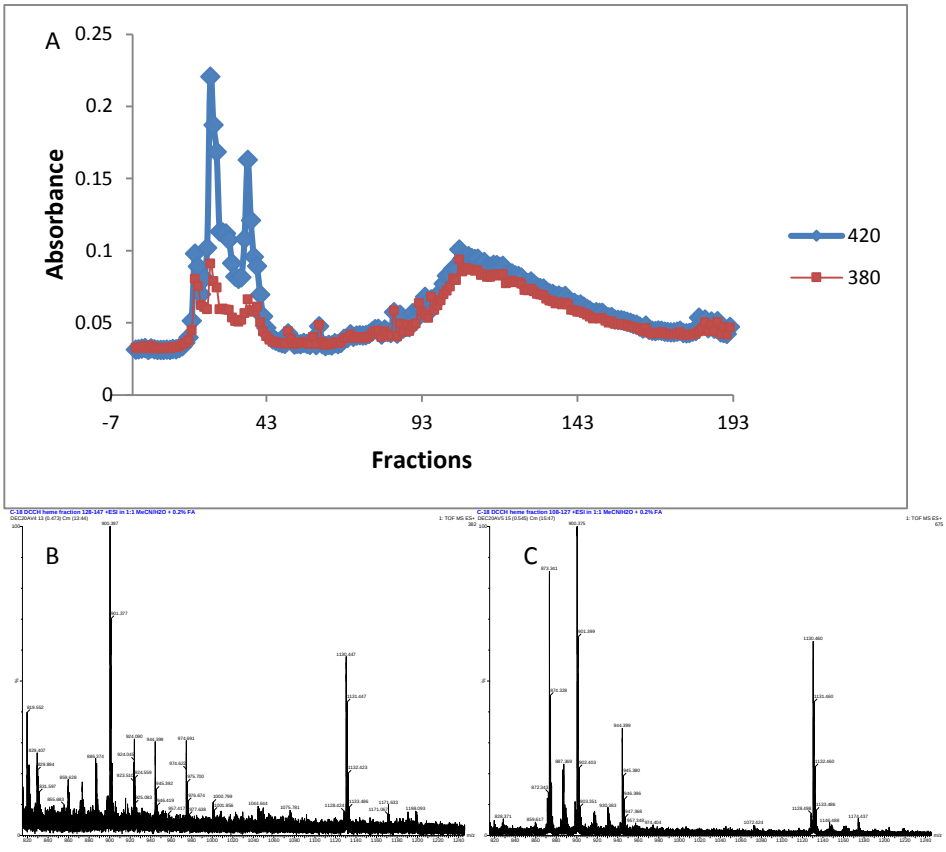

Figure 3.20: Heme-DCCH separation on a Biotage® KP-C18-HS SNAP column using gradients of solvents with increasing polarity was used to try and better separate mono from bis heme-DCCH. There was only one large peak, rather than two distinct peaks observed (A). As fractions were sampled it was observed that the later eluting product was pure bis heme-DCCH (B) and the earlier was a mixture of mono and bis heme-DCCH (C).

3.3.3.2. Heme-AAF Purification

Heme-AAF was not purified to the same extent as heme-DCCH was, and Heme-AAF was simply separated away from only the reactants. Since the aim of this research was to establish whether or not mod-heme could be inserted into Bfr, less emphasis was placed on the isolation of mono and bis heme-AAF, which decreased the time spent exploring conditions and saved expensive fluorescent reagent. Heme-AAF was separated on LH-20 resin in 100 mM phosphate buffer at pH. 8.0. It was noticed that the Heme-AAF product was soluble in aqueous buffer, which was likely due to the solubility of AAF in buffered solutions over a pH of 6. This made incorporation into Bfr much more efficient. The product would elute as the first peak, which was collected and

then incorporated directly into Bfr. The incorporated heme-AAF in Bfr was analyzed with MS/MS, as outlined below.

3.3.4. Mod-Heme Incorporation into Bfr

3.3.4.1. Incorporation and Spectral Shift of Incorporated Mod-Heme

The mod-heme was incorporated into apo His6-tag Bfr (with no traceable amount of native heme) using a method derived from a previous publication.[139] Bfr would be incubated with the desired mod-heme at 80 °C for 10 minutes and then allowed to cool to room temperature. The incorporated mod-heme would then be separated from free mod-heme on a desalting GE Sephadex^{TM} G-25 Fine column with a buffered running solution of 50 mM Tris and 100 mM NaCl at pH 8.0. Heme-AAF was used directly from the column purification, whereas bis heme-DCCH was in DMF solvent which was added directly to the protein solution (Figure 3.21). DMF caused some precipitation of apo His6-tag Bfr upon addition, and so incorporation rates were much lower. A red-shift of the heme Soret peak was observable both with chromatography and in the UV-Vis spectrum for both mod-hemes (Figure 3.21). This spectral shift was indicative of the methionine bi-coordination of heme within Bfr. If heme was not properly incorporated then this red-shift would not have been observed. The percent incorporation of heme-AAF was approximated to be close to 100%, evaluated with a Bradford assay and AAF extinction coefficients, whereas the percentage incorporation of bis heme-DCCH was approximately 2%. This large discrepancy was undoubtedly due to solubility issues experienced with bis heme-DCCH. The emission and excitation spectrums for the free fluorophore, mod-heme, and mod-heme incorporated in Bfr (Figure 3.22). The excitation and emission maxima did not seem to change between samples.

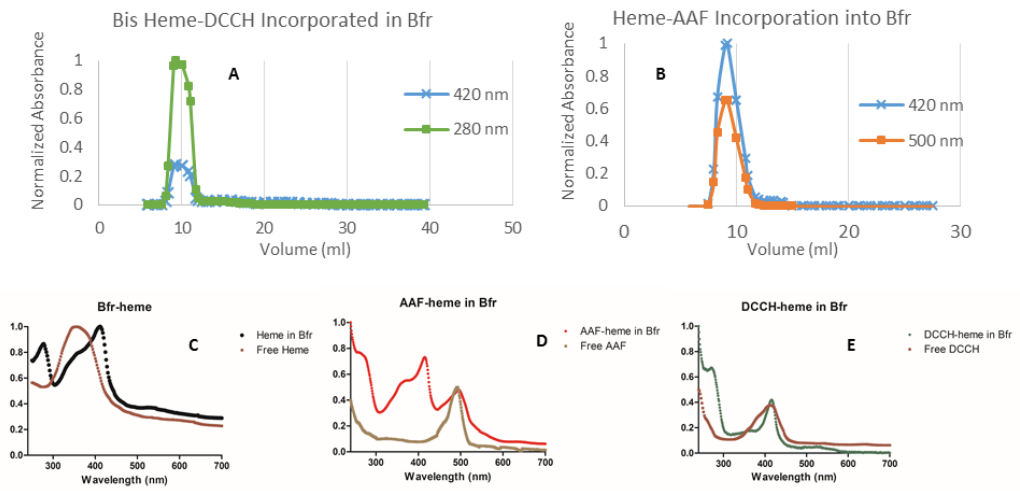

Figure 3.21: Purification of incorporated bis heme-DCCH (A) and heme-AAF (B) from unincorporated mod heme on a GE Sephadex™ G-25 Fine resin. Fractions from these separations were collected and analyzed by UV-Vis spectroscopy. A control of unmod-heme was analyzed for the spectral red shift of the heme Soret band (C), which was observed as a 38 nm peak shift. This same spectral shift was observed for both the heme-AAF (D) and heme-DCCH (E) incorporated in Bfr. The absorption spectra of free AAF had a peak that matched that of the incorporated heme-AAF, and free DCCH absorption spectra matched that of the absorption spectra of incorporated bis heme-DCCH.

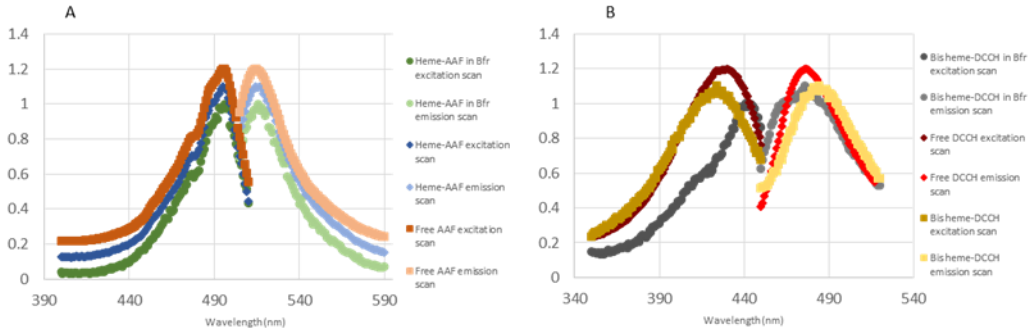

Figure 3.22: The excitation and emission spectrums for free AAF, heme-AAF, and heme-AAF incorporated in Bfr (A), and free DCCH, bis heme-DCCH, and bis heme-DCCH incorporated in Bfr (B).

3.3.4.2. MS/MS of Mod-heme Incorporated into Bfr

Mod-heme incorporated within His6-tag Bfr was analyzed using MS/MS. After separating the incorporated mod-heme from the free mod-heme with a desalting column the mod-heme-Bfr construct was free of unincorporated mod-heme. Therefore, the mod-heme examined by MS/MS should be of heme derivatives which had been incorporated into Bfr. Bis heme-DCCH was purified and incorporated in such low quantities that it was unable to be analyzed by MS/MS. Instead, the highly available mixture of mono/bis heme-DCCH was used to incorporate within Bfr, which was analyzed with MS/MS. When examining incorporated mono/bis heme-DCCH an 873 peak corresponding to mono heme-DCCH was observed (Figure 3.23). This peak was fragmented with MS/MS and peaks corresponding to the loss of water, which indicated the presence of a carboxylic acid, and a 557 Da peak, as was seen with heme fragmentation, were observed. This indicated that heme-DCCH remained bound to His6-tag Bfr during chromatographic separation, and displayed the same fragmentation signature of mono heme-DCCH. It would be reasonable to suggest that heme-DCCH was present in Bfr to some extent. The same experimentation was performed with heme-AAF incorporated within Bfr, which again exhibited the presence of mono heme-AAF (Figure 3.24). This peak was fragmented using MS/MS experiments and peaks corresponding to a carboxylic acid cleavage and a 557 peak, as was seen for heme fragmentation, were both

observed. Again, this analysis suggested that heme-AAF was incorporated within His6-tag Bfr. In addition to these experiments native polyacrylamide gel electrophoresis (PAGE) and fluorescence evaluation were used to assess proper incorporation of the mod-hemes within Bfr.

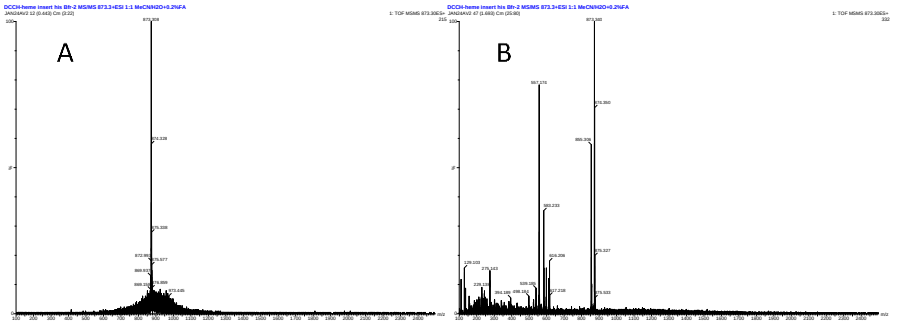

Figure 3.23: Detection of the mono heme-DCCH product (A) after incorporation into Bfr. This peak was fragmented and formed the same ions that were detected previously with mono heme-DCCH (B).

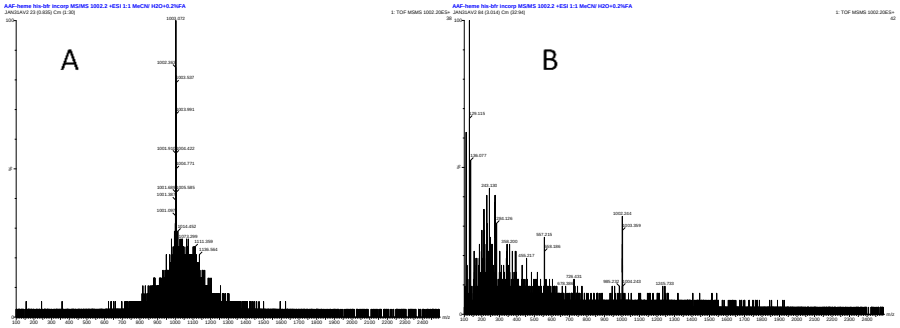

Figure 3.24: Detection of the mono heme-AAF product (A) after incorporation into Bfr. This peak was fragmented and formed the same 557 peak observed with heme fragmentation, and a 985 peak corresponding to the loss of water from carboxylic acid (B).

3.3.4.3. Native PAGE of Incorporated Mod-Heme

His6-tag Bfr incorporated with bis heme-DCCH and heme-AAF were run on native PAGE to detect fluorescent mod-hemes associated with native protein structures (Figure 3.25). These gels were fluorescently imaged to detect the presence of bis heme-DCCH and heme-AAF, and then stained to detect the presence of associated protein. Clearly, fluorescent bands were visible at the top of the gel that were also stained blue by the protein specific coomassie stain. This result showed that both mod-hemes were associated with non-denatured

protein. The gel migration of the incorporated mod-hemes in His6-tag Bfr was identical to that of the incorporated unmod-heme His6-tag Bfr control. Free heme-AAF was also run as a control, which did not generate a fluorescent band at the same position. These observations indicated that the incorporated mod-hemes seemed to be associated with the native protein structure. Anisotropy of these mod-heme incorporated samples was performed next to further demonstrate proper association of this heme labelled dye.

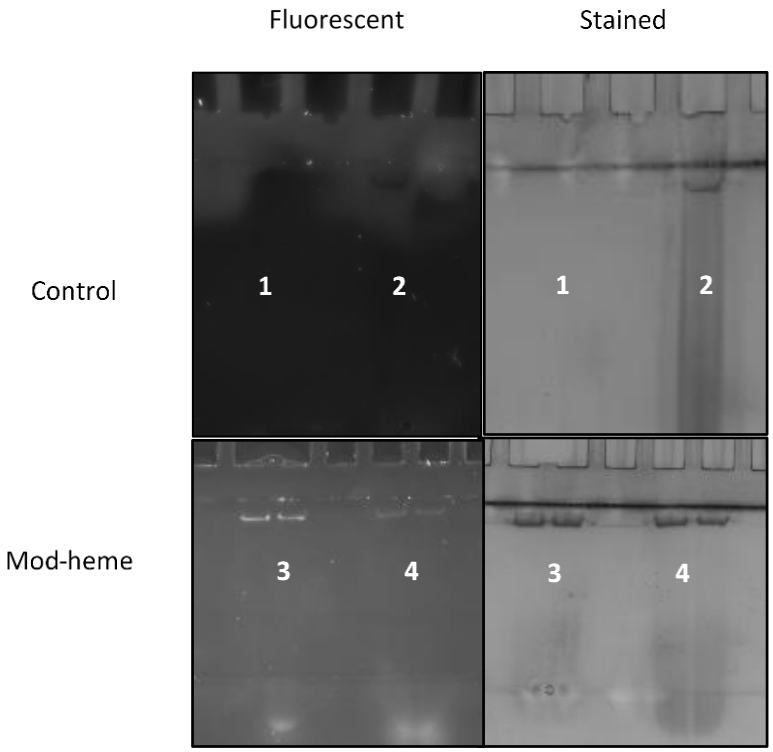

Figure 3.25: Native-PAGE of mod-heme incorporated in Bfr. Native PAGE was run with free heme-AAF (1), unmod-heme incorporated in Bfr (2), bis heme-DCCH incorporated in Bfr (3), and heme-AAF incorporated in Bfr (4). The native PAGE was first imaged fluorescently without stain and then stained with coomassie.

3.3.4.4. Fluorescence Anisotropy of Incorporated Mod-Heme

Fluorescence anisotropy experiments were performed to compare the rotational freedom of the free fluorophore, the mod-heme, and the incorporated mod-hemes. Fluorescence anisotropy measures the rotational freedom by taking two measurements of light in perpendicular polarized planes. If the value is zero then there is total freedom of rotation, whereas if the anisotropy is 1 then the

fluorophore is totally restricted in movement. When measured, the heme-AAF incorporated in Bfr had a much higher anisotropy, 0.3, than the free AAF, 0.034. This was consistent with values of other fluorescently labeled biomolecules.[182,183] The free heme-AAF showed an anisotropy of 0.059, slightly larger than the free AAF, but much smaller than the incorporated heme-AAF. This indicated that heme-AAF must have been restricted within a large structure, which slowed the rotation. DCCH was not soluble in aqueous buffer, and so the anisotropy was not measured, but the bis-DCCH-heme incorporated in Bfr had an anisotropy of 0.33, comparable to that of incorporated heme-AAF.

In addition to these anisotropy measurements, a Perrin plot was used to evaluate the size of the rotating particle that contained the fluorophore. Sucrose was titrated into the sample in increments of 3% up until a final concentration of 30% (Figure 3.26). When the volume of the rotating unit was calculated the size of the heme-AAF incorporated in Bfr was 10.5 nm, which was close to the actual size of 12 nm. The free AAF, and heme-AAF were 2.5 nm and 2.7 nm respectively. The size of the free fluorophore was much larger than expected based on the actual size of the fluorophore. This could be explained by resonance energy transfer (RET).[184] Typically in Perrin plots the lines will intersect at a common point on the y-axes, which is the r_o value.[182] If, as is known with fluorescein, there is RET between fluorophores it will cause a shift in the slope of the Perrin plot. This shift in the slope causes an overestimation of the true anisotropy value.[185] This effect might explain why the unincorporated fluorophores seemed to be larger than they truly were. Free DCCH and free heme-DCCH could not be examined due to the insolubility of these molecules in aqueous buffer, which were not appropriate comparisons to bis DCCH-heme incorporated in Bfr.

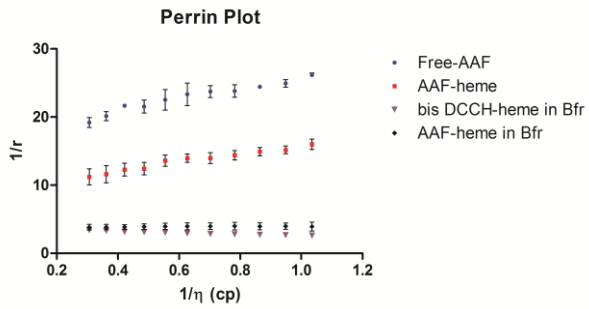

Figure 3.26: A Perrin plot of free AAF, free heme-AAF, incorporated heme-AAF, and incorporated bis heme-DCCH. Each sample was titrated with sucrose from a 60% (w/v) solution of sucrose in 3% increments until a concentration of 30%.

3.3.4.5. Heme-AAF Quenching

Quenching experiments were performed, as was done with the SF quenching experiments. It was observed that the heme-AAF incorporated in Bfr showed the same quenching pattern as the encapsulated SF, both of which had fluorescein labels (Figure 3.27). The plot of quenching confirmed that the fluorophore was protected to the same extent as the encapsulated SF. With this evidence, and the previous evidence, it was suggested that modification of heme propionate groups with fluorophores and the proper incorporation into Bfr was a viable method to functionalize the Bfr platform. This initial work will lead to future modifications to heme propionate groups for the purpose of further functionalizing the inner surface of Bfr.

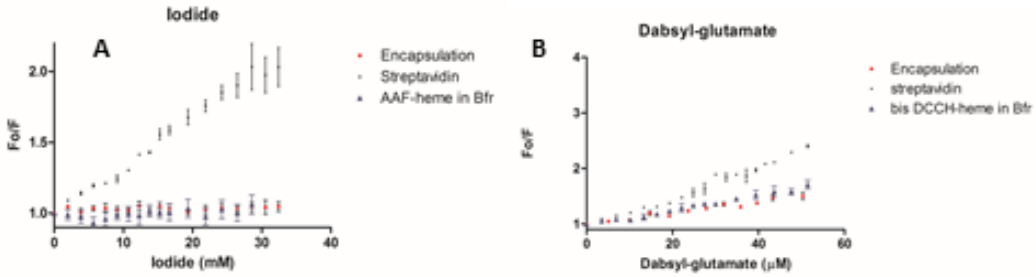

Figure 3.27: Heme-AAF incorporated into Bfr was titrated with iodide (A) and dabsyl-glutamate (B), as encapsulated SF was in chapter2. Heme-AAF incorporated into Bfr showed the same quenching patterns as encapsulated SF.

3.4. Conclusion

Here it has been shown that heme was able to be chemically modified with multiple molecules, two of which were purified and incorporated into the Bfr

protein structure. It was discovered that the use of labels with hydrazide functionalities often led to unexpected and unwanted side reactions with the heme porphyrin group. As a precaution, such functionalities should be avoided in the future. DCCH and AAF were both attached to heme, but only DCCH was purified to its constituent mono and bis products, whereas heme-AAF was purified as a mixture. The product synthesis was evaluated with MS, and later by MS/MS fragmentation patterns of the mod-heme products. All products demonstrated the expected masses and fragmentation patterns, and thus it was highly probable that these were the desired products. Both mod-hemes were incorporated into Bfr, which were evaluated by chromatography, UV-Vis spectroscopy, MS, native PAGE, fluorescence anisotropy, and fluorescence quenching. The development of this aspect of the Bfr platform was seen as critical to design new functionalities within Bfr. The introduction of fluorescent markers, and affinity interactions to the heme will provide much more control of Bfr modification, and host-guest interactions.

Chapter 4: Future Directions

4.1. Introduction

Despite the work that has been performed to develop the Bfr bionanoplatform, there remains much work to explore the full extent of its capabilities. Three projects, outlined below, intend to further the developmemt of bacterioferritin and its applications. Furthering the heme work from chapter 3 is essential to best develop Bfr. Heme is both an integral and unique aspect of Bfr, which provides a great advantage to this platform. Labelling heme with fluorophores has shown that it is possible to modify the heme and still incorporate it into Bfr. The next steps are to add functional groups that serve auxiliary functions to fluorescence, such as the lysine-NTA ligand explored, catalysts[186], or imaging agents.[187] Heme, in this sense, will act as a highly specific component for both localization to the inner surface and as a fluorescent marker. Unlike Cys or other amino acids that may be used to covalently attach functional groups onto proteins, heme can be manipulated outside of the protein environment[98] prior to its incorporation into Bfr. In addition to the synthetic advantages to heme modification, it would become possible to mix differing ratios of modified heme to derive an ensemble of modified hemes within a single Bfr. Since Bfr contains 12 heme binding pockets, it would be possible to mix ratios of, say, fluorescently labeled heme, NTA modified heme, and gadolinium complexed-heme all to the same Bfr molecule. These aspects make heme an exciting, and interesting molecule to explore further. The first of these explorations will be the addition of lysine-NTA to heme.

The second aspect of Bfr yet to be explored is the exterior surface modification. Much has been accomplished in the development of the interior of Bfr, which, to paraphrase Jeroen J.L.M. Cornelissen, is far more difficult to modify than the exterior[8], but little has been done to functionalize the exterior of Bfr. Exterior surface modification of ferritin has been accomplished in other publications, primarily in the drug delivery arena[2,18,188], but also in some of the

work in bio-materials science.[189-192] Designing specific labels on the surface of Bfr will enhance its range of applications.

Lastly, development of Bfr as a platform for NP-based catalytic conversion of small molecules will be explored. This development will follow work previously performed by Varpness, Z. *et. al.*[64]. This will involve the synthesis and characterization of a Pt NP within Bfr along with its capabilities to produce H_2 gas. By designing Bfr for this purpose, it will overcome the issues seen in the previous publication with Pt NP catalyst stability.

4.2. Heme-lysine-NTA Incorporation into Bfr

By adding an NTA functionality to heme the His6-tag-NTA interaction, used heavily in this thesis, would be reversed between host and guest. This reversal will dramatically change the range of proteinaceous guests that can be encapsulated within Bfr. His6-tags, which are commonly placed on proteins for expression purposes, could be used as the specific affinity ligand for encapsulating them within the host Bfr displaying an NTA functionality from its heme groups. Heme-lysine-NTA has already been synthesized, and now requires purification. Additional attempts to improve solubility of lysine-NTA in DMF or DMSO should be made, which may increase the reactivity with heme-NHS. Purification should be explored with both LH-20 and C-18 columns to try and separate heme from the mono heme product. The product should display enhanced solubility due to the addition of three carboxylic acid functional groups, as was exhibited with the heme-AAF product. This should improve the amount of heme-lysine-NTA able to be incorporated within Bfr. Presence of heme-lysine-NTA in Bfr should be evaluated using fragmentation with MS/MS to identify its presence with Bfr, and the heme Soret peak spectral shift upon insertion into Bfr, as outlined in chapter three.

The first His6-tag bearing guest to be explored would be green fluorescent protein (GFP). GFP is another well-established protein in molecular biology. GFP is derived from jelly fish, is intrinsically fluorescent, has a molecular weight of 26854 Da, is 238 amino acids long, has a beta barrel fold, and is

approximately 5.2 nm long and 2.4 nm wide.[193] This serves as an ideal guest molecule for encapsulation because it is relatively small, intrinsically fluorescent, and will contain a single His6-tag affinity ligand. GFP can be used in this manner as a guide for encapsulating other proteins with single His6-tag affinity interactions. Encapsulation procedures should entail declustering with varying concentrations of GndHCl and varying temperature, and exploration of different ratios of heme-lysine-NTA to native heme in Bfr. TEM and fluorescence analysis of the encapsulated GFP should be performed as with the SF encapsulation studies, outlined in chapter two. Study of GFP on this platform will surely lead to future encapsulation studies with enzymes and other functional proteins. By using the reversed His6-tag NTA interaction it will make the protein guests more similar in the nature of the affinity interaction. This should provide some consistency and continuity between the proteinaceous guest molecules and the host Bfr.

4.3. Surface Modification of Bfr

To better enable Bfr to act as a guest delivery platform it is considered critical to develop the outer surface as well. Some of this work has already begun with the design and preparation of an S-tagged Bfr, which was prepared on a plasmid by Anthony Petrie of the Honek laboratory. The S-tag was designed on the N-terminus, which faces the exterior, as mentioned in chapter two. Work has been done to express and purify this protein, as outlined in chapter two, and is currently being explored for labelling purposes by Hawa Gyamfi of the Honek laboratory. Reasons for exploring the S-tag are outlined in detail in chapter two.

Alternative means to modifying the exterior surface of Bfr could be the covalent modification of a Cys residue. Fortuitously, there are no Cys amino acids coded for in the Bfr structure. A single point mutation in the structure could enable the specific labelling of 24 Cys residues in the fully assembled cage protein. Maleimide chemistry could be used to specifically label the Cys residues with fluorophores to evaluate this labelling method, which could later

be exchanged for other targeting ligands such as the RGD peptide.[2,111] The point mutation would have to be chosen well in order to generate an exposed Cys residue on the surface. It would be ideal, as well, to choose a residue that is non-disruptive to the fold. A sequence alignment was performed to determine residues that were highly conserved in the Bfr structure. After looking at the Bfr crystal structure and a sequence alignment several candidate residues were chosen: Asp 73, Lys 76, Ser 89, and Ser 110. This method, in addition with the S-tag method would provide unique and highly specific functionalities for modification of the Bfr surface.

4.4. Platinum Core Synthesis and H_2 Gas Production

Using and re-engineering the function of protein platforms has limitations. For instance, design of a drug delivery vehicle with intrinsic toxicity or toxic metabolic products would be unwise to explore as a platform in light of other, non-toxic, choices. Proper complementation of the desired function of a platform with its native capabilities would surely benefit the final application, and limit the number of potentially detrimental modifications. This reasoning follows the rule of parsimony, where the fewest number of modifications to a platform should lead to the lowest potential for ill effects on important structural or functional features. Through examination of Bfr as a platform for nanotechnology there remains one area not explored that would complement the proteins native function. This would be to exploit its native metal nanoparticle (NP) carrying capacity. Synthesis of a Pt NP in Bfr could be explored, mimicking research previously performed with a heat shock protein.[64] This heat shock protein was approximately 12 nm in diameter, and 400-1000 atom Pt NPs were synthesized inside this cage protein. The researchers used methyl viologen and Tris(bipyridine)ruthenium(II) ($Ru(bpy)_3^{2+}$) to produce electrons from a light source and transfer them to the Pt NP. The pores of the heat shock protein were large enough to allow the transfer of electrons from the methyl viologen mediator. The advantage of using the protein cage was that it prevented the aggregation of Pt NP. The researchers were able to use the Pt NP catalyst to produce H_2 gas at reported levels of hydrogenases, but the production would

cease after a short period of time. This was thought to be due to the degradation of the electron mediator, methyl viologen, by Pt based hydrogenation. Since the pore size was large enough to allow methyl viologen to the interior space it could easily become hydrogenated by the catalyst. The problem here was to somehow get electrons to the Pt catalyst in order to produce H_2 gas without degrading the electron mediator in the process. This is where Bfr is an ideal host for such a process, and could provide many advantageous features.

Bfr has pores that are already tuned for passage of only small molecules like water, iron and phosphate. These pores would only allow small molecules, like water or H_2 gas to transit, whereas larger molecules would be generally excluded. This sieve could work to protect the catalyst from modifying molecules other than those desired. In addition to providing this unique advantage, Bfr could be used as a model to further develop the understanding of protein shell scaffolds. Recently, the importance of pore size was investigated examining the effects of protein shells and their pore size on the activity of Pt NPs for antioxidant activity.[194] It was shown that the pore size and shell were important determinants for the catalytic properties of the Pt NP. By exploring this area with the Bfr protein shell it would further develop the understanding of how pores and the platform effect catalytic rates.

Since methyl viologen was used to shuttle electrons to the Pt NP in the discussed publication, and Bfr would not allow direct contact of these two components, the natural question would be how does one move electrons into the Bfr interior without moving an electron mediator in? Bfr is well placed for this process because it has been found that electron movement across the protein shell is integral for the native processes. Bfr, along with all ferritin family proteins, is involved with iron storage and release in the cell. Regulation of the process of iron core formation and release has only recently been discussed.[81,134] In the process of reduction of iron for release from Bfr heme has been found to be the mediating cofactor for electron shuttling from the exterior to the interior.[81] Important in this process was a Bfr associating ferredoxin protein

(Bfd), which is a small protein containing an Fe-S centre that transfers electrons from ferredoxin to the centre of Bfr through the heme cofactor. This mechanism provides a unique and exciting opportunity to re-purpose this function for another application. The heme cofactor could serve as a means to deliver electrons to a Pt NP without necessitating an electron mediator to come in contact with the Pt NP. By exploiting this electron transfer pathway, along with the complementary nature of Bfr as a metal NP host, a very stable, and long lasting H_2 catalyst could be formed.

Using Bfr as a platform should be electrochemically viable since the redox potential of heme in Bfr is -225 mV[82], whereas the redox potential of methyl viologen is -446 mV. The redox potential of Pt is known to be as high as 700 mV, depending on the size of the particle.[195] This could effectively shuttle electrons from the exterior environment to the interior environment, thus protecting the Pt NP from external factors. Bfd could also be used as a means to shuttle electrons through Bfr, although it might be possible to reduce the heme with an electron mediator such as methyl viologen. These options would have to be characterized for their electron transfer capability.

Although the goal of this research direction is to replicate Pt NP catalyzed H_2 gas production, there will be milestones to meet, and each milestone will be independently impactful to the development and understanding of Bfr as a whole. These milestones are: evaluation of *E. coli* Bfd and the electron transfer characteristics to Bfr, and the synthesis of metal NP within Bfr and evaluation of their catalytic capabilities.

4.4.1. Exploration of Bfd and its ability to Transfer Electrons to Bfr Heme

Recently, work detailing the necessity of a Bfd protein for electron transfer and iron release in Bfr derived from *Pseudomonas aeruginosa* was published[81]. An *E. coli* gene with high sequence similarity for *P. aeruginosa* Bfd is known, however the crystal structure, and electrochemical evaluation of this *E. coli* protein has not been investigated. By cloning and expressing Bfd it

would provide necessary information on the physical characteristics of this protein along with its interaction with Bfr. A sequence would have to be generated, and placed on a plasmid for expression. It is possible to have this sequence generated by GenScript and placed on a plasmid for a nominal fee. Expression should be without issue since this is a native protein to the host *E.* coli bacteria that would be employed for it's over expression. After expression the protein would need to be purified. Once pure, iron release characteristics should be analyzed to determine the electron transfer capability of *E. coli* Bfd, as was done previously.[81] A co-crystallized structure of *E. coli* Bfr and Bfd could be of importance for the futher characterization of the interface between the two, and to compare against the known *Pseudomonas aeruginosa* structure. This study would be of significance because it could unite the Bfr protein family with a common Bfd architecture for liberating Fe atoms from the interior. In addition, Bfd investigation could provide a unique methodology for transferring electrons to the Bfr core for a variety of purposes.

4.4.2. Synthesis of a Platinum Nanoparticles within Bfr and Analysis of its Catalytic Capabilities

Finally, the production of Pt NP would be explored within Bfr. The advantages of exploring NP synthesis within Bfr would be: predictive NP growth, avoidance of deactivation of the catalytic surface and mediators, improvement of difficult catalytic NP recovery, and prevention of NP aggregation.n[196] NPs would be synthesized as in previous publications with Pt in the presence of Bfr followed by reduction with sodium borohydride.[64] The Pt NP would be synthesized in varying sizes to evaluate the effect of size on the catalytic function, as has been previously explored.[194,196] The formation of these NP will be evaluated with TEM, and UV-Vis spectroscopy, as with the investigation of 5 nm GNP encapsulation in chapter two.

Two methods would be explored for electron transfer to heme: Bfd reduction of heme, and methyl viologen reduction of heme. The advantage of exploring both methods is that each has different means of generating electrons. Methyl viologen can generate electrons from light using a $Ru(bpy)_3^{2+}$

cocatalyst, whereas Bfd get electrons from ferredoxin, which derives electrons from NADPH. This electron transfer to heme in Bfr could be evaluated using electron paramagnetic resonance.[77] Evaluation of the ability to transfer electrons across the protein shell will provide evidence for the ability of Bfr to act as a nanoreactor for redox reactions. The production of H_2 gas will be evaluated by the production of hydrogen gas via GC-MS. If the heme cofactor proves to be electrochemically inappropriate it may be possible to switch the heme cofactor for another porphyrin or chlorin, or to modify the methionine residues coordinating the heme.[86,197] This work will push Bfr into applications with the potential to be a highly useful nanoreactor for fuel production and other catalytic functions.

Appendix

Appendix 1: MS of Dabsyl-glutamate with the calculated mass using high resolution mass spectrometry with a Thermo Scientific Q-Exactive™. The calculated mass matched that of the expected molar mass for Dabsyl-glutamate, highlighted with the red arrow.

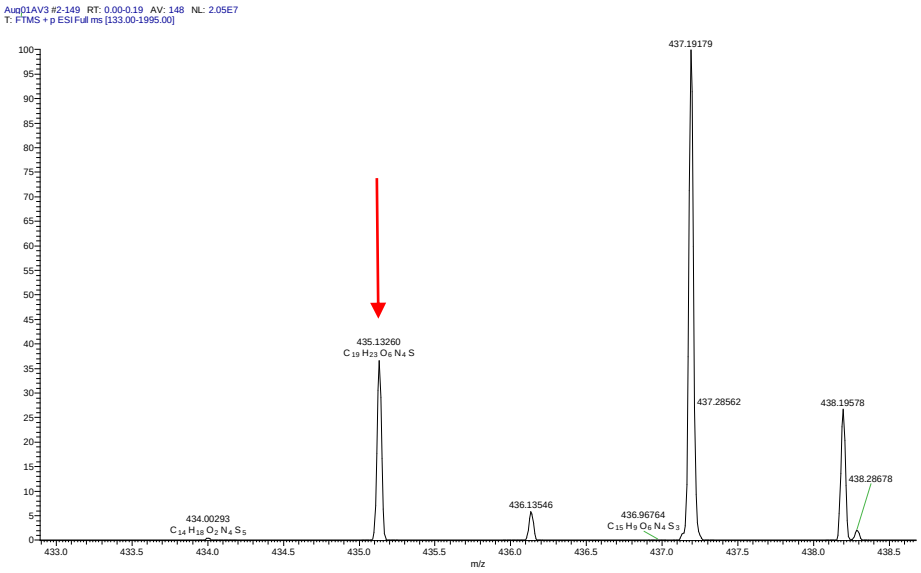

Appendix 2: Possible labelling sites for fluorescein isothiocyanate. Possible lysine labelling sites per subunit are highlighted in blue. The lysines were Lys 80, 121, 132, and 134. The number of lysine residues that were labelled on SF was unknown, with a maximum number of 16 residues being labelled per fully formed tetramer.

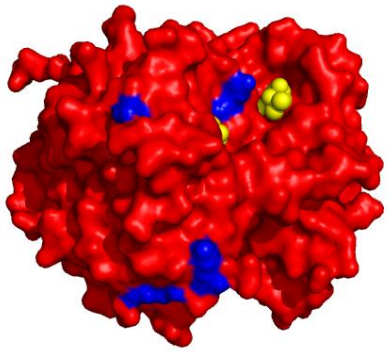

References

1. Ashley, C. E.; Carnes, E. C.; Phillips, G. K.; Durfee, P. N.; Buley, M. D.; Lino, C. A.; Padilla, D. P.; Phillips, B.; Carter, M. B.; Willman, C. L.; Brinker, C. J.; Caldeira, J. d. C.; Chackerian, B.; Wharton, W.; Peabody, D. S. Cell-Specific Delivery of Diverse Cargos by Bacteriophage MS2 Virus-like Particles. *ACS Nano* **2011**, *5*, 5729-5745.

2. Zhen, Z.; Tang, W.; Chen, H.; Lin, X.; Todd, T.; Wang, G.; Cowger, T.; Chen, X.; Xie, J. RGD-Modified Apoferritin Nanoparticles for Efficient Drug Delivery to Tumors. *ACS Nano* **2013**, *7*, 4830-4837.

3. Kostiainen, M. A.; Hiekkataipale, P.; Laiho, A.; Lemieux, V.; Seitsonen, J.; Ruokolainen, J.; Ceci, P. Electrostatic assembly of binary nanoparticle superlattices using protein cages. *Nat Nanotechnol* **2013**, *8*, 52-56.

4. Kashanian, S.; Tarighat, F. A.; Rafipour, R.; Abbasi-Tarighat, M. Biomimetic synthesis and characterization of cobalt nanoparticles using apoferritin, and investigation of direct electron transfer of Co(NPs)-ferritin at modified glassy carbon electrode to design a novel nanobiosensor. *Mol. Biol. Rep.* **2012**, *39*, 8793-8802.

5. Matsumoto, N. M.; Prabhakaran, P.; Rome, L. H.; Maynard, H. D. Smart Vaults: Thermally-Responsive Protein Nanocapsules. *ACS Nano* **2013**, *7*, 867-874.

6. Xiao, C.; Kuznetsov, Y. G.; Sun, S.; Hafenstein, S. L.; Kostyuchenko, V. A.; Chipman, P. R.; Suzan-Monti, M.; Raoult, D.; McPherson, A.; Rossmann, M. G. Structural Studies of the Giant Mimivirus. *Plos Biology* **2009**, *7*, 958-966.

7. Gauss, G. H.; Benas, P.; Wiedenheft, B.; Young, M.; Douglas, T.; Lawrence, C. M. Structure of the DPS-like protein from Sulfolobus solfataricus reveals a bacterioferritin-like dimetal binding site within a DPS-like dodecameric assembly. *Biochemistry* **2006**, *45*, 10815-10827.

8. Cornelissen, J. J. L. M. Chemical virology Packing polymers in protein cages. *Nat. Chem.* **2012**, *4*, 775-777.

9. Comellas-Aragones, M.; Engelkamp, H.; Claessen, V. I.; Sommerdijk, N. A. J. M.; Rowan, A. E.; Christianen, P. C. M.; Maan, J. C.; Verduin, B. J. M.; Cornelissen, J. J. L. M.; Nolte, R. J. M. A virus-based single-enzyme nanoreactor. *Nat Nanotechnol* **2007**, *2*, 635-639.

10. Ji, X.; Huang, L.; Huang, H. Construction of nanometer cisplatin core-ferritin (NCC-F) and proteomic analysis of gastric cancer cell apoptosis induced with cisplatin released from the NCC-F. *J Proteomics* **2012**, *75*, 3145-3157.

11. Patterson, D. P.; Schwarz, B.; El-Boubbou, K.; van der Oost, J.; Prevelige, P. E.; Douglas, T. Virus-like particle nanoreactors: programmed encapsulation of the thermostable CelB glycosidase inside the P22 capsid. *Soft Matter* **2012**, *8*, 10158-10166.

12. Patterson, D. P.; LaFrance, B.; Douglas, T. Rescuing recombinant proteins by sequestration into the P22 VLP. *Chem Commun* **2013**, *49*, 10412-10414.

13. Patterson, D. P.; Prevelige, P. E.; Douglas, T. Nanoreactors by Programmed Enzyme Encapsulation Inside the Capsid of the Bacteriophage P22. *ACS Nano* **2012**, *6*, 5000-5009.

14. O'Neil, A.; Reichhardt, C.; Johnson, B.; Prevelige, P. E.; Douglas, T. Genetically Programmed In Vivo Packaging of Protein Cargo and Its Controlled Release from Bacteriophage P22. *Angew Chem Int Edit* **2011**, *50*, 7425-7428.

15. Patterson, D. P.; Schwarz, B.; Waters, R. S.; Gedeon, T.; Douglas, T. Encapsulation of an Enzyme Cascade within the Bacteriophage P22 Virus-Like Particle. *ACS Chem Biol* **2013**, *9*, 359-365.

16. O'Neil, A.; Prevelige, P. E.; Basu, G.; Douglas, T. Coconfinement of Fluorescent Proteins: Spatially Enforced Communication of GFP and mCherry Encapsulated within the P22 Capsid. *Biomacromolecules* **2012**, *13*, 3902-3907.

17. Stephanopoulos, N.; Tong, G. J.; Hsiao, S. C.; Francis, M. B. Dual-Surface Modified Virus Capsids for Targeted Delivery of Photodynamic Agents to Cancer Cells. *ACS Nano* **2010**, *4*, 6014-6020.

18. Uchida, M.; Kosuge, H.; Terashima, M.; Willits, D. A.; Liepold, L. O.; Young, M. J.; McConnell, M. V.; Douglas, T. Protein Cage Nanoparticles Bearing the LyP-1 Peptide for Enhanced Imaging of Macrophage-Rich Vascular Lesions. *ACS Nano* **2011**, *5*, 2493-2502.

19. Lucon, J.; Qazi, S.; Uchida, M.; Bedwell, G. J.; LaFrance, B.; Prevelige, P. E., Jr.; Douglas, T. Use of the interior cavity of the P22 capsid for site-specific initiation of atom-transfer radical polymerization with high-density cargo loading. *Nat Chem* **2012**, *4*, 781-788.

20. Minten, I. J.; Nolte, R. J. M.; Cornelissen, J. J. L. M. Complex Assembly Behavior During the Encapsulation of Green Fluorescent Protein Analogs in Virus Derived Protein Capsules. *Macromol Biosci* **2010**, *10*, 539-545.

21. Buehler, D. C.; Toso, D. B.; Kickhoefer, V. A.; Zhou, Z. H.; Rome, L. H. Vaults Engineered for Hydrophobic Drug Delivery. *Small* **2011**, *7*, 1432-1439.

22. Goldsmith, L. E.; Pupols, M.; Kickhoefer, V. A.; Rome, L. H.; Monbouquette, H. G. Utilization of a Protein "Shuttle" To Load Vault Nanocapsules with Gold Probes and Proteins. *ACS Nano* **2009**, *3*, 3175-3183.

23. Uchida, M.; Morris, D. S.; Kang, S.; Jolley, C. C.; Lucon, J.; Liepold, L. O.; LaFrance, B.; Prevelige, P. E., Jr.; Douglas, T. Site-Directed Coordination Chemistry with P22 Virus-like Particles. *Langmuir* **2012**, *28*, 1998-2006.

24. Abe, S.; Hirata, K.; Ueno, T.; Morino, K.; Shimizu, N.; Yamamoto, M.; Takata, M.; Yashima, E.; Watanabe, Y. Polymerization of Phenylacetylene by Rhodium Complexes within a Discrete Space of apo-Ferritin. *J. Am. Chem. Soc.* **2009**, *131*.

25. Choi, K.; Choi, S.; Jeon, H.; Kim, I.; Ahn, H. J. Chimeric Capsid Protein as a Nanocarrier for siRNA Delivery: Stability and Cellular Uptake of Encapsulated siRNA. *ACS Nano* **2011**, *5*, 8690-8699.

26. Ma-Ham, A.; Wu, H.; Wang, J.; Kang, X.; Zhang, Y.; Lin, Y. Apoferritin-based nanomedicine platform for drug delivery: equilibrium binding study of daunomycin with DNA. *J Mater Chem* **2011**, *21*, 8700-8708.

27. Parveen, S.; Misra, R.; Sahoo, S. K. Nanoparticles: a boon to drug delivery, therapeutics, diagnostics and imaging. *Nanomed-Nanotechnol* **2012**, *8*, 147-166.

28. Choi, H. S.; Liu, W.; Misra, P.; Tanaka, E.; Zimmer, J. P.; Ipe, B. I.; Bawendi, M. G.; Frangioni, J. V. Renal clearance of quantum dots. *Nat. Biotechnol.* **2007**, *25*, 1165-1170.

29. Maeda, H.; Wu, J.; Sawa, T.; Matsumura, Y.; Hori, K. Tumor vascular permeability and the EPR effect in macromolecular therapeutics: a review. *J. Controlled Release* **2000**, *65*, 271-284.

30. Maeda, H.; Bharate, G. Y.; Daruwalla, J. Polymeric drugs for efficient tumor-targeted drug delivery based on EPR-effect. *Eur J Pharm Biopharm* **2009**, *71*, 409-419.

31. Flenniken, M.; Liepold, L.; Crowley, B.; Willits, D.; Young, M.; Douglas, T. Selective attachment and release of a chemotherapeutic agent from the interior of a protein cage architecture. *Chem Commun* **2005**, 447-449.

32. Goutayer, M.; Dufort, S.; Josserand, V.; Royere, A.; Heinrich, E.; Vinet, F.; Bibette, J.; Coll, J.; Texier, I. Tumor targeting of functionalized lipid nanoparticles: Assessment by in vivo fluorescence imaging. *Eur J Pharm Biopharm* **2010**, *75*, 137-147.

33. Ranson, M.; Cheeseman, S.; White, S.; Margison, J. Caelyx (stealth liposomal doxorubicin) in the treatment of advanced breast cancer. CRC *Cr Rev Oncol-Hem* **2001**, *37*, 115-120.

34. Zamboni, W. C. Liposomal, nanoparticle, and conjugated formulations of anticancer agents. *Clin Cancer Res* **2005**, *11*.

35. Wang, A. Z.; Langer, R.; Farokhzad, O. C. Nanoparticle Delivery of Cancer Drugs. *Annu Rev Med* **2012**, *63*, 185-198.

36. Abbing, A.; Blaschke, U.; Grein, S.; Kretschmar, M.; Stark, C.; Thies, M.; Walter, J.; Weigand, M.; Woith, D.; Hess, J.; Reiser, C. Efficient intracellular delivery of a protein and a low molecular weight substance via recombinant polyomavirus-like particles. *J. Biol. Chem.* **2004**, *279*, 27410-27421.

37. Buehler, D. C.; Toso, D. B.; Kickhoefer, V. A.; Zhou, Z. H.; Rome, L. H. Vaults Engineered for Hydrophobic Drug Delivery. *Small* **2011**, *7*, 1432-1439.

38. Inoue, T.; Kawano, M.; Takahashi, R.; Tsukarnoto, H.; Enornoto, T.; Imai, T.; Kataoka, K.; Handa, H. Engineering of SV40-based nano-capsules for delivery of heterologous proteins as fusions with the minor capsid proteins VP2/3. *J. Biotechnol.* **2008**, *134*, 181-192.

39. Lipin, D. I.; Chuan, Y. P.; Lua, L. H. L.; Middelberg, A. P. J. Encapsulation of DNA and non-viral protein changes the structure of murine polyomavirus virus-like particles. *Arch. Virol.* **2008**, *153*, 2027-2039.

40. Uchida, M.; Flenniken, M. L.; Allen, M.; Willits, D. A.; Crowley, B. E.; Brumfield, S.; Willis, A. F.; Jackiw, L.; Jutila, M.; Young, M. J.;

Douglas, T. Targeting of cancer cells with ferrimagnetic ferritin cage nanoparticles. *J. Am. Chem. Soc.* **2006**, *128*, 16626-16633.

41. Wu, H.; Engelhard, M. H.; Wang, J.; Fisher, D. R.; Lin, Y. Synthesis of lutetium phosphate-apoferritin core-shell nanoparticles for potential applications in radioimmunoimaging and radioimmunotherapy of cancers. *J Mater Chem* **2008**, *18*, 1779-1783.

42. Rae, C.; Khor, I.; Wang, Q.; Destito, G.; Gonzalez, M.; Singh, P.; Thomas, D.; Estrada, M.; Powell, E.; Finn, M.; Manchester, M. Systemic trafficking of plant virus nanoparticles in mice via the oral route. *Virology* **2005**, *343*, 224-235.

43. Kaiser, C. R.; Flenniken, M. L.; Gillitzer, E.; Harmsen, A. L.; Harmsen, A. G.; Jutila, M. A.; Douglas, T.; Young, M. J. Biodistribution studies of protein cage nanoparticles demonstrate broad tissue distribution and rapid clearance in vivo. *Int J Nanomed* **2007**, *2*, 715-733.

44. Allen, M.; Bulte, J. W. M.; Liepold, L.; Basu, G.; Zywicke, H. A.; Frank, J. A.; Young, M.; Douglas, T. Paramagnetic viral nanoparticles as potential high-relaxivity magnetic resonance contrast agents. *Magn Reson Med* **2005**, *54*, 807-812.

45. Niikura, K.; Sugimura, N.; Musashi, Y.; Mikuni, S.; Matsuo, Y.; Kobayashi, S.; Nagakawa, K.; Takahara, S.; Takeuchi, C.; Sawa, H.; Kinjo, M.; Ijiro, K. Virus-like particles with removable cyclodextrins enable glutathione-triggered drug release in cells. *Mol Biosyst* **2013**, *9*, 501-507.

46. Toita, R.; Murata, M.; Abe, K.; Narahara, S.; Piao, J. S.; Kang, J.; Ohuchida, K.; Hashizume, M. Biological evaluation of protein nanocapsules containing doxorubicin. *Int J Nanomed* **2013**, *8*, 1989-1999.

47. Zeng, Q.; Wen, H.; Wen, Q.; Chen, X.; Wang, Y.; Xuan, W.; Liang, J.; Wan, S. Cucumber mosaic virus as drug delivery vehicle for doxorubicin. *Biomaterials* **2013**, *34*, 4632-4642.

48. Lin, X.; Xie, J.; Zhu, L.; Lee, S.; Niu, G.; Ma, Y.; Kim, K.; Chen, X. Hybrid Ferritin Nanoparticles as Activatable Probes for Tumor Imaging. *Angew Chem Int Edit* **2011**, *50*, 1569-1572.

49. Kang, Y. J.; Park, D. C.; Shin, H.; Park, J.; Kang, S. Incorporation of Thrombin Cleavage Peptide into a Protein Cage for Constructing a Protease-Responsive Multifunctional Delivery Nanoplatform. *Biomacromolecules* **2012**, *13*, 4057-4064.

50. Ma-Ham, A.; Wu, H.; Wang, J.; Kang, X.; Zhang, Y.; Lin, Y. Apoferritin-based nanomedicine platform for drug delivery: equilibrium binding study of daunomycin with DNA. *J Mater Chem* **2011**, *21*, 8700-8708.

51. Li, X.; Qiu, L.; Zhu, P.; Tao, X.; Imanaka, T.; Zhao, J.; Huang, Y.; Tu, Y.; Cao, X. Epidermal Growth Factor-Ferritin H-Chain Protein Nanoparticles for Tumor Active Targeting. *Small* **2012**, *8*, 2505-2514.

52. Jeon, J. O.; Kim, S.; Choi, E.; Shin, K.; Cha, K.; So, I.; Kim, S.; Jun, E.; Kim, D.; Ahn, H. J.; Lee, B.; Lee, S.; Kim, I. Designed Nanocage Displaying Ligand-Specific Peptide Bunches for High Affinity and Biological Activity. *ACS Nano* **2013**, *7*, 7462-7471.

53. Yoffe, A. Semiconductor quantum dots and related systems: electronic, optical, luminescence and related properties of low dimensional systems. *Adv. Phys.* **2001**, *50*, 1-208.

54. Kumagai, S.; Yoshii, S.; Yamada, K.; Matsukawa, N.; Iwahori, K.; Yamashita, I. Electrostatic placement of nanodots onto silicon substrate using ferritin protein supramolecules with control of electrostatic interaction in solution. *Jpn J Appl Phys 1* **2006**, *45*, 8311-8316.

55. Miura, A.; Hikono, T.; Matsumura, T.; Yano, H.; Hatayama, T.; Uraoka, Y.; Fuyuki, T.; Yoshii, S.; Yamashita, I. Floating nanodot gate memory devices based on biomineralized inorganic nanodot array as a storage node. *Jpn J Appl Phys 2* **2006**, *45*, L1-L3.

56. Miura, A.; Uraoka, Y.; Fuyuki, T.; Yoshii, S.; Yamashita, I. Floating nanodot gate memory fabrication with biomineralized nanodot as charge storage node. *J. Appl. Phys.* **2008**, *103*, 074503.

57. Ichikawa, K.; Uraoka, Y.; Punchaipetch, P.; Yano, H.; Hatayama, T.; Fuyuki, T.; Yamashita, I. Low-temperature polycrystalline silicon thin film transistor flash memory with ferritin. *Jpn J ApplPhys 2* **2007**, *46*, L804-L806.

58. Wang, T.; Choi, H. W.; Yoo, I. S.; Kim, J. S.; Park, S. J. Preparation of Two-dimensional Array of Nanodots by Ferritin Template. *Mol Cryst Liq Cryst* **2009**, *505*, 386-395.

59. Li, F.; Li, K.; Cui, Z.; Zhang, Z.; Wei, H.; Gao, D.; Deng, J.; Zhang, X. Viral Coat Proteins as Flexible Nano-Building-Blocks for Nanoparticle Encapsulation. *Small* **2010**, *6*, 2301-2308.

60. Minten, I. J.; Claessen, V. I.; Blank, K.; Rowan, A. E.; Nolte, R. J. M.; Cornelissen, J. J. L. M. Catalytic capsids: the art of confinement. *Chemical Science* **2011**, *2*, 358-362.

61. Chen, Q.; Schoenherr, H.; Vancso, G. J. Block-Copolymer Vesicles as Nanoreactors for Enzymatic Reactions. *Small* **2009**, *5*, 1436-1445.

62. Giacomini, C.; Villarino, A.; Franco-Fraguas, L.; Batista-Viera, F. Immobilization of beta-galactosidase from Kluyveromyces lactis on silica and agarose: comparison of different methods. *J Mol Catal B-Enzym* **1998**, *4*, 313-327.

63. Song, Y. S.; Lee, J. H.; Kang, S. W.; Kim, S. W. Performance of beta-galactosidase pretreated with lactose to prevent activity loss during the enzyme immobilisation process. *Food Chem.* **2010**, *123*, 1-5.

64. Varpness, Z.; Peters, J.; Young, M.; Douglas, T. Biomimetic synthesis of a H-2 catalyst using a protein cage architecture. *Nano Letters* **2005**, *5*, 2306-2309.

65. Iwahori, K.; Yamashita, I. Bio-template synthesis of nanoparticle by cage-shaped protein supramolecule, apoferritin. *J Clust Sci* **2007**, *18*, 358-370.

66. Douglas, T.; Stark, V. Nanophase cobalt oxyhydroxide mineral synthesized within the protein cage of ferritin. *Inorg. Chem.* **2000**, *39*, 1828-1830.

67. Dominguez-Vera, J.; Colacio, E. Nanoparticles of Prussian blue ferritin: A new route for obtaining nanomaterials. *Inorg. Chem.* **2003**, *42*, 6983-6985.

68. Clemente-Leon, M.; Coronado, E.; Soriano-Portillo, A.; Galvez, N.; Dominguez-Vera, J. M. Permanent magnetism in apoferritin-encapsulated Pd nanoparticles. *J Mater Chem* **2007**, *17*, 49-51.

69. Iwahori, K.; Yamashita, I. Size-controlled one-pot synthesis of fluorescent cadmium sulfide semiconductor nanoparticles in an apoferritin cavity. *Nanotechnology* **2008**, *19*, 495601.

70. Iwahori, K.; Yoshizawa, K.; Muraoka, M.; Yamashita, I. Fabrication of ZnSe nanoparticles in the apoferritin cavity by designing a slow chemical reaction system. *Inorg. Chem.* **2005**, *44*, 6393-6400.

71. Klem, M. T.; Young, M.; Douglas, T. Biomimetic synthesis of photoactive alpha-Fe2O3 templated by the hyperthermophilic ferritin from Pyrococus furiosus. *J Mater Chem* **2010**, *20*, 65-67.

72. Warren, Martin J. Smith,Alison G. *Tetrapyrroles birth, life, and death /;* Austin, Tex. N.Y. Landes Bioscience, Springer Science & Business Media, 2009.

73. Perutz, M.; Wilkinson, A.; Paoli, M.; Dodson, G. The stereochemical mechanism of the cooperative effects in hemoglobin revisited. *Annu. Rev. Biophys. Biomol. Struct.* **1998**, *27*, 1-34.

74. Dorman, S.; Kenny, C.; Miller, L.; Hirsch, R.; Harrington, J. Role of redox potential of hemoglobin-based oxygen carriers on methemoglobin reduction by plasma components. *Artif Cell Blood Sub* **2002**, *30*, 39-51.

75. Popovic, D. M.; Leontyev, I. V.; Beech, D. G.; Stuchebrukhov, A. A. Similarity of cytochrome c oxidases in different organisms. *Proteins* **2010**, *78*, 2691-2698.

76. Saraste, M. Structure and Evolution of Cytochrome-Oxidase. *Anton Leeuw Int J G* **1994**, *65*, 285-287.

77. Cheesman, M.; Kadir, F.; Albasseet, J.; Almassad, F.; Farrar, J.; Greenwood, C.; Thomson, A.; Moore, G. Epr and Magnetic Circular-Dichroism Spectroscopic Characterization of Bacterioferritin from Pseudomonas-Aeruginosa and Azotobacter-Vinelandii. *Biochem. J.* **1992**, *286*, 361-367.

78. Wrighton, S.; Stevens, J. The Human Hepatic Cytochromes-P450 Involved in Drug-Metabolism. *Crit. Rev. Toxicol.* **1992**, *22*, 1-21.

79. Nelson, D.; Koymans, L.; Kamataki, T.; Stegeman, J.; Feyereisen, R.; Waxman, D.; Waterman, M.; Gotoh, O.; Coon, M.; Estabrook, R.; Gunsalus, I.; Nebert, D. P450 superfamily: Update on new sequences, gene mapping, accession numbers and nomenclature. *Pharmacogenetics* **1996**, *6*, 1-42.

80. Das, A.; Grinkova, Y. V.; Sligar, S. G. Redox potential control by drug binding to cytochrome p450 3A4. *J. Am. Chem. Soc.* **2007**, *129*, 13778-+.

81. Yao, H.; Wang, Y.; Lovell, S.; Kumar, R.; Ruvinsky, A. M.; Battaile, K. P.; Vakser, I. A.; Rivera, M. The Structure of the BfrB-Bfd Complex

Reveals Protein-Protein Interactions Enabling Iron Release from Bacterioferritin. *J. Am. Chem. Soc.* **2012**, *134*, 13470-13481.

82. Watt, G.; Frankel, R.; Papaefthymiou, G.; Spartalian, K.; Stiefel, E. Redox Properties and Mossbauer-Spectroscopy of Azotobacter-Vinelandii Bacterioferritin. *Biochemistry* **1986**, *25*, 4330-4336.

83. Guallar, V.; Olsen, B. The role of the heme propionates in heme biochemistry. *J. Inorg. Biochem.* **2006**, *100*, 755-760.

84. Takayama, S.; Mikami, S.; Terui, N.; Mita, H.; Hasegawa, J.; Sambongi, Y.; Yamamoto, Y. Control of the redox potential of Pseudomonas aeruginosa cytochrome c(551) through the Fe-Met coordination bond strength and pK(a) of a buried heme propionic acid side chain. *Biochemistry* **2005**, *44*, 5488-5494.

85. Zheng, Z.; Gunner, A. R. Analysis of the electrochemistry of hemes with E(m)s spanning 800 mV. *Proteins* **2009**, *75*, 719-734.

86. Chapman, S.; Daff, S.; Munro, A. Heme: The most versatile redox centre in biology? *Struct Bond* **1997**, *88*, 39-70.

87. Watanabe, H.; Hirakawa, H.; Nagamune, T. Phosphite-driven Self-sufficient Cytochrome P450. *Chemcatchem* **2013**, *5*, 3835-3840.

88. Schwaneberg, U.; Appel, D.; Schmitt, J.; Schmid, R. P450 in biotechnology: zinc driven omega-hydroxylation of p-nitrophenoxydodecanoic acid using P450BM-3 F87A as a catalyst. *J. Biotechnol.* **2000**, *84*, 249-257.

89. Turbe-Doan, A.; Arfi, Y.; Record, E.; Estrada-Alvarado, I.; Levasseur, A. Heterologous production of cellobiose dehydrogenases from the basidiomycete Coprinopsis cinerea and the ascomycete Podospora anserina and their effect on saccharification of wheat straw. *Appl. Microbiol. Biotechnol.* **2013**, *97*, 4873-4885.

90. Trifonov, A.; Herkendell, K.; Tel-Vered, R.; Yehezkeli, O.; Woerner, M.; Willner, I. Enzyme-Capped Relay-Functionalized Mesoporous Carbon Nanoparticles: Effective Bioelectrocatalytic Matrices for Sensing and Biofuel Cell Applications. *ACS Nano* **2013**, *7*, 11358-11368.

91. Urlacher, V.; Lutz-Wahl, S.; Schmid, R. Microbial P450 enzymes in biotechnology. *Appl. Microbiol. Biotechnol.* **2004**, *64*, 317-325.

92. Kee, H. L.; Kirmaier, C.; Tang, G.; Diers, J. R.; Muthiah, C.; Taniguchi, M.; Laha, J. K.; Ptaszek, M.; Lindsey, J. S.; Bocian, D. F.; Hoten, D. Effects of substituents on synthetic analogs of chlorophylls. Part 2: Redox properties, optical spectra and electronic structure. *Photochem. Photobiol.* **2007**, *83*, 1125-1143.

93. Mahboob, A.; Vassiliev, S.; Poddutoori, P. K.; van der Est, A.; Bruce, D. Factors Controlling the Redox Potential of ZnCe6 in an Engineered Bacterioferritin Photochemical 'Reaction Centre'. *Plos One* **2013**, *8*.

94. Fruk, L.; Mueller, J.; Weber, G.; Narvaez, A.; Dominguez, E.; Niemeyer, C. M. DNA-Directed immobilization of horseradish peroxidase-DNA conjugates on microelectrode arrays: Towards electrochemical screening of enzyme libraries. *Chem-Eur J* **2007**, *13*, 5223-5231.

95. Fruk, L.; Mueller, J.; Niemeyer, C. M. Kinetic analysis of semisynthetic peroxidase enzymes containing a covalent DNA-heme adduct as the cofactor. *Chem-Eur J* **2006**, *12*, 7448-7457.

96. Fruk, L.; Kuhlmann, J.; Niemeyer, C. M. Analysis of heme-reconstitution of apoenzymes by means of surface plasmon resonance. *Chem Commun* **2009**, 230-232.

97. Fruk, L.; Kuo, C.; Torres, E.; Niemeyer, C. M. Apoenzyme Reconstitution as a Chemical Tool for Structural Enzymology and Biotechnology. *Angew Chem Int Edit* **2009**, *48*, 1550-1574.

98. Kuo, C.; Fruk, L.; Niemeyer, C. M. Addressable DNA-Myoglobin Photocatalysis. *Chem-Asian J* **2009**, *4*, 1064-1069.

99. Onoda, A.; Himiyama, T.; Ohkubo, K.; Fukuzumi, S.; Hayashi, T. Photochemical properties of a myoglobin-CdTe quantum dot conjugate. *Chem Commun* **2012**, *48*, 8054-8056.

100. Sato, H.; Hayashi, T.; Ando, T.; Hisaeda, Y.; Ueno, T.; Watanabe, Y. Hybridization of modified-heme reconstitution and distal histidine mutation to functionalize sperm whale-myoglobin. *J. Am. Chem. Soc.* **2004**, *126*, 436-437.

101. Feng, J.; Liu, J.; Ji, L. Thermostability, solvent tolerance, catalytic activity and conformation of cofactor modified horseradish peroxidase. *Biochimie* **2008**, *90*, 1337-1346.

102. Gorton, L.; Lindgren, A.; Larsson, T.; Munteanu, F.; Ruzgas, T.; Gazaryan, I. Direct electron transfer between heme-containing enzymes

and electrodes as basis for third generation biosensors. *Anal. Chim. Acta* **1999**, *400*, 91-108.

103. Tahir, M. N.; Andre, R.; Sahoo, J. K.; Jochum, F. D.; Theato, P.; Natalio, F.; Berger, R.; Branscheid, R.; Kolb, U.; Tremel, W. Hydrogen peroxide sensors for cellular imaging based on horse radish peroxidase reconstituted on polymer-functionalized TiO2 nanorods. *Nanoscale* **2011**, *3*, 3907-3914.

104. Brase, S.; Gil, C.; Knepper, K.; Zimmermann, V. Organic azides: An exploding diversity of a unique class of compounds. *Angew Chem Int Edit* **2005**, *44*, 5188-5240.

105. Lin, F.; Hoyt, H.; van Halbeek, H.; Bergman, R.; Bertozzi, C. Mechanistic investigation of the Staudinger ligation. *J. Am. Chem. Soc.* **2005**, *127*, 2686-2695.

106. Huisgen, R. 1.3-Dipolare Cycloadditionen - Ruckschau Und Ausblick. *Angew Chem Int Edit* **1963**, *75*.

107. de Araujo, A.; Palomo, J.; Cramer, J.; Kohn, M.; Schroder, H.; Wacker, R.; Niemeyer, C.; Alexandrov, K.; Waldmann, H. Diels-Alder ligation and surface immobilization of proteins. *Angew Chem Int Edit* **2006**, *45*, 296-301.

108. Sletten, E. M.; Bertozzi, C. R. From Mechanism to Mouse: A Tale of Two Bioorthogonal Reactions. *Acc. Chem. Res.* **2011**, *44*.

109. Debets, M. F.; van der Doelen, C. W. J.; Rutjes, F. P. J. T.; van Delft, F. L. Azide: A Unique Dipole for Metal-Free Bioorthogonal Ligations. *Chembiochem* **2010**, *11*, 1168-1184.

110. Smith,J.C., Lee, K., Wang, Q., Finn, M.G., Johnson, J.E., Mrksich, M., and Mirkin, C.A. Nanopatterning the Chemospecific Immobilization of Cowpea Mosaic Virus Capsid. *Nano Lett* **2003**, *3*, 883-886.

111. Kim, Y.; Ho, S. O.; Gassman, N. R.; Korlann, Y.; Landorf, E. V.; Collart, F. R.; Weiss, S. Efficient site-specific Labeling of proteins via cysteines. *Bioconjug. Chem.* **2008**, *19*, 786-791.

112. Chatterji, A.; Ochoa, W. F.; Paine, M.; Ratna, B. R.; Johnson, J. E.; Lin, T. W. New addresses on an addressable virus nanoblock: Uniquely reactive lys residues on cowpea mosaic virus. *Chem. Biol.* **2004**, *11*, 855-863.

113. Prasuhn, D. E.,Jr.; Yeh, R. M.; Obenaus, A.; Manchester, M.; Finn, M. G. Viral MRI contrast agents: coordination of Gd by native virions and attachment of Gd complexes by azide-alkyne cycloaddition. *Chem Commun* **2007**, 1269-1271.

114. Wang, Q.; Lin, T. W.; Johnson, J. E.; Finn, M. G. Natural supramolecular building blocks: Cysteine-added mutants of cowpea mosaic virus. *Chem. Biol.* **2002**, *9*, PII S1074-5521(02)00166-7.

115. Hooker, J. M.; Kovacs, E. W.; Francis, M. B. Interior surface modification of bacteriophage MS2. *J. Am. Chem. Soc.* **2004**, *126*, 3718-3719.

116. Tilley, S. D.; Francis, M. B. Tyrosine-selective protein alkylation using pi-allylpalladium complexes. *J. Am. Chem. Soc.* **2006**, *128*.

117. Wong, K. K. W.; Whilton, N. T.; Colfen, H.; Douglas, T.; Mann, S. Hydrophobic proteins: synthesis and characterisation of organic-soluble alkylated ferritins. *Chem Commun* **1998**, 1621-1622.

118. Vaughan, M. D.; Robertson, V. J.; Honek, J. F. Experimental and theoretical studies on inversion dynamics of dichloro(L-difluoromethionine-N,S)platinum(II) and dichloro(L-trifluoromethionine-N,S)platinum(II) complexes. *J. Fluorine Chem.* **2007**, *128*, 65-70.

119. Ngo, J. T.; Tirrell, D. A. Noncanonical Amino Acids in the Interrogation of Cellular Protein Synthesis. *Acc. Chem. Res.* **2011**, *44*, 677-685.

120. Lin, C. W.; Ting, A. Y. Transglutaminase-catalyzed site-specific conjugation of small-molecule probes to proteins in vitro and on the surface of living cells. *J. Am. Chem. Soc.* **2006**, *128*.

121. Seebeck, F. P.; Woycechowsky, K. J.; Zhuang, W.; Rabe, J. P.; Hilvert, D. A simple tagging system for protein encapsulation. *J. Am. Chem. Soc.* **2006**, *128*, 4516-4517.

122. Li, Y. G.; Tseng, Y. D.; Kwon, S. Y.; D'Espaux, L.; Bunch, J. S.; Mceuen, P. L.; Luo, D. Controlled assembly of dendrimer-like DNA. *Nat Mater* **2004**, *3*, 38-42.

123. Uchida, M.; Morris, D. S.; Kang, S.; Jolley, C. C.; Lucon, J.; Liepold, L. O.; LaFrance, B.; Prevelige, P. E.,Jr.; Douglas, T. Site-Directed Coordination Chemistry with P22 Virus-like Particles. *Langmuir* **2012**, *28*, 1998-2006.

124. Minten, I. J.; Claessen, V. I.; Blank, K.; Rowan, A. E.; Nolte, R. J. M.; Cornelissen, J. J. L. M. Catalytic capsids: the art of confinement. *Chemical Science* **2011**, *2*, 358-362.

125. Sarikaya, M.; Tamerler, C.; Jen, A. K. Y.; Schulten, K.; Baneyx, F. Molecular biomimetics: nanotechnology through biology. *Nat Mater* **2003**, *2*, 577-585.

126. Huang, J.; Ru, B.; Dai, P. Bioinformatics Resources and Tools for Phage Display. *Molecules* **2011**, *16*, 694-709.

127. Frolow, F.; Kalb, A.; Yariv, J. Structure of a Unique Twofold Symmetrical Heme-Binding Site. *Nat. Struct. Biol.* **1994**, *1*, 453-460.

128. Andrew, S.; Lebrun, N.; Barynin, V.; Thomson, A.; Moore, G.; Guest, J.; Harrison, P. Site-Directed Replacement of the Coaxial Heme Ligands of Bacterioferritin Generates Heme-Free Variants. *J. Biol. Chem.* **1995**, *270*, 23268-23274.

129. Grossman, M.; Hinton, S.; Minakbernero, V.; Slaughter, C.; Stiefel, E. Unification of the Ferritin Family of Proteins. *Proc. Natl. Acad. Sci. U. S. A.* **1992**, *89*, 2419-2423.

130. Dunford, H. Oxidations of iron(II)/(III) by hydrogen peroxide: from aquo to enzyme. *Coord. Chem. Rev.* **2002**, *233*, 311-318.

131. Pulliainen, A.; Kauko, A.; Haataja, S.; Papageorgiou, A.; Finne, J. Dps/Dpr ferritin-like protein: insights into the mechanism of iron incorporation and evidence for a central role in cellular iron homeostasis in Streptococcus suis. *Mol. Microbiol.* **2005**, *57*, 1086-1100.

132. Crow, A.; Lawson, T. L.; Lewin, A.; Moore, G. R.; Le Brun, N. E. Structural Basis for Iron Mineralization by Bacterioferritin. *J. Am. Chem. Soc.* **2009**, *131*, 6808-6813.

133. Yang, X.; Le Brun, N.; Thomson, A.; Moore, C.; Chasteen, N. The iron oxidation and hydrolysis chemistry of Escherichia coli bacterioferritin. *Biochemistry* **2000**, *39*, 4915-4923.

134. Wong, S. G.; Abdulqadir, R.; Le Brun, N. E.; Moore, G. R.; Mauk, A. G. Fe-haem bound to Escherichia coil bacterioferritin accelerates iron core formation by an electron transfer mechanism. *Biochem. J.* **2012**, *444*.

135. Dautant, A.; Meyer, J.; Yariv, J.; Precigoux, G.; Sweet, R.; Kalb, A.; Frolow, F. Structure of a monoclinic crystal form of cytochrome b1 (bacterioferritin) from E-coli. *Acta Crystallogr. Sect. D* **1998**, *54*, 16-24.

136. Macedo, S.; Romao, C. V.; Mitchell, E.; Matias, P. M.; Liu, M. Y.; Xavier, A. V.; LeGall, J.; Teixeira, M.; Lindley, P.; Carrondo, M. A. The nature of the di-iron site in the bacterioferritin from Desulfovibrio desulfuricans. *Nat. Struct. Biol.* **2003**, *10*, 285-290.

137. Fan, R.; Boyle, A. L.; Cheong, V. V.; Ng, S. L.; Orner, B. P. A Helix Swapping Study of Two Protein Cages. *Biochemistry* **2009**, *48*, 5623-5630.

138. Ardejani, M. S.; Li, N. X.; Orner, B. P. Stabilization of a Protein Nanocage through the Plugging of a Protein-Protein Interfacial Water Pocket. *Biochemistry* **2011**, *50*, 4029-4037.

139. Wong, S. G.; Abdulqadir, R.; Le Brun, N. E.; Moore, G. R.; Mauk, A. G. Fe-haem bound to Escherichia coil bacterioferritin accelerates iron core formation by an electron transfer mechanism. *Biochem. J.* **2012**, *444*, 553-560.

140. Conlan, B.; Cox, N.; Su, J.; Hillier, W.; Messinger, J.; Lubitz, W.; Dutton, P. L.; Wydrzynski, T. Photo-catalytic oxidation of a di-nuclear manganese centre in an engineered bacterioferritin 'reaction centre'. *BBA Bioenergetics* **2009**, *1787*, 1112-1121.

141. Suttisansanee, U. Biochemistry in Bacterioferritin, Unpublished doctoral dissertation, University of Waterloo, Waterloo, Ontario Canada. 2006.

142. Huang, Z.; Park, J. I.; Watson, D. S.; Hwang, P.; Szoka, F. C., Jr. Facile synthesis of multivalent nitrilotriacetic acid (NTA) and NTA conjugates for analytical and drug delivery applications. *Bioconjug. Chem.* **2006**, *17*, 1592-1600.

143. Garner, D. K.; Vaughan, M. D.; Hwang, H. J.; Savelieff, M. G.; Berry, S. M.; Honek, J. F.; Lu, Y. Reduction potential tuning of the blue copper center in Pseudomonas aeruginosa azurin by the axial methionine as probed by unnatural amino acids. *J. Am. Chem. Soc.* **2006**, *128*, 15608-15617.

144. Dautant, A.; Meyer, J.; Yariv, J.; Precigoux, G.; Sweet, R.; Kalb, A.; Frolow, F. Structure of a monoclinic crystal form of cytochrome b1 (bacterioferritin) from E-coli. *Acta Crystallogr D* **1998**, *54*, 16-24.

145. Raines, R.; McCormick, M.; Van Oosbree, T.; Mierendorf, R. The S center dot tag fusion system for protein purification. *Method Enzymol* **2000**, *326*, 362-376.

146. KIM, J.; RAINES, R. Ribonuclease S-Peptide as a Carrier in Fusion Proteins. *Protein Sci.* **1993**, *2*, 348-356.

147. Motoki, M.; Seguro, K. Transglutaminase and its use for food processing. *Trends Food Sci. Technol.* **1998**, *9*, 204-210.

148. Lee, J.; Song, C.; Kim, D.; Park, I.; Lee, S.; Lee, Y.; Kim, B. Glutamine (Q)-peptide screening for transglutaminase reaction using mRNA display. *Biotechnol. Bioeng.* **2013**, *110*, 353-362.

149. Sugimura, Y.; Hosono, M.; Wada, F.; Yoshimura, T.; Maki, M.; Hitomi, K. Screening for the preferred substrate sequence of transglutaminase using a phage-displayed peptide library - Identification of peptide substrates for TGase 2 and Factor XIIIA. *J. Biol. Chem.* **2006**, *281*, 17699-17706.

150. Kamiya, N.; Tanaka, T.; Suzuki, T.; Takazawa, T.; Takeda, S.; Watanabe, K.; Nagamune, T. S-peptide as a potent peptidyl linker for protein cross-linking by microbial transglutaminase from Streptomyces mobaraensis. *Bioconjug. Chem.* **2003**, *14*, 351-357.

151. CHAIET, L.; WOLF, F. Properties of Streptavidin Biotin-Binding Protein Produced by Streptomycetes. *Arch. Biochem. Biophys.* **1964**, *106*, 1-5.

152. Le Trong, I.; Wang, Z.; Hyre, D. E.; Lybrand, T. P.; Stayton, P. S.; Stenkamp, R. E. Streptavidin and its biotin complex at atomic resolution. *Acta Crystallogr D* **2011**, *67*, 813-821.

153. Stayton, P.; Freitag, S.; Klumb, L.; Chilkoti, A.; Chu, V.; Penzotti, J.; To, R.; Hyre, D.; Le Trong, I.; Lybrand, T.; Stenkamp, R. Streptavidin-biotin binding energetics. *Biomol. Eng.* **1999**, *16*, 39-44.

154. Xing, D.; Dorr, R.; Cunningham, R.; Scholes, C. Endonuclease-Iii Interactions with Dna Substrates .2. the Dna-Repair Enzyme Endonuclease-Iii Binds Differently to Intact Dna and to Apyrimidinic Apurinic Dna Substrates as shown by Tryptophan Fluorescence Quenching. *Biochemistry* **1995**, *34*, 2537-2544.

155. De Carlo, S.; Harris, J. R. Negative staining and cryo-negative staining of macromolecules and viruses for TEM. *Micron* **2011**, *42*, 117-131.

156. Zhang, Y.; Raudah, S.; Teo, H.; Teo, G. W. S.; Fan, R.; Sun, X.; Orner, B. P. Alanine-shaving Mutagenesis to Determine Key Interfacial Residues Governing the Assembly of a Nano-cage Maxi-ferritin. *J. Biol. Chem.* **2010**, *285*, 12078-12086.

157. Zhou, H.; Gan, N.; Li, T.; Cao, Y.; Zeng, S.; Zheng, L.; Guo, Z. The sandwich-type electrochemiluminescence immunosensor for alpha-fetoprotein based on enrichment by Fe3O4-Au magnetic nano probes and signal amplification by CdS-Au composite nanoparticles labeled anti-AFP. *Anal. Chim. Acta* **2012**, *746*, 107-113.

158. Neely, A.; Perry, C.; Varisli, B.; Singh, A. K.; Arbneshi, T.; Senapati, D.; Kalluri, J. R.; Ray, P. C. Ultrasensitive and Highly Selective Detection of Alzheimer's Disease Biomarker Using Two-Photon Rayleigh Scattering Properties of Gold Nanoparticle. *ACS Nano* **2009**, *3*, 2834-2840.

159. Andrews, S.; Smith, J.; Hawkins, C.; Williams, J.; Harrison, P.; Guest, J. Overproduction, Purification and Characterization of the Bacterioferritin of Escherichia-Coli and a C-Terminally Extended Variant. *Eur J Biochem* **1993**, *213*, 329-338.

160. Martsev, S.; Vlasov, A.; Arosio, P. Distinct stability of recombinant L and H subunits of human ferritin: calorimetric and ANS binding studies. *Protein Eng.* **1998**, *11*, 377-381.

161. Ardejani, M. S.; Li, N. X.; Orner, B. P. Stabilization of a Protein Nanocage through the Plugging of a Protein-Protein Interfacial Water Pocket. *Biochemistry (N. Y.)* **2011**, *50*, 4029-4037.

162. Zhang, Y.; Raudah, S.; Teo, H.; Teo, G. W. S.; Fan, R.; Sun, X.; Orner, B. P. Alanine-shaving Mutagenesis to Determine Key Interfacial Residues Governing the Assembly of a Nano-cage Maxi-ferritin. *J. Biol. Chem.* **2010**, *285*, 12078-12086.

163. Wong, S. G.; Abdulqadir, R.; Le Brun, N. E.; Moore, G. R.; Mauk, A. G. Fe-haem bound to Escherichia coil bacterioferritin accelerates iron core formation by an electron transfer mechanism. *Biochem. J.* **2012**, *444*, 553-560.

164. Chang, J. Y.; Knecht, R.; Braun, D. G. Amino-Acid-Analysis at the Picomole Level - Application to the C-Terminal Sequence-Analysis of Polypeptides. *Biochem. J.* **1981**, *199*.

165. Harris, J.; Scheffler, D. Routine preparation of air-dried negatively stained and unstained specimens on holey carbon support films: a review of applications. *Micron* **2002**, *33*, 461-480.

166. Sobott, F.; Benesch, J.; Vierling, E.; Robinson, C. Subunit exchange of multimeric protein complexes - Real-time monitoring of subunit exchange between small heat shock proteins by using electrospray mass spectrometry. *J. Biol. Chem.* **2002**, *277*, 38921-38929.

167. Sobott, F.; Hernandez, H.; McCammon, M.; Tito, M.; Robinson, C. A tandem mass spectrometer for improved transmission and analysis of large macromolecular assemblies. *Anal. Chem.* **2002**, *74*, 1402-1407.

168. Tang, G.; Peng, L.; Baldwin, P. R.; Mann, D. S.; Jiang, W.; Rees, I.; Ludtke, S. J. EMAN2: An extensible image processing suite for electron microscopy. *J. Struct. Biol.* **2007**, *157*, 38-46.

169. Ludtke, S. J. http://blake.bcm.edu/emanwiki/EMAN2. 2013-2014.

170. Fan, R.; Boyle, A. L.; Cheong, V. V.; Ng, S. L.; Orner, B. P. A Helix Swapping Study of Two Protein Cages. *Biochemistry* **2009**, *48*, 5623-5630.

171. Fischer, M.; Georges, J. Limitations arising in the study of the fluorescence quenching of rhodamine 6G by iodides using cw-laser thermal lens spectrometry. *Spectroc. Acta Pt. A-Molec. Biomolec. Spectr.* **1998**, *54*, 101-110.

172. Crisalli, P.; Hernandez, A. R.; Kool, E. T. Fluorescence Quenchers for Hydrazone and Oxime Orthogonal Bioconjugation. *Bioconjug. Chem.* **2012**, *23*, 1969-1980.

173. Sando, S.; Abe, H.; Kool, E. Quenched auto-ligating DNAs: Multicolor identification of nucleic acids at single nucleotide resolution. *J. Am. Chem. Soc.* **2004**, *126*, 1081-1087.

174. Hink, M.; Visser, N.; Borst, J.; van Hoek, A.; Visser, A. Practical use of corrected fluorescence excitation and emission spectra of fluorescent proteins in Forster resonance energy transfer (FRET) studies. *J. Fluoresc.* **2003**, *13*, 185-188.

175. Minten, I. J.; Hendriks, L. J. A.; Nolte, R. J. M.; Cornelissen, J. J. L. M. Controlled Encapsulation of Multiple Proteins in Virus Capsids. *J. Am. Chem. Soc.* **2009**, *131*, 17771-17773.

176. De Carlo, S.; Harris, J. R. Negative staining and cryo-negative staining of macromolecules and viruses for TEM. *Micron* **2011**, *42*, 117-131.

177. Kourkoutis, L. F.; Plitzko, J. M.; Baumeister, W. Electron Microscopy of Biological Materials at the Nanometer Scale. *Ann Rev Mater Res* **2012**, *42*, 33-58.

178. Tang, G.; Peng, L.; Baldwin, P. R.; Mann, D. S.; Jiang, W.; Rees, I.; Ludtke, S. J. EMAN2: An extensible image processing suite for electron microscopy. *J. Struct. Biol.* **2007**, *157*, 38-46.

179. Dautant, A.; Meyer, J.; Yariv, J.; Precigoux, G.; Sweet, R.; Kalb, A.; Frolow, F. Structure of a monoclinic crystal form of cytochrome b1 (bacterioferritin) from E-coli. *Acta Crystallogr D* **1998**, *54*, 16-24.

180. Liu, J.; Konermann, L. Protein-Protein Binding Affinities in Solution Determined by Electrospray Mass Spectrometry. *J. Am. Soc. Mass Spectrom.* **2011**, *22*, 408-417.

181. Preimesberger, M. R.; Wenke, B. B.; Gilevicius, L.; Pond, M. P.; Lecomte, J. T. J. Facile Heme Vinyl Posttranslational Modification in a Hemoglobin. *Biochemistry* **2013**, *52*, 3478-3488.

182. Ferguson, B.; Yang, D. Methionyl-Transfer Rna-Synthetase Induced 3'-Terminal and Delocalized Conformational Transition in Transfer Rnafmet - Steady-State Fluorescence of Transfer-Rna with a Single Fluorophore. *Biochemistry* **1986**, *25*, 529-539.

183. Lim K; Jameson DM; FAU - Gentry, C. A.; Gentry CA; FAU - Herron, J. N.; Herron JN Molecular dynamics of the anti-fluorescein 4-4-20 antigen-binding fragment. 2. Time-resolved fluorescence spectroscopy. *Biochemistry* **1995**, *34*, 6975-6984.

184. Weber, G.; Shinitzk, M. Failure of Energy Transfer between Identical Aromatic Molecules on Excitation at Long Wave Edge of Absorption Spectrum. *Proc. Natl. Acad. Sci. U. S. A.* **1970**, *65*, 823-&.

185. Kawski, A. Excitation-Energy Transfer and its Manifestation in Isotropic Media. *Photochem. Photobiol.* **1983**, *38*, 487-508.

186. Abe, S.; Niemeyer, J.; Abe, M.; Takezawa, Y.; Ueno, T.; Hikage, T.; Erker, G.; Watanabe, Y. Control of the coordination structure of organometallic palladium complexes in an apo-ferritin cage. *J. Am. Chem. Soc.* **2008**, *130*.

187. Makino, A.; Harada, H.; Okada, T.; Kimura, H.; Amano, H.; Saji, H.; Hiraoka, M.; Kimura, S. Effective encapsulation of a new cationic gadolinium chelate into apoferritin and its evaluation as an MRI contrast agent. *Nanomed. -Nanotechnol. Biol. Med.* **2011**, *7*, 638-646.

188. Wu, Z.; Tang, L.; Zhang, X.; Jiang, J.; Tan, W. Aptamer-Modified Nanodrug Delivery Systems. *ACS Nano* **2011**, *5*, 7696-7699.

189. Park, C. W.; Park, H. J.; Kim, J. H.; Won, K.; Yoon, H. H. Immobilization and characterization of ferritin on gold electrode. *Ultramicroscopy* **2009**, *109*, 1001-1005.

190. Shin, K. M.; Watt, R. K.; Watt, G. D.; Choi, S. H.; Kim, H.; Kim, S. I.; Kim, S. J. Characterization of ferritin core on redox reactions as a nanocomposite for electron transfer. *Electrochim. Acta* **2010**, *55*, 3486-3490.

191. Wang, T.; Choi, H. W.; Kim, W.; Kim, J. S.; Park, S. J. Two-Dimensional Array of ZnSe-Ferritin Nanodots as a Sensor Media for Gamma-Aminobutyric Acid. *Mol Cryst Liq Cryst* **2010**, *519*, 27-35.

192. Zhao, J.; Liu, M.; Zhang, Y.; Li, H.; Lin, Y.; Yao, S. Apoferritin protein nanoparticles dually labeled with aptamer and horseradish peroxidase as a sensing probe for thrombin detection. *Anal. Chim. Acta* **2013**, *759*, 53-60.

193. Yang, F.; Moss, L.; Phillips, G. The molecular structure of green fluorescent protein. *Nat. Biotechnol.* **1996**, *14*, 1246-1251.

194. San, B. H.; Moh, S. H.; Kim, K. K. The effect of protein shells on the antioxidant activity of protein-encapsulated platinum nanoparticles. *J Mater Chem* **2012**, *22*, 1774-1780.

195. Godinez-Salomon, F.; Arce-Estrada, E.; Hallen-Lopez, M. Electrochemical Study of the Pt Nanoparticles Size Effect in the Formic Acid Oxidation. *Int J Electrochem Sc* **2012**, *7*, 2566-2576.

196. Yang, C.; Manocchi, A. K.; Lee, B.; Yi, H. Viral templated palladium nanocatalysts for dichromate reduction. *Appl Catal B-Environ* **2010**, *93*, 282-291.

197. Mahboob, A.; Vassiliev, S.; Poddutoori, P. K.; van der Est, A.; Bruce, D. Factors Controlling the Redox Potential of ZnCe6 in an Engineered Bacterioferritin Photochemical 'Reaction Centre'. *Plos One* **2013**, *8*.